INFORMATION TO USERS

This manuscript has been reproduced from the microfilm master. UMI films the text directly from the original or copy submitted. Thus, some thesis and dissertation copies are in typewriter face, while others may be from any type of computer printer.

The quality of this reproduction is dependent upon the quality of the copy submitted. Broken or indistinct print, colored or poor quality illustrations and photographs, print bleedthrough, substandard margins, and improper alignment can adversely affect reproduction.

In the unlikely event that the author did not send UMI a complete manuscript and there are missing pages, these will be noted. Also, if unauthorized copyright material had to be removed, a note will indicate the deletion.

Oversize materials (e.g., maps, drawings, charts) are reproduced by sectioning the original, beginning at the upper left-hand corner and continuing from left to right in equal sections with small overlaps. Each original is also photographed in one exposure and is included in reduced form at the back of the book.

Photographs included in the original manuscript have been reproduced xerographically in this copy. Higher quality 6" x 9" black and white photographic prints are available for any photographs or illustrations appearing in this copy for an additional charge. Contact UMI directly to order.

UMI

A Bell & Howell Information Company
300 North Zeeb Road, Ann Arbor MI 48106-1346 USA
313/761-4700 800/521-0600

Direct Optimal Control of Flexible Structures With Application to Adaptive Optics Systems

by

Chellabi Abdelkader
Eng. Dip., Ecole National Polytechnique (Algeria), 1988
MASc University Laval, Quebec, 1992

A Thesis Submitted in Partial Fulfillment of the
Requirements for the Degree of
DOCTOR OF PHILOSOPHY
in the
Mechanical Engineering.

We accept this thesis as conforming
to the required standard

Dr. Y. Stepanenko, Supervisor (Mechanical Engineering)

Dr. S. Dost, Co-Supervisor (Mechanical Engineering)

Dr. R. Podhorodeski, Department Member (Mechanical Engineering)

Dr. P. Agathoklis, Outside Member (Electrical & Computer Engineering)

Dr. M. Epstein, External Examiner (Mechanical Engineering, University of Calgary)

Supervisors: Dr. Y. Stepanenko, and Dr. S. Dost

Abstract

An adaptive optics system consists mainly of a wavefront sensor to detect optical aberrations, a control system to reconstruct the wavefront and compute a correction, and a deformable mirror to apply the correction. In this dissertation, the problem of optimal control of an adaptive optics system is investigated. A direct optimal control approach is used in the controller design.

The direct optimal control methodology developed for discrete parameter systems is extended in this study to distributed parameter systems, where the Rayleigh-Ritz method is used for both spatial and temporal variables. The displacement field is written as the product of spatial functions (mode shapes for a vibrating structure, and Zernike modes for deformable mirror) and the generalized coordinates. These generalized coordinates and the control input functions (voltages) are written as simple series expansions in time in terms of selected functions and unknown coefficients. Substitution of these selected functions and their variations into Hamilton's law of varying action results in algebraic equations of motion (AEM) of the structure. These AEM are then considered as the algebraic state equations where the unknown expansion coefficients of the time series (assumed time-modes) for the generalized coordinates are recognized as the states and those of the input functions are recognized as the controls.

Using the space-time assumed mode method, the usual variational optimal control problem is transformed into an equivalent algebraic problem. Optimal solutions are then obtained in a closed form and the solution is a global optimum within the time period considered. The solution procedure does not lead to any Ricatti equation or alike. The direct method proved to be simple, computationally efficient, attractive from implementation point of view, and it is general and allows a deterministic modelling of many physical problems.

Applied to active vibration control of plates with piezoelectric transducers, the direct methodology exhibits results similar to those obtained through conventional methods. Active shape control of a deformable mirror using the direct approach results in high performance of the controller. The method allows direct control of Zernike modes, and highlights the relationship between the control inputs and Zernike modes through an algebraic controllability measurement index. Robustness of the controller is shown through simulation of smooth and severe random variations of the optical aberrations.

In the same line of thought, a space-time finite element method is developed and applied to structural optimal control problems. Finite element method is used for both spatial and temporal discretizations. The unique feature of this method is its ability to analyse the structure-control interaction in the same mathematical framework, which allows simultaneous control and structural model design iterations. However, due to its high dimensionality, the space-time finite element method is computationally less efficient than its counterpart assumed mode.

Examiners:

Dr. Y. Stepanenko, Supervisor (Mechanical Engineering)

Dr. S. Dost, Co-Supervisor (Mechanical Engineering)

Dr. R. Podhorodeski, Department Member (Mechanical Engineering)

Dr. P. Agathoklis, Outside Member (Electrical & Computer Engineering)

Dr. M. Epstein, External Examiner (Mechanical Engineering, University of Calgary)

Table of Contents

List of Tables

List of Figures

Acknowledgements

First and formost, I would like to express my sincere appreciation to the patient guidance of my supervisor Dr. Yury Stepanenko. I thank him for his encouragement, advice and moral support I received during the course of this research, and for his help in the preparation of this dissertation. Financial assistance received from Professor Yury Stepanenko through IRIS-Precran is also gratefully acknowleged.

I would like also to thank My Co-Supervisor Dr. Sadik Dost, for his guidance, encouragement, assistance in the preparation of this work, and for creating a pleasant atmosphere for the success of this research.

My thanks are extended to Dr. Behrouz Tabarrok who was of great help from day one of my Ph.D. program till this point, for his assistance, and for reviewing some material of the thesis. Dr. Ronald Podhorodeski, and Dr. Panajotis Agathoklis deserve special thanks for their encouragement, support and assistance.

I also would like to thank Dr. Marcelo Epstein for accepting to be my external examiner.

Lastly, I would like to thank all my friends who made my stay in Victoria enjoyable among them Amirouche Cherfi and Belkacem Chergui.

Finally, I thank my wife Naima for her patience and support during the critical times of this work.

To my family

Chapter 1

Introduction

1.1 System Description

As suggested by the title of this thesis, the focus of this investigation is the adaptive optics control system. Particularly, the problem of optimal control of a deformable mirror is studied.

In general terms, adaptive optics deals with *the control of light in a real time closed-loop fashion* and refers to optical components whose characteristics are controlled during actual operation in order to improve the quality of an optical signal [5, 6, 27, 44, 72].

A typical adaptive optics system consists of three main components: deformable mirrors, wavefront sensors, and a control system. Figure 1.1 illustrates the design of a typical adaptive optics system. An optical wavefront is collected by a telescope and is reflected off a deformable mirror. The reflected wavefront is observed by a wavefront sensor. The wavefront sensor measures an array of local phase gradients/curvatures, which are processed in a wavefront reconstructor to estimate the phase/curvature of

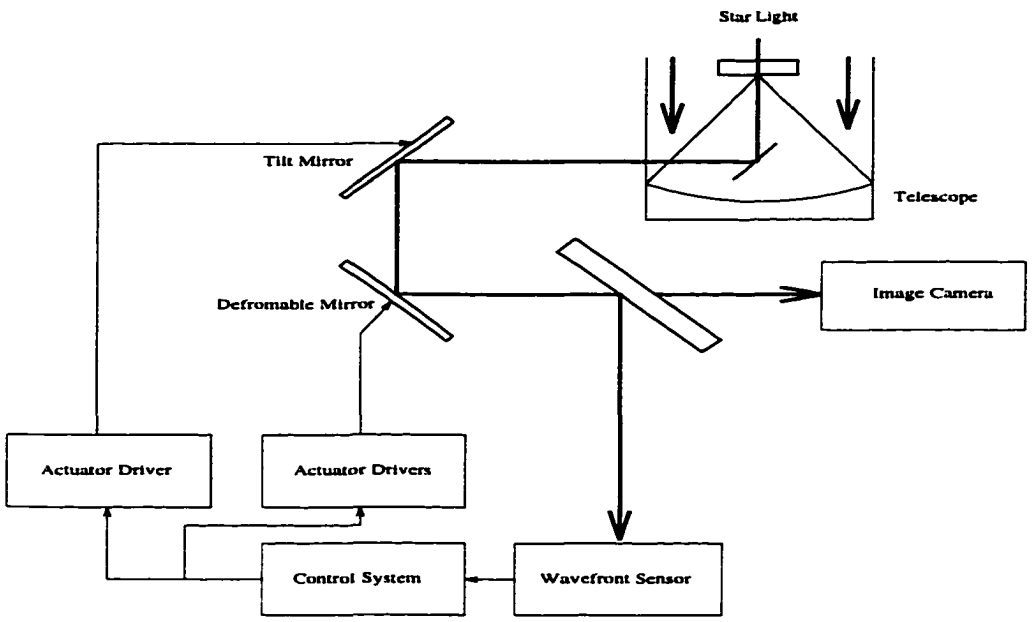

Figure 1.1: Adaptive Optics System

the incoming wavefront. These estimates are then used by the control system driving the deformable mirror to compensate for the incoming wavefront distortions.

Adaptive optics includes correction of both amplitude/intensity and phase of a light beam. Amplitude/intensity variations (also called scintillation) contribute to image quality degradation much less than phase variations and are therefore generally ignored in the planning and evaluation of adaptive optics systems [17].

Wavefronts represent surfaces of constant phase for the electromagnetic field. Wavefront for plane and spherical waves are considered as a reference. Any deviation from a reference sphere or plane results in an aberrated wavefront. This deviation occurs when the index of refraction of the propagating medium, the atmosphere, changes due to density and temperature changes. As a result, the wavefront of light traveling through the medium is distorted. An adaptive optics system seeks to adjust the shape of the deformable mirror so as to cancel out this deviation exactly; this is called phase conjugation.

Deformable mirrors are typically continuous surface mirrors deformed by actuators to have peaks and valleys. These actuators are usually piezoelectric actuators which are attached to the bottom of the mirror at preselected points. One form of frequently used actuators is the stacked piezoelectric actuator. When a voltage is applied. the piezoelectric material either expands or shrinks (depending on the polarity of the voltage) and shapes the surface of the deformable mirror. Instead of stacked actuators, *bimorph mirrors* use two thin plates of oppositely polarized piezoelectric materials [31, 50, 41, 55]. The plates are bonded together and controlled by a set of electrodes deposited on the back side of one plate.

In adaptive optics, there are mainly two types of wavefront sensors, namely wavefront slope sensors which measure the two-dimensional spatial gradients of the phase at a discrete number of points, and curvature sensors which measure local curvatures of the phase at discrete locations. The information about phase, phase gradient and/or curvature is used in the control system to reconstruct the wavefront. There are various types of common wavefront sensors which differ in the manner by which the gradients are measured [34, 49, 45, 73].

Adaptive optics finds its major application in astronomy. There are many telescopes in the world which use adaptive optics, among them the Keck telescope in Hawaii, the Bonnette system at the Dominion observatory in Victoria (Canada), and the European Southern Observatory in Germany and Chile. Other application fields of adaptive optics include communications, biomedicine and laser welding. Atmospheric distortions affect ground-based, free space laser communications. Medical devices (e.g., endoscopes) image tissue through bodily fluids that cause optical aberrations and degrade image quality. These aberrations also affect precise delivery of laser power in endoscopic and retinal surgery. Likewise, heat induced aberrations affect the delivery of laser power in welding and cutting applications.

1.2 Problem Description

Adaptive compensation in large optical telescopes, or in airborne imaging or missile systems, requires deformable mirrors capable of correcting large optical path errors at high speed. This is due to the requirement on the control bandwidth to be 10kHz or more [26].

Controlling a deformable flexible mirror is part of structural control. A critical problem in structural control is the interaction between the active control system and the structural dynamics. The overlap of the control bandwidth with modal frequency spectrum is a major issue in the active control of flexible structures. The classical method for avoiding control instability relies on having a wide separation between the lowest-frequency resonance and the highest frequency for the control closed loop response. The effectiveness of the control system depends on the degree of interaction between the control system and the structural resonances, which, in turn, depends on the details of the control law used.

An equally critical problem in adaptive optics control design, is the random nature of the turbulent atmosphere which prohibits a deterministic expression relating turbulent effect to optical image quality. The quality of the received image depends on such factors as wavelength, refractive-index structure constant, zenith angle to the source, wind velocity, and wind velocity distribution over altitude. The combination of these effects results in a randomly distorted wavefront. Past research [19, 63, 32, 68] has always considered a stochastic description of the wavefront distortions. A possible representation for describing atmospheric phase distortion is by a set of Zernike polynomials. The Zernike function space provides an orthogonal basis set of functions corresponding to aberrations commonly studied in optics [63]. The total phase

distortion $\phi(r, \theta, t)$ is described by a linear combination of the Zernike functions:

$$\phi(r, \theta, t) = \sum_{i=0}^{N} A_i(t) Z_i(r, \theta)$$

where $Z_i(r, \theta)$ are the Zernike basis functions (which will be explained in the next chapter) spanning the space within the aperture as functions of radial and angular coordinates r and θ, and $A_i(t)$ are *random* time-varying coefficients. However, control design using deterministic -as opposed to stochastic- control laws, requires that the phase distortion present in the wavefront is to be described deterministically.

For high speed applications several types of mirrors have been proposed, such as thin-plate mirrors on piezoelectric stacks, and bimorph mirrors. The bimorph mirror is especially appealing since it provides large-amplitude continuous deformations at high speed with low voltages [31].

The potential of using bimorph mirrors for high speed adaptive compensation has been convincingly demonstrated in some experiments [31] where the device performs to frequencies in excess of 10 kHz. Nevertheless, there are many issues which still need to be resolved before appropriate control design procedures are developed. Specifically, given a piezoelectric material, electromechanical coupling, the structure (mirror) and the control domain, a designer should be able to obtain an optimum procedure for controlling the shape of the given mirror's surface. To meet this design goal, one must be able to obtain -deterministically- a measure of the wavefront aberrations and correlate them to the variables used in the controller design.

To resolve some of these issues, the research in this thesis is directed towards the following major objectives:

1. The first objective is to develop models for the active structure (i.e., deformable mirror) consisting of a thin-plate structure and piezoceramic actuators. This

also includes a deterministic representation of the wavefront aberrations (i.e. mirror's surface).

2. The second objective is to develop an optimal control methodology for distributed parameter systems based on the developed models. This also includes optimal regulator problem for active vibration control of a tip/tilt mirror, and an optimal tracking problem control for active shape control of a deformable mirror.

1.3 Literature Survey and Proposed Approach

Since the adaptive optics system consists of a multi-actuator deformable mirror and multiple wavefront sensor gradient/curvature measurements, it is a multi-dimensional control system. The required speed of this system is dictated by the frequency content of the incoming optical wavefront [38, 39]. As the signal bandwidth increases, the control system will be required to respond faster. Currently control bandwidths of a few hundred Hertz are in use for most applications [33, 48]. The word bandwidth is often cited in adaptive optics literature, without regard to the multivariable nature of the system. Some articles assume that the overall system operates at one bandwidth, thus analyzing the adaptive optics system as a single-input single-output system [38, 39, 74], which results in lower performance when applied to multi-input multi-output systems. In some other papers it is recognized that there are multiple loops and therefore multiple "bandwidths" but without considering the possible coupling between the different loops [4, 22, 64, 36, 51]. Huang [48] considered the multivariable nature of the system and proposed multivariable H_∞ control design, but this was computationally non-efficient due the high dimensionality of the controller.

For systems using curvature sensors, Roddier [67] suggests coupling this type of

sensors with a bimorph mirror to remove the intermediate stage of reconstructing the wavefront. This is done by connecting the output of each curvature detector to the corresponding input of the bimorph which results in a very fast time response of the system. This claim was contested by Shwartz [69] who showed that indeed an intermediate stage is necessary to correct for the mismatching terms between the bimorph mirror surface and the wavefront. Furthermore, the multivariable problem for the bimorph mirror coupled with a curvature sensor remain unresolved to date, and the existing controller was designed based only on the quasi-static model of the mirror.

Control of a deformable mirror is strongly related to control of flexible structures for which a well established theory and algorithms exist in the literature. Meirovitch [59] has written what is already a classical book on control of flexible structures. He develops models of flexible structures and gives frequency and time domain methods of systems analysis and synthesis. Porter [65] introduces modal control which can be considered as a predecessor to balanced control. Junkins and Kim [54] give an up-to-date introduction to control of flexible structure. Also Junkins [53] edited a monograph that consists of up-to date contributions to the dynamics, identification and control of flexible structures. Lin [58] gives a good and wide-ranging review of methods used in advanced system analysis and synthesis: H_2 and H_∞ controllers, robust design , nonlinear systems fuzzy controllers, and control using neural network. The monograph by Joshi [52] presents his own developments in the area of control of flexible space structures, supported by numerous applications; it concentrates on robust dissipative controllers and LQG controllers. However, application of these conventional control approaches to adaptive optics was not possible without resort to stochastic methods in describing the random variation of the atmospheric aberrations.

A recently developed control methodology called "Direct" methodology is seen

as an alternative to the stochastic problem of the wavefront representation. The foremost feature of the proposed methodology is that the conventional differential state space formulation is replaced by an equivalent algebraic representation. The source of inspiration here has been the work of Adiguzel [1] who developed the direct optimal approach for discrete systems. His development is based on the analyses of response problems of mechanics introduced for the first time by Bailey [8, 9] and consists in essence of utilizing Hamilton's Law of Varying Action, in short HLVA.

To help understand the premise of the direct methodology via HLVA, a brief summary would be appropriate at this point. HLVA was set forth by William Rowan Hamilton in 1834-1835 in his classical papers on a general methodology in dynamics [42, 43]. It manifests a natural law of mechanical systems, mathematically expressing minimization of an energy functional of the system. As in extremization of any functional, one can then bring in mathematical tools of calculus of variations to attempt a solution. When this is done without deducing or resorting to any differential equation of motion, the approach is referred to as *direct method.* When the governing laws are expressed by differential equations, which can also be obtained from HLVA, the approach is simply *indirect* [1].

Central to generating the solution directly to the response problem of mechanics espoused by Bailey, is the concept of expressing the displacement field during a time interval of motion in the form of truncated simple power series in time with constant expansion coefficients which are treated as the unknowns of the response problem. In essence, this is the method of Ritz [12], [11], [1]. Application of this concept to the time varying coefficients in Zernike expansion represents an alternative to the stochastic problem.

Following Bailey's papers in mid and late 1970's, a trend has emerged and others have obtained direct solutions to dynamics problems either based on HLVA or ref-

erencing to it. From the latest articles, to mention a few, are those of Borri *et al.* [21], Ben-Tal and Bar-Yoseph [18], Bar-Yospeh *et al.* [15], Atilgan and Hodges [3], and Hodges and Hou [47] with various emphases, who successfully applied the direct approach and provided numerical results that could get as close to known exact solutions as desired. The remarkable feature of this approach is not only the capability to solve these problems (solution to some of them are available by other means), but also the simplicity of the procedure with which the results are obtained considering their accuracy.

Since the direct method in response analysis proved successful, addressing the control (inverse response) problem directly via HLVA becomes an appealing technique to investigate. In particular, its demonstrated simplicity, generality and accuracy provides the motivation to search for possibilities of devising a direct control approach to mechanical systems. To this end , a direct open-loop control methodology using HLVA was demonstrated by Oz and Raffie [62]. Adiguzel [1] successfully developed and demonstrated through a few examples, a direct optimal control methodology for discrete systems. It was concluded in [1] that: *Many issues still remain to be addressed ... Perhaps more practically and readily, an immediate extension would be the study of distributed parameter systems using the direct control concept of this study. An on-line implementation task can be undertaken. A comparative study can be pursued by applying the proposed direct method and others.* And many other questions need to be studied as to how such a direct (control) approach would fit into the problem of controllability, observability, optimality, and feedback control, etc. All of these aspects of the direct control problem are investigated in this study.

Another similar but somehow different approach, is the *space-time finite element optimal control approach.* Nagurka and Wang [60], and Yen and Nagurka [77] proposed an approach to solving an optimal structural control problem. The approach consists

of discretization of the equations of motion and the performance index by expanding the states in terms of a finite number of prespecified basis functions and undetermined parameters. This formulation leads to a constrained quadratic programming problem that is solved analytically. An alternative approach for solving optimal control problems by discretization in time was studied by Hodges and Bless [46]. In their approach, the optimal control problem was formulated via *temporal* finite elements resulting in a two point boundary value problem whose solution yields a discrete-time control law. This was applied only to discrete systems. Following Ben-Tal's [18] approach, the optimal control problem is solved while performing simultaneous temporal and spatial discretization. Therefore, this method can be viewed as a generalization and extension of the above approaches. Ben-Tal *et. al* [18] use dynamic programming method to solve for the control law, while in this study the control law is simply derived using the conventional methods of discrete optimal control theory.

To address the optimal control problems directly, the spatial part of displacement fields are prescribed and curve fitted by known shape functions which represent the Zernike polynomials in an adaptive optics system or the mode shape in a vibrating structure. The temporal part is expanded in power series up to desired accuracy. This concept is extended to the input fields, which are the ultimate unknowns in a control problem. The spatial expansion is prescribed according to the geometrical distribution of the actuators, for the temporal part, the expansion is in simple power series with unknown coefficients, and the series are truncated to match the order of the accelerations. The expansion coefficients of displacement and control field in their respective time-series, together, constitute the control unknowns of the problem. Direct application of HLVA to these yields a set of algebraic equations for the control problem. Thus without any resort to differential equations, the control problem can also be studied directly via such algebraic equations. Through the proposed

direct methodology, the conventional variational optimal problem involving integral functionals, is transformed to an equivalent algebraic optimal problem, from which, solutions are obtained in closed form with a straightforward procedure. The space-time finite element -another direct methodology- based optimal control methodology is also developed and analysed through some examples.

1.4 Thesis Contribution

The contribution of this thesis can be summerized as follows:

I. An optimal control design for high speed adaptive optics compensation has been developed. The design methodology is applicable to a wide spectrum of problems, whether the problem considered is deterministic or stochastic. It is simple, computationally efficient and possesses a great flexibilty for hardware implementations.

II. As a consequence of this study, a new technique for modelling stochastic problems by deterministic models is developed. Application of this technique to conventional stochastic control problems could simplify the controller design for such problems.

III. Beside the direct optimal control methodology, the space-time optimal control approach newly developed in the course of this thesis, offers another alternative for structural control for both stochastic and deterministic problems. The unique feature of this method is its ability to analyse the structure-control interaction in the same mathematical framework, allowing a better understanding of this interaction, which results in better control designs.

1.5 Thesis Organisation

Chapter 2 provides a description in a more detailed fashion about adaptive optics systems, in particular the concept of atmospheric aberrations and their polynomial representation. Adaptive optics using phase conjugation is described along with the components which constitute an adaptive optics system. Wavefront sensing methods, and the corresponding correction methods associated with each sensing system are introduced. Attention is finally drawn to adaptive systems using bimorph mirrors and curvature sensor which constitute the motivating application of this study. The chapter closes with some remarks and conclusions.

Chapter 3 is dedicated solely to the descriptions and definitions for the flexible structure in terms of the assumed mode technique. The preliminary formulations of system dynamics via HLVA and the resulting algebraic state equations (based on assumed mode expansion) are derived. Equations of time continuity required in a time marching process are also included, followed by discussions on controllability from the perspective of direct control approach. This discussion is undertaken to shed light on the controllable and uncontrollable modes of a deformable structure.

In chapter 4, the optimal regulator control problem is studied. The formulation of an algebraic optimal control problem for a classical linear regulator is introduced after the introduction of the assumed modes into the control performance measure. Then a straightforward solution of the optimal problem is given and an illustrative example demonstrating the method is included. Formulation and applications of the direct optimal control are then extended to tracking problems in Chapter 5, where an optimal controller is designed for a flexible deformable mirror. A simulation of the deformable mirror (bimorph mirror) with and without the controller is included at the end of the chapter.

Chapter 6 introduces the space-time finite element formulation applied to structures with discrete and/or continuous piezoelectric transducers. The optimal control is reconsidered here. An optimal controller is designed using space and time discretization, and the resulting controller is compared with the direct optimal controller in overall performance via simulation of the deformable mirror introduced previously. Some concluding remarks close this chapter.

This study is concluded in chapter 7 with an overall summary and assessment of the findings and directions for future research.

Chapter 2

Adaptive Optics Systems

In this chapter, we will present a general overview of an adaptive optics system as found in the literature. We will describe and explain in a more detailed fashion, the major functions and components that constitute an adaptive optics system. We first define a block diagram representation of the closed loop adaptive optics system, then using the diagram, we will explain the function of each component in the diagram. Since the control system is the focus of this study, reconstruction and control of the wavefront are given more attention.

2.1 Introduction

Figure 2.1 represents a block diagram of the closed loop adaptive optics system. The atmospheric aberrations are represented as additive disturbances by the vector $\boldsymbol{d}$. Note that all the components of $\boldsymbol{d}$ can have different and perhaps independent temporal variations that must be compensated for by the adaptive optics control system. The wavefront is reflected from a deformable mirror, and the resulting wavefront

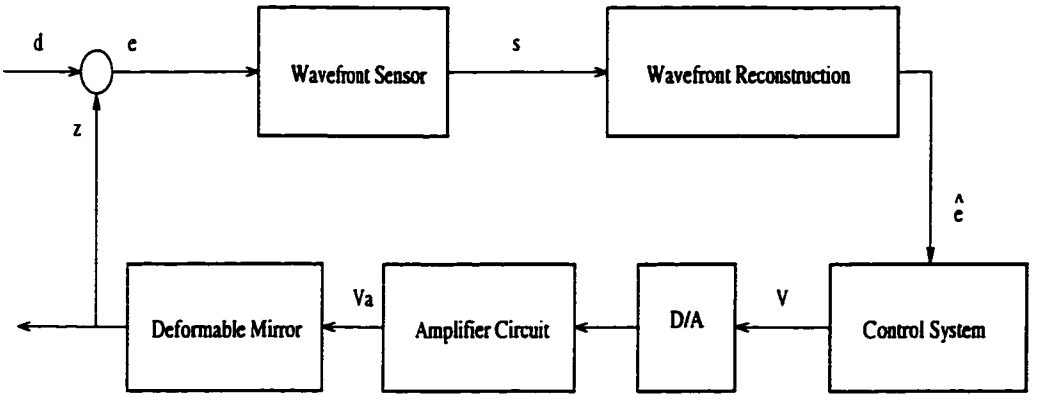

Figure 2.1: Block diagram of an AO system

error vector $\boldsymbol{e}$ is introduced into the sensor. The wavefront sensor measures local subaperture slopes in the x and y directions and/or wavefront curvature which are represented by the vector $\boldsymbol{s}$. The wavefront reconstructor combines these measurements and produce an estimate of the wavefront error $\hat{e}$. The wavefront estimates are passed to the control system, which selects control signals for each actuator (for discrete actuator mirror) or electrode (for a bimorph mirror) to reduce the estimated error $\hat{e}$. The output of the control system $\boldsymbol{V}$ is amplified by an amplifier circuit, which produces the mirror drive voltages $\boldsymbol{V}_a$. The voltages $\boldsymbol{V}_a$ drive the piezoelectric actuators which deflect the surface of the deformable mirror. When the closed loop system is operating properly, the shape of the deformable mirror will match the shape of the incoming disturbance in steady state, producing zero wavefront error.

2.2 Phase Conjugation

The principle of phase conjugation is the core of adaptive optics. It can be analyzed by a number of ways. The method can be shown by observing Figure 2.2. The wavefront of a beam entering from the left (a) is distorted by a piece of glass because the index of refraction is higher than 1. The wavefront is retarded as it goes through the glass

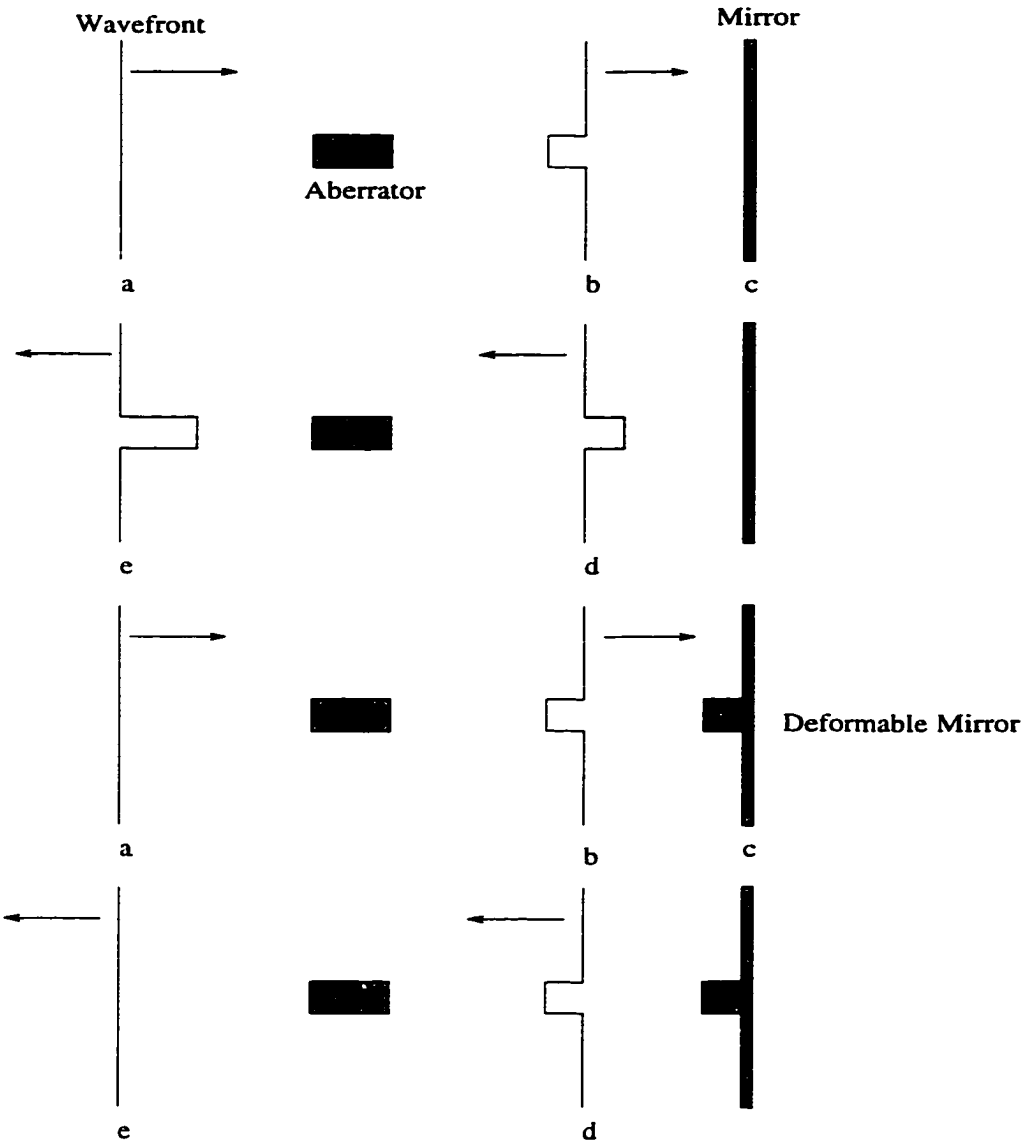

Figure 2.2: Principle of phase conjugation

(b). After reflection from the mirror (c), the wavefront has the same shape but it is propagating in the opposite direction. As it traverses the glass again, it receives the same retardation as before. The exiting wavefront (e) is greatly distorted, since it passed through the aberrator twice.

If we want to achieve a plane wavefront after a beam passes through the glass twice, there may be a way to alter the surface of the mirror in such a way as to invert the wavefront so that the second passage leaves no residual distortion. Looking at figure 2.2, we can see that a bump in the mirror *at just the right place* and *at just the right amount* can cause the leading edge of the wavefront to be reversed. When this wavefront (d) passes through the aberrator again, the final wavefront (e) is once again plane. This is called conjugation of the phase which comes from the fact that the correction is proportional and inverse in sign to the amount of aberration in the wavefront. Note that if the aberration is dynamic -in reality it is-, we must place the phase conjugate on the beam *at the right time* [72].

2.3 Representation of the Wavefront

For imaging applications, atmospheric turbulence (which is referred in the literature to the changes of air density due to temperature variations) along the propagation path causes continuous spatial and temporal variations in the index of refraction. Such variations in index of refraction result in spatial and temporal modulation of intensity and phase of the optical image.

The random nature of the turbulent atmosphere prohibits a deterministic expression relating turbulent effects to optical image quality. The quality of the received image depends on such factors as wavelength, refractive-index structure constant, zenith angle to the source, wind velocity, and wind velocity distribution over alti-

tude. The combination of these effects results in a randomly distorted wavefront. Thus it becomes necessary to have means of mathematically describing the phase distortion present in the wavefront.

A number of mathematical constructs are used to describe the phase of a beam. These include power series representation and a set polynomials called Zernike Polynomials.

The power series representation is, unfortunately, not an orthonormal set over a circle. Many such series exist. The set of polynomials that is orthonormal over a circle introduced by Zernike has some very useful properties. The series called *Zernike series*, is composed of sums of power series terms with appropriate normalizing factors. A detailed description of the Zernike series is given by Born and Wolf [20], and an analysis of Zernike Polynomials and atmospheric turbulence including their Fourier transforms was done by Noll [61].

Z_j	n	m	Expression (ρ, θ)	Expression (x, y)	Description
Z_1	0	0	1	1	Piston
Z_2	1	1	$2\rho\cos\theta$	$2x$	y Tilt
Z_3	1	1	$2\rho\sin\theta$	$2y$	x Tilt
Z_4	2	0	$\sqrt{3}[2\rho^2 - 1]$	$\sqrt{3}[2x^2 + 2y^2 - 1]$	Defocus
Z_5	2	2	$\sqrt{6}\rho^2\cos 2\theta$	$\sqrt{6}[x^2 - y^2]$	Astigmatism
Z_6	2	2	$\sqrt{6}\rho^2\sin 2\theta$	$\sqrt{62}xy$	Astigmatism
Z_7	3	1	$\sqrt{8}[(3\rho^3 - 2\rho)\cos\theta]$	$\sqrt{8}[3x(x^2 + y^2) - 2x]$	Coma
Z_8	3	1	$\sqrt{8}[(3\rho^3 - 2\rho)\sin\theta]$	$\sqrt{8}[3y(x^2 + y^2) - 2y]$	Coma
Z_9	3	3	$\sqrt{8}[\rho^3\cos 3\theta]$	$\sqrt{8}[x(x^2 - 3y^2)]$	Trefoil
Z_{10}	3	3	$\sqrt{8}[\rho^3\sin 3\theta]$	$\sqrt{8}[y(3x^2 - y^2)]$	Trefoil

Table 2.1: First 10 Zernike Polynomials

The general Zernike series contains all aberration terms, including piston [1] and tilt. The analytic expressions of the first 10 Zernike terms are given in table 2.1. In

[1] *Piston* is the constant retardation or advancement of the phase over the entire beam.

polar coordinates, these polynomials are defined by [61, 75]

$$\begin{aligned} Z_{even\ j} &= \sqrt{2(n+1)}R_n^m(\rho)\cos m\theta\ ; \quad m \neq 0 \\ Z_{odd\ j} &= \sqrt{2(n+1)}R_n^m(\rho)\sin m\theta\ ; \quad m \neq 0 \\ Z_j &= \sqrt{2(n+1)}R_n^m(\rho)\ ; \quad m = 0 \end{aligned} \tag{2.1}$$

Where $\rho = \frac{r}{R}$, r is a radial distance, R is the aperture radius , θ is the azimuth angle. n is the degree of radial mode, m is the azimuthal frequency, and

$$R_n^m(\rho) = \sum_{s=0}^{(n-m)/2} \frac{(-1)^s(n-s)!}{s![(n+m)/2-s]![(n-m)/2-s]!}\rho^{n-2s} \tag{2.2}$$

Therefore, a wavefront W can be described by a linear combination of the Zernike functions as:

$$W(r,\theta,t) = A_0(t) + \sum_{k=1}^{N} A_k(t)Z_k(r,\theta) \tag{2.3}$$

where $Z_k(r,\theta)$ are the Zernike basis functions spanning the space within the aperture as functions of radial and angular coordinates r and θ, and $A_k(t)$ are random time-varying coefficients which have to be determined using information about the wavefront obtained through phase measurements.

Mathematically, an infinite number of Zernike functions are required to characterize the wavefront completely. However, approximately 92% of the root mean square (rms) phase information is contained in the first 14 Zernike modes excluding the piston (zeroth mode) [63]. The piston mode represents the average phase within the aperture. It is nondistortive and unobservable by the wavefront sensor. As such the piston is removed from the summation in Eq. 2.3.

An important property of the Zernike functions is that they form an orthogonal basis set of functions that satisfy the relation [63]

$$\frac{1}{\pi R^2}\int_0^{2\pi} d\theta \int_0^R Z_i Z_j r dr = \delta_{ij} \tag{2.4}$$

Where δ_{ij} is the Kroneker symbol:

$$\delta_{ij} = \begin{cases} 1, & \text{i=j} \\ 0, & \text{i}\neq\text{j} \end{cases} \tag{2.5}$$

From Eqs. (2.3), (2.4) it can be shown that the rms value of phase across an aperture is simply the root sum square of the Zernike coefficients:

$$\sigma = \sqrt{(c_1^2 + c_2^2 + c_3^2 + \ldots + c_N^2)} \tag{2.6}$$

The Zernike coefficients for an arbitrary value of phase are obtained as:

$$A_i(t) = \frac{\int d\theta \int \Phi(r,\theta) W(r,\theta,t) Z_i(r,\theta) r dr}{\int d\theta \int \Phi(r,\theta) r dr} \tag{2.7}$$

Where $\Phi(r,\theta)$ is the aperture weighting function defined in this study as:

$$\Phi(r,\theta) = \begin{cases} 1, & \text{r}\leq\text{R} \\ 0, & \text{r}>\text{R} \end{cases} \tag{2.8}$$

2.4 Wavefront Sensing

The wavefront information that is derived from measured data, will be used by the control system for phase correction. The actual reconstruction of the phase from this data is discussed in subsequent sections. Two basic types of wavefront information are used. When the wavefront is expressed in terms of Optical Path Differences (OPD) over a small spatial area, or zone, the wavefront is said to be *zonal.* When the wavefront is expressed in terms of coefficients of the modes of a polynomial expansion (such as Zernike Polynomials) over the entire pupil, it is said to be *modal.*

The wavefront sensors (WFS) in adaptive optics do not measure directly the wavefront but its first and/or second spatial derivatives. Hartmann-Shack sensors are the most commonly used for the measurement of the first spatial derivative (or tilt), and curvature sensors are used to measure the second spatial derivative which is the curvature of the wavefront.

2.4.1 Hartmann-Shack Wavefront Sensor

The principle of Hartmann-Shack WFS is presented in Figure 2.3. A lenslet array is placed in a conjugate pupil plane in order to sample the incoming wavefront. If the wavefront is plane, each lenslet forms an image of the source at its focus Figure 2.3a. If the wavefront is distorted, each lenslet receives a tilted wavefront in the first approximation and forms an image out of axis in its focal plane Figure 2.3b. The measure of the image position gives directly the angle of arrival of the wave at each lenslet.

Usually, the Shack-Hartmann WFS requires the use of a reference plane wave generated from a reference source in the instrument, in order to calibrate precisely the focus positions of the lenslet array. A good feature of this sensor is the simultaneous determination of the x and y slopes by the measurement of the image position (x and y coordinates)

A number of methods can be used to measure the Hartmann-Shack images formed by the lenslet array. The simplest technique is to use a quad-cell detector for each subaperture [2],[72]. The main drawbacks of this technique are generally the limited dynamic range and spot size dependent response. Another solution is the use of a CCD as a detector to record simultaneously all the images. The good feature of a CCD is the perfectly determined pixel positions and the 100% fill factor. Even a CCD can be used as an array of quad-cells. But it allows in principle to calculate the centroid of the spot at the price of a large number of pixels per subaperture. [2]

2.4.2 Curvature Sensor

This type of sensor was developed by Roddier [67] to measure curvature instead of wavefront slope measurement as in Hartmann-Shack WFS described previously. The

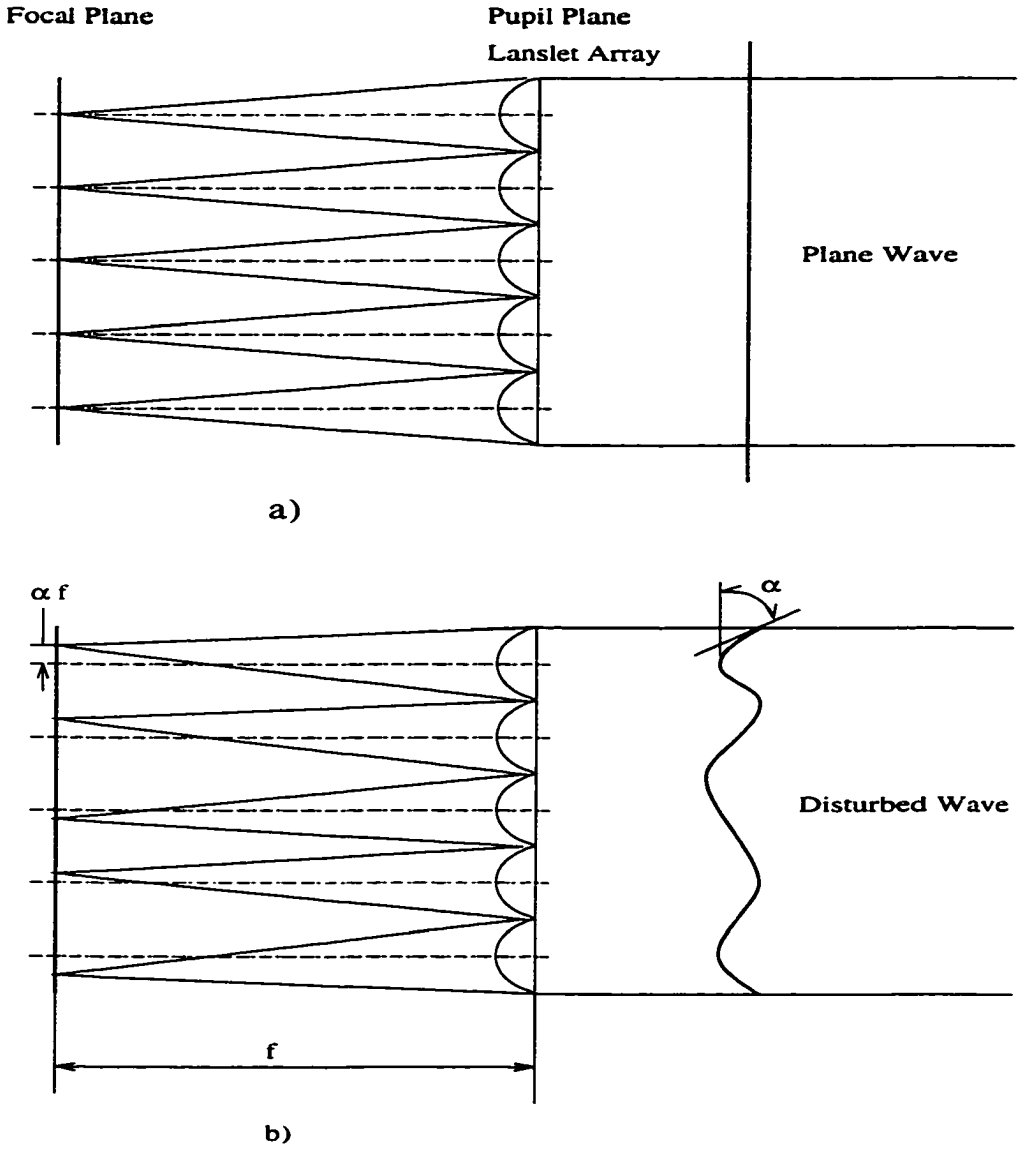

Figure 2.3: Principle of Hartmann-Shack Wavefront Sensor: a) Plane Wave b) Disturbed Wave

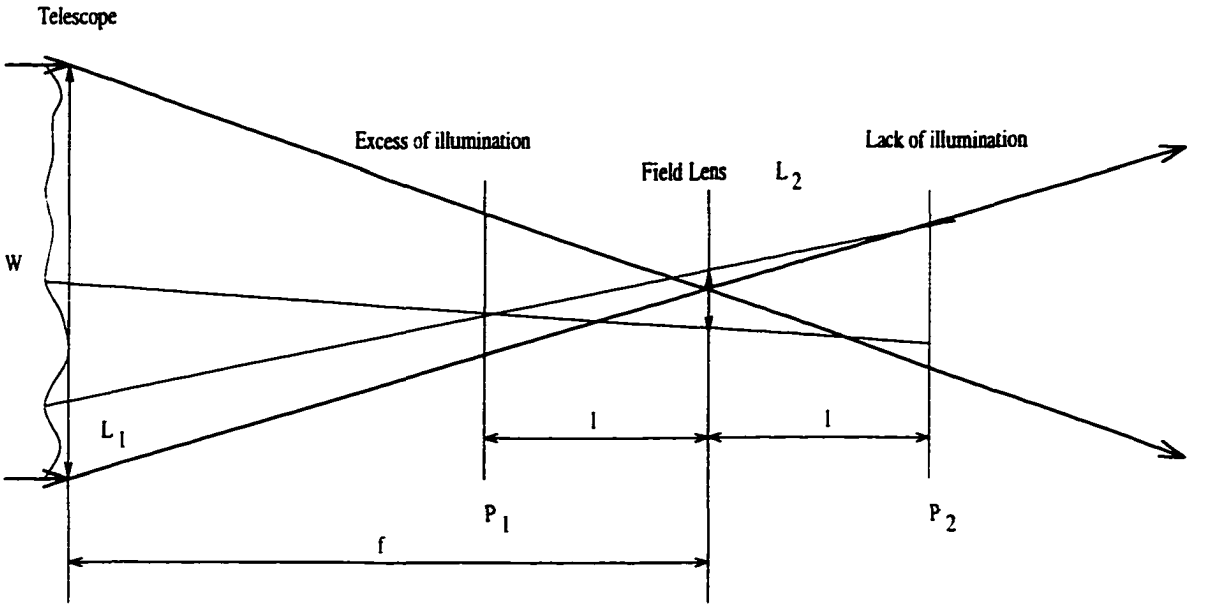

Figure 2.4: Principle of the Curvature Sensor

Laplacian of the wavefront together with the wavefront tilts at the aperture edge are measured, providing data to solve Poisson's equation to reconstruct the wavefront. Contrary to what is claimed in the literature [2] this type of sensor cannot be used directly with a bimorph mirror to solve Poisson's equation. Rather, an intermediate stage is needed for correction [69].

The principle of this sensor is presented in Figure 2.4. The telescope of focal length f images the source in its focal plane. The curvature sensor consists of two image detectors placed out-of-focus. The first detector records the irradiance distribution in plane P_1 at a distance l before the focal plane. The second one records the irradiance distribution in plane P_2 at the same distance l behind the focus. A local wavefront curvature will produce an excess of illumination in one plane and a lack of illumination in the other (Figure 2.4). A field lens is used for symmetry in order to reimage the pupil. The planes P_1 and P_2 can be also seen as two defoculized pupil planes. It can

be shown that in the geometrical optics approximation, the difference between the two irradiance distributions is a measure of the local wavefront inside the beam and the radial first derivative at the edge of the beam [2, 67]. The geometrical optics is approximated by:

$$\lambda \frac{f-l}{r_0} \ll r_0 \frac{l}{f} \tag{2.9}$$

The measured signal S is the normalized difference between the illuminations $I_1(\boldsymbol{r})$ and $I_2(\boldsymbol{r})$ in the planes P_1 and P_2 and is given by [67]

$$S(\boldsymbol{r}) = \frac{I_1(\boldsymbol{r}) - I_2(-\boldsymbol{r})}{I_1(\boldsymbol{r}) + I_2(-\boldsymbol{r})} = \frac{f(f-l)}{2l}[\nabla^2 W(\frac{f\boldsymbol{r}}{l}) + \frac{\partial}{\partial \boldsymbol{n}} W(\frac{f\boldsymbol{r}}{l})\delta_c] \tag{2.10}$$

Where $\boldsymbol{r}$ is a position vector, $W = W(\boldsymbol{r})$ is the measured wavefront surface, $\nabla^2 W$ is the Laplacian of the wavefront, $\frac{\partial W}{\partial \boldsymbol{n}}$ is the wavefront slope at the edge of the aperture, and δ_c is a linear impulse distribution around the pupil edge.

For high order aberration measurements, the distance l must be larger than for the case of low order aberrations measurements. For extended sources, the distance l must also be larger than the case of point sources. An increase of the distance l means a decrease in the sensitivity (and an increase of the dynamic) of the curvature sensor as expressed by Eq. 2.10. The distance l of the curvature sensor is very similar to the lenslet focal length of the Hartmann-Shack sensor. Note that when the distance l is decreased to the minimum, the curvature sensor is only able to measure tilts and is reduced to quad-cell. In the limiting case the curvature sensor provides four edge measurements and no more curvature.

The setup used at the University of Hawaii [37] employs a variable curvature mirror placed at the focus of the telescope as a field lens. It allows to reimage on the detector array the inside and outside focus blurred pupil images by its concave and convex deformation. This produces a modulation of the illumination on the detector

array. The curvature signals are recovered by synchronous detection. The pixels inside the beam give the local curvatures, the pixels on the edge of the beam give the local wavefront slopes. The modulation frequency is the temporal sampling frequency of the wavefront, the deformation amplitude directly determines the working distance l. A good feature of this device is its capability to modify easily the sensitivity of the sensor by changing the amplitude of the mirror vibrations (i.e. l). Because of the low number of subapertures in the sensor, photo-counting avalanche photodiodes are used as detectors, taking advantage of their quantum efficiency. For curvature sensing, only two detectors are required per subaperture [2].

2.5 Wavefront Correction

As with sensing, there are both modal and zonal means of correction as well. The need to engineer better systems, with higher spatial resolution, more stroke capability, and higher operational bandwidth, has been a catalyst in developing actuators, faceplate materials, and analytical techniques that apply to many other areas of engineering.

Mirrors that have an actively controlled reflective surface are the most common devices used for wavefront correction.

2.5.1 Modal Tilt Correction

The simplest form of wavefront correction is variation of the beam direction, or the tilt of the wavefront. The amount of energy needed to control the tilt mode in an optical system is directly related to the stroke and bandwidth requirements for the steering mirror [72]

2.5.2 Modal Higher-order Correction

The next most common form of correction is an active focus system. While peering through a telescope, an image is brought into focus by one's knowledge that a "fuzzy" image is out of focus while a "sharp" image is not. By cycling through the position of the sharpest focus, the system can be made to adapt to variations in the receiver's lens system, the observer's eye (or a camera).

It can be shown that astigmatism can be corrected by moving a single lens or mirror. If a cylindrical mirror or lens is aligned with the beam and moved along the optic axis, astigmatism is changed. By having two mirrors or lenses with their cylinder axes oriented 45° to each other, astigmatism for all orientations can be corrected [72].

2.5.3 Multichannel Correction

When it is necessary to correct for modes higher than astigmatism, the wavefront can be divided spatially. Each part of the beam is corrected by applying the required strength of correction to that part. Devices that work in this manner are called *multichannel correctors.*

Segmented mirrors

As reported in [72], the earliest implementation of a multichannel corrector was the segmented mirror. This is a mirror made up of a number of closely spaced small mirrors with piston or tilt correction capabilities. See Figure 2.5. In this way the higher-order modes of correction can be applied by determining the individual contribution of each of the segments. Some segmented mirrors of this type have been operated in a *piston-only* mode, whereby each segment is confined to simple up-and-down motion. The *piston/tip/tilt* has been shown also. Each segment operates with

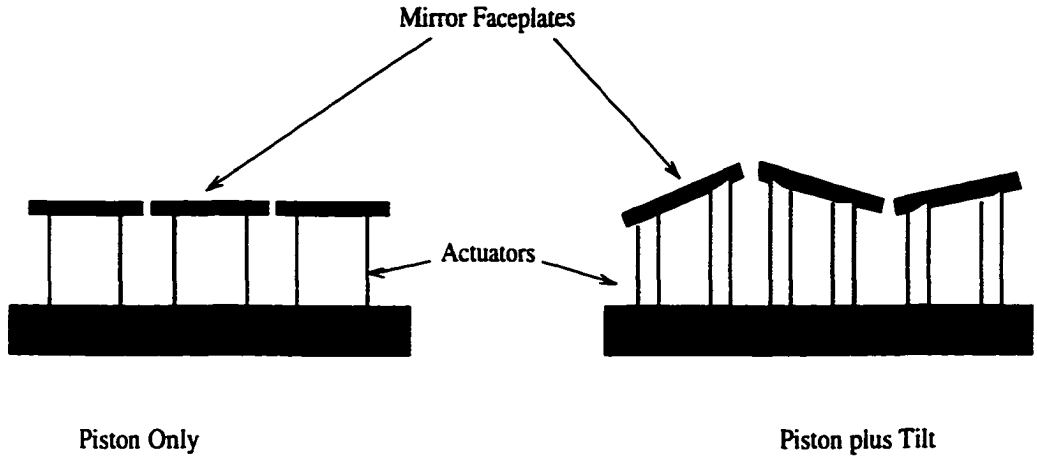

Figure 2.5: Segmented multichannel mirror

three degrees of freedom: the up/down piston mode and two orthogonal axes of tilt. A further consideration is the shape of the segments. Square, hexagonal, and circular segments have been used.

The discontinuities (gaps) between segments have an impact on overall performance. Energy is lost through the gaps. It is important that the area of the gaps is below 2% [72]. Because each segment operates independently, there is no cross-coupling or need for actuator preloading. The step response for a segment can be as low as $100\mu s$

Continuous Faceplate Mirrors

The continuous faceplate mirrors as opposed to segmented mirrors, automatically maintain continuity and therefore can work with a reduced number of actuators. Actuators are generally of the push-pull type using mostly piezoelectric or electrostrictive materials. The actuators can be discrete actuators perpendicular to the surface as in Figure 2.6 or discrete actuators on the edges that impart bending moments. They can also be continuous such as in membrane mirror or bimorph mirror. See Figures

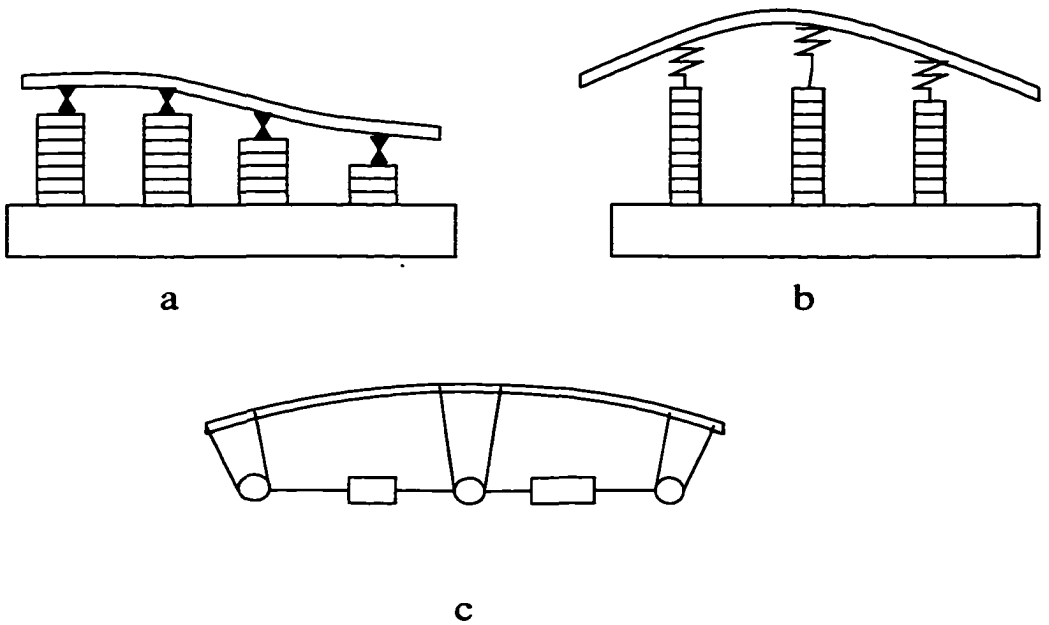

Figure 2.6: Discrete Actuators mirrors: a) discrete position actuators; b) discrete force actuator; c) bending moment actuators

2.7, and 2.8

Discrete Actuators Deformable Mirrors

SADM (*Stacked Actuator Deformable Mirror*) correctors, with discrete sets of actuators in the form of a stack of piezoceramic disks supported on a rigid base were first developed in the late 1970's [30] to address the large stroke requirements of infrared systems. A mirror deformation of 0.8μm was obtained, but the total voltage required for each stack is more than 1 kV. In the beginning of 1980's the range of displacement is increased to $\pm$ 8μm. The high supply of voltage required for control, the large hysteresis and the limitation on the number of actuators made this type of mirrors not an ideal one. Miniaturization of actuators, low operating voltages, position accuracy, and low hysteresis become then important parameters to consider. A review made by Ealey [29] and Raybova and Zakharenkov [66] discussed other developments of

deformable mirrors.

Membrane Mirrors

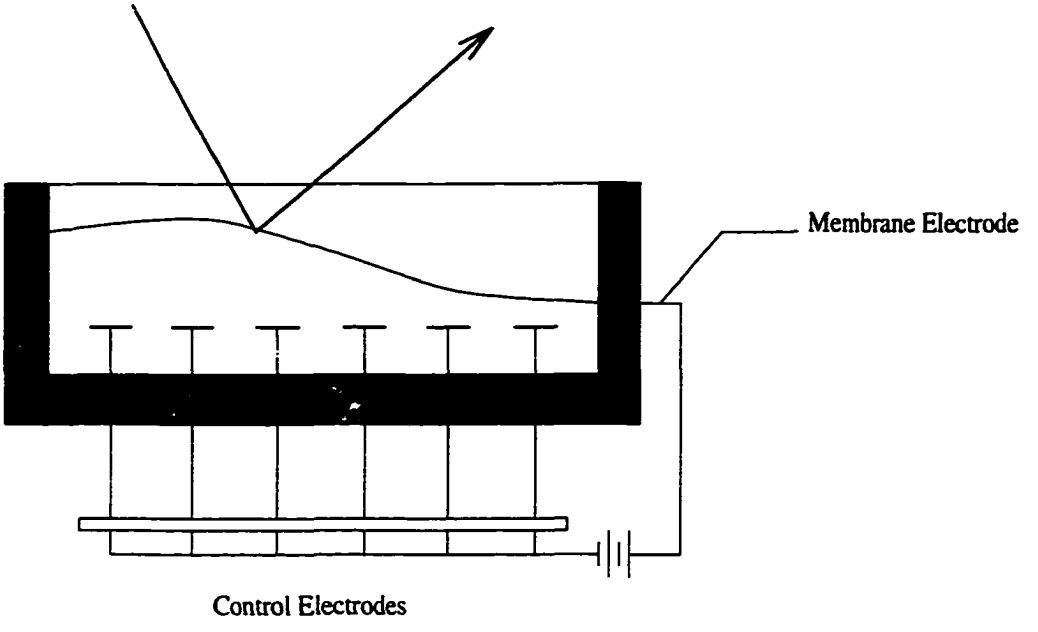

Figure 2.7: A membrane mirror

New types of deformable mirror designs have also been developed in recent years, such as the *membrane mirror* [40]. From Figure 2.7, a reflective surface is positioned between a transparent electrode and a series of electrodes at the back of the mirror. The deformation is caused by electrostatic forces. The membrane is suspended in a partially evacuated environment to reduce damping. For large-stroke designs, damping has been found to be needed since the surface tends to be unstable and pin the membrane against the electrodes. Additionally a membrane mirror requires the use of a window which complicates applications in the infrared.

Bimorph Mirrors

A bimorph mirror is made of two thin plates of piezoelectric materials bonded together. The two plates are oppositely poled. When a voltage is applied, the piezoelectric effects leads to an opposite variation of the transverse length of the two plates, and this results in bending of the mirror. See Figure 2.8. The use of curvature adaptive optics is strongly advocated for correction of the lower order aberrations on the basis of its economy, of its simplicity of control, and because its influence function which is global across the entire mirror has a spatial behavior similar to that of the Kolmogorov-based atmospheric wavefront structure [17]

2.6 Wavefront Reconstruction

Wavefront sensors, described earlier measure the condition of the wavefront and produce signals that represent the wavefront. Both zonal and modal sensors may be used in a particular system. It is up to the reconstructor to sort out the meaning of those signals, and then it is the control system that must determine how to treat the signals and relay them to the appropriate correction device.

2.6.1 Phase from wavefront slopes

Retrieving the phase from slope measurements is the determination of the phase at various points from the knowledge of the wavefront slopes at other points of the wavefront plane. This is a fundamental problem of adaptive optics. The most common wavefront sensors (Hartmann-Shack sensors or shearing interferometers) produce output signals proportional to the wavefront slopes.

The number of unknown phase points is N and the number of wavefront slope measurements is M. The problem of phase determination from wavefront slopes

depends upon the geometry of the problem. The phase estimation at N locations is ϕ_n. The measured slopes at M locations are s_m. The matrix connecting the two is determined by the geometry of the problem. For instance, for the geometry given by Figure 2.9a, the measured slopes from the wavefront sensor are represented by s_m^x or s_m^y. The superscripts represent the slope in the x or y direction. The phase is to be determined at the points $\phi_{-1,-1}$, $\phi_{-1,0}$, ..., where the subscripts represent the coordinates of the unknown points. A set of equations can then be constructed

$$\begin{aligned} s_1^x &= \phi_{-1,-1} - \phi_{0,-1} \\ s_2^y &= \phi_{0,-1} - \phi_{0,0} \\ \vdots &\quad \vdots \end{aligned}$$

that can be written in a matrix form as

$$\boldsymbol{s} = \boldsymbol{B}\phi \tag{2.11}$$

Where the matrix $\boldsymbol{B}$ is the *reconstruction matrix.* Often, $\boldsymbol{B}$ is simply composed of sums and differences based on the geometrical configuration of wavefront sensor positions and phase determination positions. Many of the elements are +1 or -1. In some cases, however, $\boldsymbol{B}$ can be quite complex. In wavefront sensors, the slope measurements is seldom a simple difference between two different points, but usually it is a spatial average over the subaperture. In adaptive optics control system problems, one often encounters the case where the number of equations M is greater than the number of unknowns N. This *overdetermined system* is the basis for much research in numerical techniques, many of which apply to adaptive optics systems.

The problem reduces to calculating the values of the unknowns such that the error between the measured, or known parameters s_i and the actual values of s is small. An inverse for a non-square matrix cannot be calculated directly. An approximation

can be determined based on a specific merit function. Solving for the phase φ, the *least squares solution* of Eq. (2.11) is given by

$$\phi = [\boldsymbol{B}^T\boldsymbol{B}]^{-1}\boldsymbol{B}^T\boldsymbol{s} \tag{2.12}$$

where $\boldsymbol{B}^T$ is the transpose of the matrix $\boldsymbol{B}$. The matrix $[\boldsymbol{B}^T\boldsymbol{B}]^{-1}\boldsymbol{B}^T$ is called the *pseudoinverse* of $\boldsymbol{B}$ for which, the norm $\|\boldsymbol{s} - \boldsymbol{B}\boldsymbol{\phi}\|$ is minimum. Although, this method apears starightforward, a number of difficulties can arise. The inversion of matrix $[\boldsymbol{B}^T\boldsymbol{B}]$ is impossible if it is singular or if, numerically, it is close to singular. To get around this problem, the *method of singular value decomposition* (SVD) can be used to invert $[\boldsymbol{B}^T\boldsymbol{B}]$ and reconstruct the phase from the measured slopes. If noise measurement is considered, and correlated with a covariance matrix $\boldsymbol{C}_n$, the phase is then given by

$$\phi = [\boldsymbol{B}^T\boldsymbol{C}_n^{-1}\boldsymbol{B}]^{-1}\boldsymbol{B}^T\boldsymbol{C}_n^{-1}\boldsymbol{s} \tag{2.13}$$

To go into a detailed description of numerical methods used to overcome the singularity problems is beyond the scope of this thesis, however, a good overview and analysis regarding these points can be found in [72]

Several wavefront reconstruction algorithms have been published [34, 28, 49, 71]. Fried [34] and Southwell [71] (see Figure 2.9) discussed zonal wavefront reconstruction methods for different configurations of Hartmann-Shack wavefront sensor subapertures with respect to actuators of wavefront corrector.

2.6.2 Modes from wavefront slopes

Another common method, that constitutes the basis of this study, is the phase representation in terms of its modal coefficients. The problem of phase modes from

wavefront slopes is similar to reconstruction of phase values at various points discussed in the previous section. The wavefront phase W is described by a polynomial expansion as in Eq. (2.3), rewriting the same expansion without the piston mode one obtains,

$$W(x,y,t) = \sum_{k=1}^{N} A_k(t) Z_k(x,y) \tag{2.14}$$

A Hartmann-Shack wavefront sensor measures the slopes of the wavefront at various points m. There are M total measurements. It is assumed that the wavefront sensor measures the x-directional derivative p of the phase, and/or the y-directional derivative q of the phase at a particular location in a subaperture. That is

$$p_i(x,y,t) = \left.\frac{\partial W(x,y,t)}{\partial x}\right|_i$$

$$q_i(x,y,t) = \left.\frac{\partial W(x,y,t)}{\partial y}\right|_i \tag{2.15}$$

where the index i implies evaluation at the coordinates (x_i,y_i). From Eqs.(2.14) and (2.15) we can express

$$p_i = \sum_{k=1}^{N} A_k(t) \left.\frac{\partial Z_k(x,y)}{\partial x}\right|_i$$

$$q_i = \sum_{k=1}^{N} A_k(t) \left.\frac{\partial Z_k(x,y)}{\partial y}\right|_i \tag{2.16}$$

In a matrix form this set can be represented by the matrix equation

$$\boldsymbol{s} = \boldsymbol{B}\boldsymbol{A} \tag{2.17}$$

where the $\boldsymbol{s}$ is the slope vector and $\boldsymbol{A}$ is the mode coefficient vector

$$\boldsymbol{s} = \begin{bmatrix} p_1 \\ p_2 \\ \vdots \\ p_M \\ q_1 \\ q_2 \\ \vdots \\ q_M \end{bmatrix}; \quad \boldsymbol{A} = \begin{bmatrix} A_1 \\ A_2 \\ \vdots \\ A_N \end{bmatrix} \tag{2.18}$$

while the reconstruction matrix $\boldsymbol{B}$ is

$$\boldsymbol{B} = \begin{bmatrix} Z^1_{1,x} & Z^1_{2,x} & \dots & Z^1_{N,x} \\ Z^2_{1,x} & Z^2_{2,x} & \dots & Z^2_{N,x} \\ \vdots & \vdots & \dots & \vdots \\ Z^M_{1,x} & Z^M_{2,x} & \dots & Z^M_{N,x} \\ Z^1_{1,y} & Z^1_{2,y} & \dots & Z^1_{N,y} \\ Z^2_{1,y} & Z^2_{2,y} & \dots & Z^2_{N,y} \\ \vdots & \vdots & \dots & \vdots \\ Z^M_{1,y} & Z^M_{2,y} & \dots & Z^M_{N,y} \end{bmatrix} \tag{2.19}$$

for which an element $Z^m_{i,x}$ is given by

$$Z^m_{i,x} = \left.\frac{\partial Z_i(x,y)}{\partial x}\right|_m \tag{2.20}$$

As it can be seen in this case, the matrix $\boldsymbol{B}$ is not simply sums and differences based on the geometrical configuration of the wavefront sensor positions and phase determination positions. The elements are the derivatives of the polynomial basis functions evaluated at the wavefront subaperture positions. Since this system is overdetermined, the solution is found by finding the pseudoinverse of $\boldsymbol{B}$,

$$\boldsymbol{A} = [\boldsymbol{B}^T\boldsymbol{B}]^{-1}\boldsymbol{B}^T\boldsymbol{s} \tag{2.21}$$

If the basis functions (modes) are Zernike polynomials, the derivatives can be found explicitly and a straightforward approach can be used to compute the pseudoinverse matrix.

If the noise covariance matrix of the measurements is C_n, the pseudoinverse least-squares solution is

$$\boldsymbol{A} = \left[(\boldsymbol{B}^T \boldsymbol{C}_n^{-1} \boldsymbol{B})^{-1} \boldsymbol{B}^T \boldsymbol{C}_n^{-1}\right] \boldsymbol{s} \tag{2.22}$$

The accuracy of the modal estimation is determined by noise and the amount of overdetermination of the system. Southwell [71] defines *undermodeling* as a system of reconstruction equations where there are fewer modes required than can be actually projected out of the data. A more serious problem occurs when undersampling occurs. When the sampling density of the wavefront slopes is insufficient for the modes required, higher order modes will appear as perturbations on the lower order modes. Elimination of this from a wavefront aliasing requires careful examination of the number and form of the polynomials for the modes in terms of the number and placement of available wavefront slope measurements. In general if there are more modes desired, there should be more samples acquired. They should be in a geometry sufficient for coding the wavefront information [72].

2.6.3 Modes from Curvature Measurements

Another method of reconstructing the modes of a wavefront is using information obtained by a curvature sensor instead of a slope sensor, as suggested by Xin and Xueye [76]. As explained earlier, the signals obtained from a curvature sensor are local curvature in the inner region of the aperture and normal slope at the aperture edges.

Using Eq. (2.10), and considering polynomial expansion in Zernike modes of Eq. (2.3) the measured signal from the curvature sensor can be expressed as:

$$S(\boldsymbol{r},t) = C_0 \sum_{i=2}^{N} A_i(t) \left[\nabla^2 Z_i(C_1\boldsymbol{r}) + \frac{\partial}{\partial \boldsymbol{n}} Z_i(C_1\boldsymbol{r})\delta_c \right] \tag{2.23}$$

where

$$C_0 = \frac{f(f-l)}{2l}; \qquad C_1 = \frac{f}{l}$$

A measurement signal S_j given by a detector j can be written in the form

$$S_j(\boldsymbol{r},t) = C_0 \sum_{i=2}^{N} A_i(t) b_{ij} \tag{2.24}$$

where

$$b_{ij} = \left[\nabla^2 Z_i(C_1\boldsymbol{r}) + \frac{\partial}{\partial \boldsymbol{n}} Z_i(C_1\boldsymbol{r})\delta_c \right] \tag{2.25}$$

from which we can write

$$\begin{cases} s_0 = S_0/C_0 = A_2 b_{20} + A_3 b_{30} + \ldots + A_N b_{N0} \\ s_1 = S_1/C_0 = A_2 b_{21} + A_3 b_{31} + \ldots + A_N b_{N1} \\ \vdots = \vdots = \vdots \\ s_M = S_M/C_0 = A_2 b_{2M} + A_3 b_{3M} + \ldots + A_N b_{NM} \end{cases} \tag{2.26}$$

or in a matrix form

$$\boldsymbol{s} = \boldsymbol{B}\boldsymbol{A} \tag{2.27}$$

Where

$$\boldsymbol{s} = \begin{bmatrix} s_1 \\ s_2 \\ \vdots \\ s_M \end{bmatrix}; \quad \boldsymbol{B} = \begin{bmatrix} b_{20} & b_{30} & \ldots & b_{N0} \\ b_{21} & b_{31} & \ldots & b_{N1} \\ \vdots & \vdots & \ldots & \vdots \\ b_{2M} & b_{3M} & \ldots & b_{NM} \end{bmatrix}; \quad \boldsymbol{A} = \begin{bmatrix} A_1 \\ A_2 \\ \vdots \\ A_N \end{bmatrix} \tag{2.28}$$

Since the matrix $\boldsymbol{B}$ is rectangular, the Zernike polynomials coefficients vector $\boldsymbol{A}$ can be determined using least squares method resulting in

$$\boldsymbol{A} = [\boldsymbol{B}^T \boldsymbol{B}]^{-1} \boldsymbol{B}^T \tag{2.29}$$

and for a correlated noise with a correlation matrix $\boldsymbol{C}_n$ the solution is obtained in a weighted least square sens with a weighting matrix $\boldsymbol{C}_n$ as

$$\boldsymbol{A} = \left[(\boldsymbol{B}^T \boldsymbol{C}_n^{-1} \boldsymbol{B})^{-1} \boldsymbol{B}^T \boldsymbol{C}_n^{-1} \right] \boldsymbol{s} \tag{2.30}$$

With this method, the difficulty in detecting the normal slopes at pupil edges is overcome and the compensation of high order aberrations could be realized with high accuracy.

2.6.4 Modes from wavefront phase

Finally, for control purposes (modal control), it is necessary to extract the modes of a wavefront to be processed by the control system. If OPD (Optical Path Difference) information is provided, in this case, the modes are extracted from the phase information given by the OPD data. For Zernike polynomials, the modal coefficients can be computed using Eq. (2.7).

2.7 Control System

In this section, conventional control methods used in adaptive optics are presented, where only continuous faceplate mirrors with discrete actuator or segmented mirrors are considered. Control of bimorph mirrors will be presented subsequently.

2.7.1 Zonal control from continuous phase

Once a phase map or a modal representation is constructed, it is necessary to determine the application of that information for driving a wavefront corrector which is a deformable mirror in most of the cases.

A deformable mirror is assumed to be a linear system of electro-mechanical actuators that deform a mirror surface into a desired shape. The details of the shape are not important in the general case; however the precise influence of each actuator of discrete actuators mirror is a very important consideration in the wavefront control scheme. A desired surface $\varphi(x,y)$ is generated by applying the proper amplitude a_i to n actuators. The effect of each actuator on the surface $W_i(x,y)$ is its influence function. A set of linear equations can be constructed

$$\varphi(x,y) = \sum_{i=1}^{n} a_i W_i(x,y) \tag{2.31}$$

which can be written in a matrix form,

$$\boldsymbol{\varphi} = \boldsymbol{W}\boldsymbol{a} \tag{2.32}$$

For a surface represented by k points, the influence matrix $\boldsymbol{W}$ has k rows and n columns. A pseudoinverse of $\boldsymbol{W}$ is required. The actuator commands are then derived from the actuator amplitude a_i by multiplying a suitbale gain factors and voltage conversions, and by accounting for the factor of $2\cos\beta$ multiplier between the wavefront and the mirror surface with an incidence angle of β.

Constructiong the influence matrix $\boldsymbol{W}$ is not trivial. The effect of each actuator on a point (x,y) in the wavefront plane must be determined. Although the influences often couple, they are assumed to be linear. The influences are often unsymmetric, and are especially so when the edge of the mirror is caged. The geometric effect of

clamping neighboring actuators has a complicated effect on the influence of each actuator. These considerations, and their temporal characteristics, must be considered before constructing the influence matrix and inverting it [72].

2.7.2 Modal control from continuous phase

In this case, the wavefront φ to be constructed by the modal control system, is a sum of modes with basis functions $Z_i(x, y)$ and coefficients A_i,

$$\varphi = \sum_{i=1}^{N} A_i Z_i \tag{2.33}$$

The modes of the wavferont for the controller can be determined by inverting the linear set to solve for A_i

$$\boldsymbol{A} = \boldsymbol{Z}^{\dagger}\boldsymbol{\varphi} \tag{2.34}$$

where $\boldsymbol{Z}^{\dagger} = [\boldsymbol{Z}^T\boldsymbol{Z}]^{-1}\boldsymbol{Z}^T$ is the minimum norm pseudoinverse of the matrix $\boldsymbol{Z}$. If the Z_i are orthogonal, the matrix is diagonal and the inversion is simple. If the modal correctors do not form an orthogonal set, the inverson is more complicated but achievable.

2.7.3 Zonal control from modal phase

If the phase is constructed and the corrector devices respond to commands in a zonal sense, another set of linear equations must be formed. Two similar reconstruction problems are combined. The zonal corrector commands are derived by inverting the linear sum of influence functions

$$\varphi(x, y) = \sum_{i=1}^{n} a_i W_i(x, y)$$

If the wavefront Φ is represented by a sum of modes with basis functions $Z_i(x, y)$ and coefficients A_i

$$\boldsymbol{\Phi} = \sum_{i=1}^{N} A_i Z_i$$

and the two summations can be equated

$$\varphi = \Phi = \sum_{i=1}^{n} a_i W_i(x, y) = \sum_{i=1}^{N} A_i Z_i$$

Using matrix notation

$$\boldsymbol{ZA} = \boldsymbol{Wa} \tag{2.35}$$

which gives

$$\boldsymbol{A} = \boldsymbol{Z}^{\dagger}\boldsymbol{Wa} \tag{2.36}$$

2.7.4 Zonal control from wavefront slopes

The most common and perhaps the most interesting problem in adaptive optics controls is the indirect method applied when the input is a number of wavefront slopes measured with a wavefront sensor and the output of the control are signals to various actuators that apply a correction to the wavefront. Unfortunately, there is hardly ever one-to-one correspondence between the slope measurements and the actuator drive signals. If there were, the signals would be corrupted by noise. Fortunately the problem is linear and can be treated as in previous sections.

Recalling Eq. (2.11), knowing that the slope vector $\boldsymbol{s}$ is given by (cf. Eq. (2.11))

$$\boldsymbol{s} = \boldsymbol{B\phi}$$

and the phase is corrected by a surface φ which is the sum of the actuator influence functions (cf. Eq. (2.31))

$$\boldsymbol{\phi} = \boldsymbol{\varphi} = \boldsymbol{Wa}$$

Combining the two equations eliminates the central step of explicit phase representation

$$\boldsymbol{s} = \boldsymbol{BWa} \tag{2.37}$$

and the actuator commands a_i are given by

$$\boldsymbol{a} = [\boldsymbol{BW}]^{\dagger}\boldsymbol{s} \tag{2.38}$$

Where,

$$[\boldsymbol{BW}]^{\dagger} = [(\boldsymbol{BW})^{T}(\boldsymbol{BW})]^{-1}[(\boldsymbol{BW})^{T}]$$

2.7.5 Modal control from wavefront curvature

In a similar way, an indirect method for correcting wavefront modes as applied to non-discrete actuator mirror, specifically to a bimorph mirror was suggested by Chellabi, Stepanenko and Dost [23].

Field equations governing the deformation of the bimorph mirror are reduced to Poisson's equation [55]. The displacement of the ith surface position z_i is linear in electrode voltages V_j and may therefore, be written in the form of

$$z_i = \sum_{i=1}^{N_e} P_{ij} V_j \tag{2.39}$$

where A_{ij} are coefficients derived from solutions of Poisson's equation, and N_e is the total number of electrodes. Displacement along the boundary is taken to be zero. The influence function at each position of the surface is obtained through the column vector A_{ij} by fixing j and varying i, in other words, the values of an influence function at surface positions labeled $i = 1, ..., N_p$, where N_p is the number of surface points. Each influence function is the surface displacement caused by a unit voltage applied

to a single electrode and is combined linearly with the other influence functions to give the total surface displacement z_i.

The problem in controlling the mirror configuration to a desired shape, is to find a set of voltages V_j that best fit the mirror surface z to a desired surface z' at a selected set of surface-matching points.

The control algorithm is based on least-squares optimization method proposed initially by Claflin and Bareket [25] and applied to configure a membrane electrostatic mirror.

The quantity to be minimized is

$$J = \sum_{i=1}^{N_p} (z_i - z_i')^2 \tag{2.40}$$

Eq. (2.39) may be written in matrix form

$$\boldsymbol{z} = \boldsymbol{PV} \tag{2.41}$$

where $\boldsymbol{P}$ is the influence function matrix with elements P_{ij}, and z_i and V_j are the components of the vectors $\boldsymbol{z}$ and $\boldsymbol{V}$ respectively. Solving Eq. (2.41) for V in the least squares sense of minimizing Eq.(2.40), one finds the solution

$$\boldsymbol{V} = (\boldsymbol{P}^T\boldsymbol{P})^{-1}\boldsymbol{P}^T\boldsymbol{z}' \tag{2.42}$$

The components P_{ij} of the influence matrix $\boldsymbol{P}$ are computed by solving Poisson's equation that governs the static behavior of a bimorph mirror as given by Kokorowski [55].

2.8 Concluding Remarks

In sections 2.7.1-2.7.4, dealing with the control system, only the required deflection vector is calculated without mentioning the driving voltages that produce such deflec-

tions. However, in most cases, for piezoelectric actuators, the relationship between the displacements and their driving voltages is assumed to be linear.

Other components of the adaptive optics system include the D/A converters, which imposes a fixed gain in each channel. The amplifier circuit is based on resistors, capacitors, and operational amplifiers. The piezoelectric actuator can be modelled depending on the type of the faceplate material, the number of actuators and the dimension of the active region [48].

From a mathematical standpoint, zonal and modal correction methods are very similar. For the zonal correction method, the wavefront to be corrected is decomposed in terms of localized zonal influence functions. This decomposition produces a set of phase slopes or tilts which correspond to the drive signal required to implement correction at the actuator location of the respective zone or node. The coefficients are selected to minimize the mean square error between the aberrated wavefront and the implemented correction. For modal correction, the wavefront is decomposed into various modes. As was previously described, Zernike Polynomials describe aberration modes for a circular aperture. As for the zonal case, a set of coefficients which correspond to actuator drive voltages is chosen to minimize the wavefront error. From a purely theoretical standpoint, the performance of both the zonal and the modal corrector is the same provided that enough zones or modes are used in the wavefront corrector. Zonal correction utilizes a localized influence function whose shape is tailored to the contour of the spatial content of the aberrated wavefront to effect an optimal local surface deformation. Modal correction utilizes a global influence function to effect a full aperture deformation which is tailored to match the modal surface contour with minimal error. In either case, the goal is to minimize the curve fitting error by matching the wavefront aberration with a best-fit conjugate (mirror image) mirror surface provided by the deformable mirror.

Note that all the control methods -except the last one- presented in this chapter are the ones used and found in the literature. None of these methods use the dynamic model of the mirror in their design, relying only on the static behavior of the mirror. Except for few designs, most control strategies ignore the time dimension in their design given the delay in measurement, temporal consideration which has a direct effect on the bandwidth of the system, is a very important parameter in the design of the controller.

2.9 Conclusion of Chapter 2

In this chapter, the principle of adaptive optics based on phase conjugation correction was described. The major steps in adaptive optics system are explained, starting with wavefront mathematical representation passing by wavefront sensing and finishing with wavefront correction and control. We have shown that the wavefront can be represented by a set of orthogonal polynomials (Zernike polynomials) which can be used later to design the control system. In wavefront sensing, two methods, namely, slope sensing and curvature sensing were introduced. After sensing, the next main component of an adaptive optics is the corrector, this is mainly a deformable mirror. Different types of mirrors used in adaptive optics were presented. Segmented mirrors, continuous faceplate mirrors with discrete actuators and bimorph mirrors were among the correctors described. Wavefront reconstruction algorithms were presented and their mathematical description was explained. Control systems including modal and zonal approaches were presented.

Next chapter will deal with the development of the dynamic model of the structure (deformable mirror) based on the space-time assumed mode method. This model will be used later in the design of an optimal controller of a bimorph mirror. The model

of the discrete actuator mirror will be given in chapter 5 where the finite element model of the active structure is formulated.

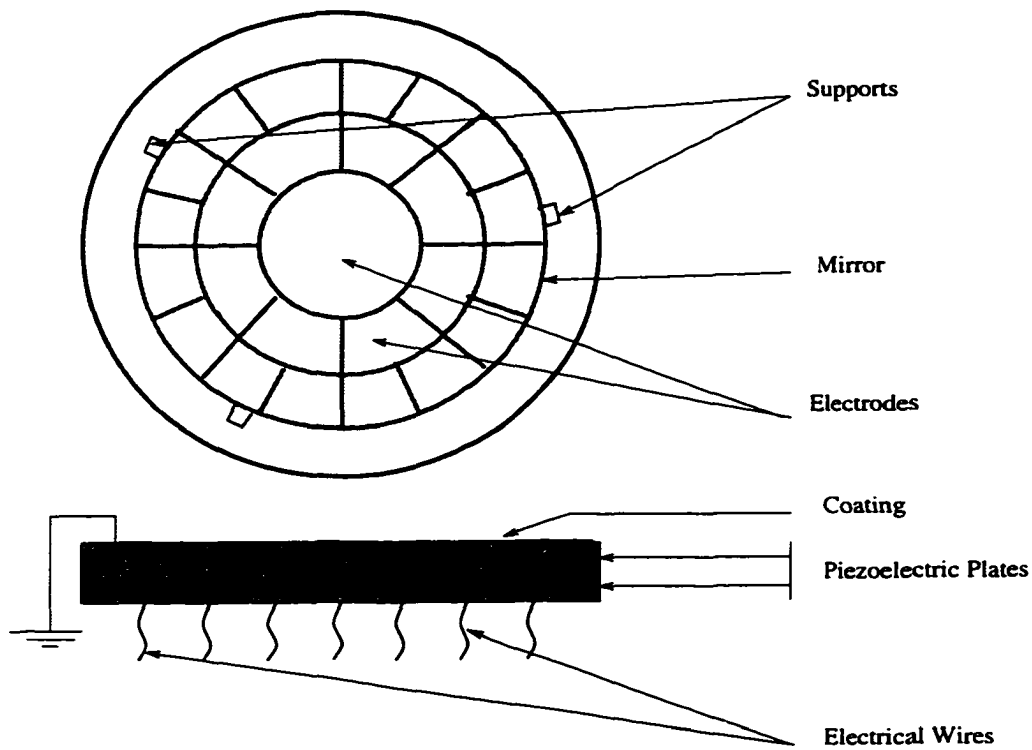

Figure 2.8: A bimorph mirror

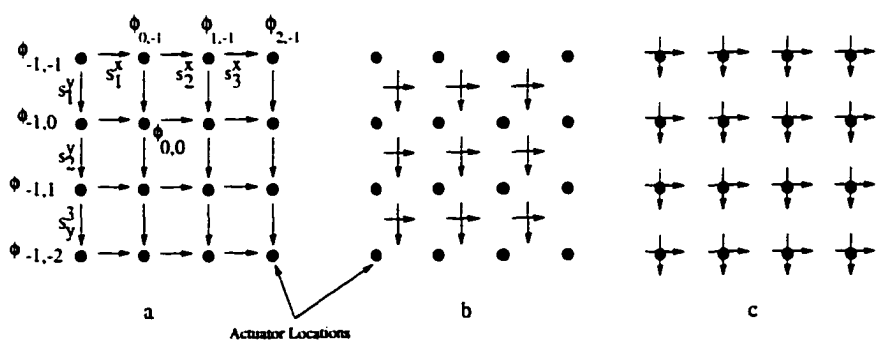

Figure 2.9: Configuration of zonal wavefront reconstruction a) Hudgin; b) Fried; c) Southwell

Chapter 3

System Dynamics: Assumed Modes

3.1 System Representation

The general system is represented in Figure (3.1). It is composed of an elastic body with inclusions of piezoelectric material which are poled and electroded arbitrarily. This configuration reflects the structure of a bimorph mirror, where a shim metal (elastic body) is inserted between two oppositely poled piezoelectric plates. The shim metal plays the role of a common electrode. The electrodes represents the continuous actuators, where a distributed electric charge is applied.

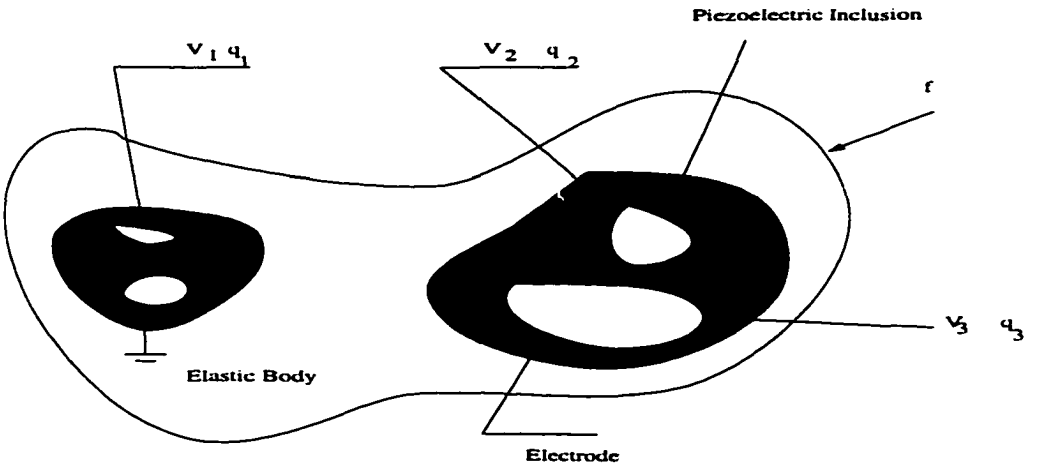

Figure 3.1: Electroelastic Continuum System

3.2 Electromechanical Constitutive Relation

Using the IEEE standard notation, the linear constitutive equations of a piezoelectric material written in a Cartesian coordinate system are given by:

$$\begin{aligned} \boldsymbol{T} &= \boldsymbol{C}\boldsymbol{S} - \boldsymbol{e}^T\boldsymbol{E} \\ \boldsymbol{D} &= \boldsymbol{e}\boldsymbol{S} + \epsilon\boldsymbol{E} \end{aligned} \tag{3.1}$$

where $\boldsymbol{T}(x,y)$ is the stress tensor, $\boldsymbol{C}$ is the elasticity matrix, $\boldsymbol{S}(x,y)$ is the inifinitesimal strain tensor, $\boldsymbol{e}$ is the piezoelectric matrix, $\boldsymbol{E}(x,y)$ is the electrical field in the material, $\boldsymbol{D}(x,y)$ is the electric displacement vector, and ϵ is the dielectric matrix, with

$$\boldsymbol{D} = \begin{bmatrix} D_1 \\ D_2 \\ D_3 \end{bmatrix}; \quad \boldsymbol{E} = \begin{bmatrix} E_1 \\ E_2 \\ E_3 \end{bmatrix}; \quad \boldsymbol{S} = \begin{bmatrix} S_{11} \\ S_{22} \\ S_{33} \\ 2S_{23} \\ 2S_{31} \\ 2S_{12} \end{bmatrix} = \begin{bmatrix} S_1 \\ S_2 \\ S_3 \\ S_4 \\ S_5 \\ S_6 \end{bmatrix}; \quad T = \begin{bmatrix} T_1 \\ T_2 \\ T_3 \\ T_4 \\ T_5 \\ T_6 \end{bmatrix} \tag{3.2}$$

$$\epsilon = \begin{bmatrix} \epsilon_1 & 0 & 0 \\ 0 & \epsilon_1 & 0 \\ 0 & 0 & \epsilon_3 \end{bmatrix} \tag{3.3}$$

The matrix $\boldsymbol{e}$ can be expressed in terms of the more commonly used piezoelectric $\boldsymbol{d}$ matrix

$$\boldsymbol{d} = \begin{bmatrix} 0 & 0 & 0 & 0 & d_{15} & 0 \\ 0 & 0 & 0 & d_{15} & 0 & 0 \\ d_{31} & d_{32} & 0 & 0 & 0 & d_{66} \end{bmatrix} \tag{3.4}$$

as:

$$\boldsymbol{e} = \boldsymbol{dC} \tag{3.5}$$

Equation (3.1) then becomes with $\boldsymbol{C} = \boldsymbol{C}^T$ ($\boldsymbol{C}$ is always symmetric)

$$\boldsymbol{T} = \boldsymbol{CS} - \boldsymbol{Cd}^T\boldsymbol{E} \tag{3.6}$$

A piezoelectric structure is an electro-mechanical system which involves both mechanical degree of freedom (dof) represented by a generalized displacement vector $\boldsymbol{u}$ as well as an electrical dof denoted by a generalized electrical potential $\boldsymbol{v}$.

In the traditional Rayleigh-Ritz approach to response of dynamic systems, the generalized displacements $\boldsymbol{u}$ and the generalized electrical potential $\boldsymbol{v}$ are treated as assumed or known vectors (or functions) of some spatial basis vectors (or functions) $\boldsymbol{U}(x, y, z)$ and $\boldsymbol{V}(x, y, z)$ multiplied by unknown coefficients $\boldsymbol{q}(t)$ and $\boldsymbol{\phi}(t)$.

Note that specifically, for a deformable mirror, the spatial basis functions $\boldsymbol{U}(x, y, z)$ represent the shape of the mirror surface. They also represent the spatial functions of Zernike polynomials such as given in Table (2.1). For other applications such as vibration control, these spatial basis functions represent the mode shapes of the

vibrating structure. The assumed modes representation can thus be written as

$$\boldsymbol{u} = [u \;\; v \;\; w]^T = \boldsymbol{U}(x,y,z)\boldsymbol{q}(t) \tag{3.7}$$

$$\boldsymbol{v} = \boldsymbol{V}(x,y,z)\boldsymbol{\phi}(t) \tag{3.8}$$

where

$$\boldsymbol{U} = \begin{bmatrix} \boldsymbol{U}_1 & \mathbf{0} & \mathbf{0} \\ \mathbf{0} & \boldsymbol{U}_2 & \mathbf{0} \\ \mathbf{0} & \mathbf{0} & \boldsymbol{U}_3 \end{bmatrix}; \qquad \boldsymbol{V} = \begin{bmatrix} \boldsymbol{V}_1 & \mathbf{0} & \mathbf{0} \\ \mathbf{0} & \boldsymbol{V}_2 & \mathbf{0} \\ \mathbf{0} & \mathbf{0} & \boldsymbol{V}_3 \end{bmatrix} \tag{3.9}$$

$$\boldsymbol{q} = \begin{bmatrix} \boldsymbol{q}_1^T & \boldsymbol{q}_2^T & \boldsymbol{q}_3^T \end{bmatrix}^T; \quad \boldsymbol{\phi} = \begin{bmatrix} \boldsymbol{\phi}_1^T & \boldsymbol{\phi}_2^T & \boldsymbol{\phi}_3^T \end{bmatrix}^T \tag{3.10}$$

$$\boldsymbol{U}_i = \begin{bmatrix} U_{i1} \\ \vdots \\ U_{ir} \end{bmatrix}^T; \; \boldsymbol{q}_i = \begin{bmatrix} q_{i1} \\ \vdots \\ q_{ir} \end{bmatrix}; \; \boldsymbol{V}_i = \begin{bmatrix} V_{i1} \\ \vdots \\ V_{iK} \end{bmatrix}^T; \; \boldsymbol{\phi}_i = \begin{bmatrix} \phi_{i1} \\ \vdots \\ \phi_{iK} \end{bmatrix}; \; i = 1,2,3 \tag{3.11}$$

$\boldsymbol{U}$ denotes the matrix of spatial mode shape functions of the mechanical displacement, with r modes, $\boldsymbol{V}$ is the matrix of spatial mode shape functions of the electrical potential with K modes, $\boldsymbol{q}$ is the generalized mechanical coordinate, and $\boldsymbol{\phi}$ is the electrical generalized coordinate.

We consider only the deflection in the z direction, which describes the bending of a thin plate, thus only the coordinate w is considered in this study. For the electrical dof we also consider the voltage applied only in one direction namely in the z direction (poling direction), thus only one electrical coordinate will be used throughout the following development. Generalization to all three coordinates can be readily accomplished by augmenting the appropriate matrices and vectors by the additional dofs. Therefore, we use

$$\boldsymbol{U} = \boldsymbol{U}_3; \quad \boldsymbol{V} = \boldsymbol{V}_3; \quad \boldsymbol{q} = \boldsymbol{q}_3; \quad \boldsymbol{\phi} = \boldsymbol{\phi}_3 \tag{3.12}$$

3.3 Variables Definitions

3.3.1 Generalized Mechanical Coordinates

For distributed parameter systems, the basis functions (mode shapes) are affiliated with the spatial information. The coefficients of these functions are the unknown parameters to solve for in a dynamic system. Solution of the problems requires obtaining these unknown time-dependent coefficients either explicitly or numerically from the differential equations. As with any other function, however, an unknown function $q_j(t)$ can also be represented over any time (t_i, t_f) by a set of basis functions in time.

Denoting the set of m basis functions over (t_i, t_f) of $q_j(t)$ by $A_k(t)$ one can write the expansion in time as

$$q_j(t) = \sum_{k=0}^{m} \alpha_{jk} A_k(t), \quad (j = 1, 2, \ldots, r) \tag{3.13}$$

where $A_k(t)$ are independent continuous functions in time with continuous derivatives over (t_i, t_f) and α_{jk} are the unknown constant coefficients of expansion in that interval. Analogous to the spatial basis functions as assumed-modes of expansion, the functions $A_k(t)$ constitute the assumed-time modes of the unknown generalized coordinates $q_j(t)$ with m time-modes.

Many choices exist for m and associated $A_k(t)$ combinations and a selection may be made depending on convenience, computational efficiency and desired accuracy, to mention a few factors. In this work, we shall employ the same time-basis functions as those used by previous researchers such as Adiguzel and Bailey in [1, 8]. Specifically, the functions $A_k(t)$ are in the form

$$A_k = (t - t_i)^k \qquad (k = 1, 2, \ldots, m), \qquad t_i < t < t_f \tag{3.14}$$

which constitute the simplest basis functions, leading to a simple power series expansion of $q_j(t)$ in time. However, the derivation that follows does not depend on the specific form of the basis functions.

Introducing (3.14) into (3.13) results in

$$q_j(t) = \alpha_{j_0} + \alpha_{j_1}(t - t_i) + \sum_{k=2}^{m} \alpha_{jk}(t - t_i)^k \tag{3.15}$$

From which we recognise

$$\alpha_{j_0} = q_j(t_i), \qquad \alpha_{j_1} = \left.\frac{dq_j}{dt}\right|_{t=t_i}, \qquad \alpha_{j_k} = (k!)^{-1}\left.\frac{d^k q_j}{dt^k}\right|_{t=t_i} \tag{3.16}$$

It is convenient to introduce the non-dimensional time τ defined as

$$\tau = \frac{t - t_i}{\theta}, \text{where} \quad \theta = t_f - t_i; \quad t_i \le t \le t_f, \quad \text{then } dt = \theta d\tau \tag{3.17}$$

Thus the expansion in (3.13) becomes

$$q_j(\tau) = a_{j_0} + a_{j_1}\tau + \sum_{k=2}^{m} a_{jk}\tau^k \tag{3.18}$$

where now,

$$a_{j_1} = \left.\frac{dq_j}{d\tau}\right|_{\tau=0}, \qquad a_{j_k} = \left.\frac{d^k q_j}{d\tau^k}\right|_{\tau=0} \tag{3.19}$$

The factors θ and $(k!)^{-1}(\theta)^k$ that should surface in the new form are absorbed by the constants a_{j_1} and a_{j_k}, respectively. Defining

$$\boldsymbol{a}_{j_0} = \begin{bmatrix} a_{j_0} \\ a_{j_1} \end{bmatrix}, \qquad \boldsymbol{a}_j = \begin{bmatrix} a_{j_2} \\ \vdots \\ a_{j_m} \end{bmatrix} \tag{3.20}$$

$$\boldsymbol{A}_{j_0}(\tau) = [1 \ \tau], \qquad \boldsymbol{A}_j(\tau) = [\tau^2 \ \dots \ \tau^m] \tag{3.21}$$

in matrix form, equation (3.18) becomes

$$q_j(\tau) = \boldsymbol{A}_{j_0}(\tau)\boldsymbol{a}_{j_0} + \boldsymbol{A}_j(\tau)\boldsymbol{a}_j; \quad j = 1, 2, \cdots, r \tag{3.22}$$

and for all of the r coordinates, we have

$$\boldsymbol{q}(\tau) = \boldsymbol{A}_0(\tau)\boldsymbol{a}_0 + \boldsymbol{A}(\tau)\boldsymbol{a} \tag{3.23}$$

where $\boldsymbol{A}_0$ a matrix of order $r \times 2r$, and $\boldsymbol{A}$ a matrix of order $r \times r(m-1)$ along with the vectors $\boldsymbol{a}_0$ and $\boldsymbol{a}$ with dimensions $2r \times 1$ and $(m-1)r \times 1$ respectively are given by

$$\boldsymbol{A}_0 = \begin{bmatrix} \boldsymbol{A}_{10} & \mathbf{0} & \dots & \mathbf{0} \\ \mathbf{0} & \boldsymbol{A}_{20} & \dots & \mathbf{0} \\ \vdots & \vdots & \dots & \vdots \\ \mathbf{0} & \mathbf{0} & \dots & \boldsymbol{A}_{r0} \end{bmatrix} \; ; \quad \boldsymbol{A} = \begin{bmatrix} \boldsymbol{A}_1 & \mathbf{0} & \dots & \mathbf{0} \\ \mathbf{0} & \boldsymbol{A}_2 & \dots & \mathbf{0} \\ \vdots & \vdots & \dots & \vdots \\ \mathbf{0} & \mathbf{0} & \dots & \boldsymbol{A}_r \end{bmatrix} \tag{3.24}$$

$$\boldsymbol{a}_0 = \begin{bmatrix} \boldsymbol{a}_{10} \\ \boldsymbol{a}_{20} \\ \vdots \\ \boldsymbol{a}_{r0} \end{bmatrix} \; ; \quad \boldsymbol{a} = \begin{bmatrix} \boldsymbol{a}_1 \\ \boldsymbol{a}_2 \\ \vdots \\ \boldsymbol{a}_r \end{bmatrix} \tag{3.25}$$

Hence, the initial states are represented by $\boldsymbol{a}_0$ and other generalized states are represented by $\boldsymbol{a}$. For an initial value problem in dynamics, $\boldsymbol{a}_0$ is given and the vector $\boldsymbol{a}$ constitutes the unknowns of the response problem. Finally, the complete assumed modes model of the generalized displacement in Eq. (3.7) becomes

$$\boldsymbol{u} = \boldsymbol{U}[\boldsymbol{A}_0\boldsymbol{a}_0 + \boldsymbol{A}\boldsymbol{a}] \tag{3.26}$$

$$= \boldsymbol{U}\bar{\boldsymbol{A}}\bar{\boldsymbol{a}} \tag{3.27}$$

where

$$\bar{\boldsymbol{A}} = [\boldsymbol{A}_0 \;\; \boldsymbol{A}] \tag{3.28}$$

$$\bar{\boldsymbol{a}} = \begin{bmatrix} \boldsymbol{a}_0 \\ \boldsymbol{a} \end{bmatrix} \tag{3.29}$$

in which, the argument τ is dropped from $\boldsymbol{A}_0$ and $\boldsymbol{A}$ for simplicity. Dimensions of $\bar{\boldsymbol{A}}$ are $r \times (m+1)r$ and those of $\bar{\boldsymbol{a}}$ are $(m+1)r \times 1$.

3.3.2 Generalized Electrical Coordinate

Similar to the development above, the electrical counterpart of Eq. (3.23) gives the form of the electrical generalized coordinate as

$$\phi(\tau) = \boldsymbol{B}_v(\tau)\boldsymbol{b}_v \tag{3.30}$$

where $\boldsymbol{B}$ has dimensions $K \times K(l+1)$ and $\boldsymbol{b}_v$ dimensions of $K(l+1) \times 1$ and written as

$$\boldsymbol{B}_v = \begin{bmatrix} \boldsymbol{B}_{v1} & \mathbf{0} & \dots & \mathbf{0} \\ \mathbf{0} & \boldsymbol{B}_{v2} & \dots & \mathbf{0} \\ \vdots & \vdots & \dots & \vdots \\ \mathbf{0} & \mathbf{0} & \dots & \boldsymbol{B}_{vK} \end{bmatrix} \quad ; \quad \boldsymbol{b}_v = \begin{bmatrix} \boldsymbol{b}_{v0} \\ \boldsymbol{b}_{v1} \\ \vdots \\ \boldsymbol{b}_{vK} \end{bmatrix} ; \quad K \leq r \tag{3.31}$$

$$\boldsymbol{B}_{vj}(\tau) = \begin{bmatrix} 1 & \tau & \tau^2 & \dots & \tau^l \end{bmatrix} \qquad j = 1, 2, \cdots, K \tag{3.32}$$

The complete assumed modes for the electrical dof given by Eq. (3.8) can then be written as:

$$\boldsymbol{v} = \boldsymbol{V}\boldsymbol{B}_v\boldsymbol{b}_v \tag{3.33}$$

Note that the assumed displacement distributions (mode shape) $\boldsymbol{U}$ must satisfy the geometric boundary conditions as stated above, while the assumed potential distributions $\boldsymbol{V}$ must be consistent with the prescribed voltage boundary conditions (*e.g.* the grounded potential is null). Note also that for a potential applied only in the poling direction of the piezoelectric material, the matrix $\boldsymbol{V}$ degenerates to a vector.

3.3.3 Generalized Applied Forces

Following the same line of thought, the applied forces (non-conservative) and electrical charge may also be expanded into a series of modal forces and charge, generating

consequently the generalized forces and charge. Neglecting body forces, the applied forces $\boldsymbol{P}_s$ along with the electrical charge $\boldsymbol{\sigma}$ can be written as

$$\boldsymbol{P}_s = \boldsymbol{W}(x,y)\boldsymbol{f}(t) = \boldsymbol{W}(x,y)\boldsymbol{B}_f\boldsymbol{b}_f \tag{3.34}$$

$$\boldsymbol{\sigma} = \boldsymbol{V}(x,y)\boldsymbol{\varphi}(t) = \boldsymbol{V}(x,y)\boldsymbol{B}_v\boldsymbol{\beta} \tag{3.35}$$

where $\boldsymbol{W}$ and $\boldsymbol{V}$ represent spatial distribution matrices with dimensions $1 \times J$ and $1 \times K$ respectively, $\boldsymbol{B}_f$ is equivalent to $\boldsymbol{B}_v$ with dimensions $J \times J(l+1)$, $\boldsymbol{\beta}$ and $\boldsymbol{b}_f$ are coefficient vectors.

Discrete actuators can be treated as distributed by writing the elements W_j of the matrix $\boldsymbol{W}(x,y)$ present in Eq. (3.34) as

$$W_j(x,y) = \delta(x - x_j)\delta(y - y_j) \tag{3.36}$$

where $\delta(x - x_j)$ and $\delta(y - y_j)$ are Dirac delta functions.

$$\boldsymbol{b}_f = \begin{bmatrix} \boldsymbol{b}_{f0} \\ \boldsymbol{b}_{f1} \\ \vdots \\ \boldsymbol{b}_{fl} \end{bmatrix}; \quad \boldsymbol{\beta} = \begin{bmatrix} \boldsymbol{\beta}_0 \\ \boldsymbol{\beta}_1 \\ \vdots \\ \boldsymbol{\beta}_l \end{bmatrix} \tag{3.37}$$

3.4 Statement of Hamilton's Law

Consider a distributed parameter dynamic system whose motion can be described by a vector of generalized displacement $\boldsymbol{u}$. For any time span $(t_f - t_i)$ of motion of this system, Hamilton's law of varying action (HLVA) is expressed as:

$$\int_{t_i}^{t_f} (\delta L + \delta W)dt - \int_V \delta \boldsymbol{u}^T \boldsymbol{p}\Big|_{t_i}^{t_f} = 0 \tag{3.38}$$

Where L is the Lagrangian of a bounded volume V defined by a difference of a kinetic energy T and a potential energy U, δW is the virtual work done by external forces

and applied surface charges, and $\boldsymbol{p}$ is the generalized momentum. Writing

$$L = T - U \tag{3.39}$$

Eq. (3.38) becomes

$$\delta \int_{t_i}^{t_f} (T - U)dt + \int_{t_i}^{t_f} \delta W dt - \int_V \delta \boldsymbol{u}^T \boldsymbol{p} \Big|_{t_i}^{t_f} = 0 \tag{3.40}$$

For a system consisting of an elastic body characterized by a material density ρ_s and bounded by a volume V_s with inclusions of piezoelectric material having a material density ρ_p, bounded by a volume V_p poled and electroded arbitrarily:

$$\widehat{T} = \frac{1}{2}\rho_s \dot{\boldsymbol{u}}^T \dot{\boldsymbol{u}} + \frac{1}{2}\rho_p \dot{\boldsymbol{u}}^T \dot{\boldsymbol{u}} \tag{3.41}$$

$$T = \int_{V_s} \frac{1}{2}\rho_s \dot{\boldsymbol{u}}^T \dot{\boldsymbol{u}} dV + \int_{V_p} \frac{1}{2}\rho_p \dot{\boldsymbol{u}}^T \dot{\boldsymbol{u}} dV \tag{3.42}$$

$$U = \int_{V_s} \frac{1}{2}\boldsymbol{S}^T \boldsymbol{T} dV + \int_{V_p} \frac{1}{2}[\boldsymbol{S}^T \boldsymbol{T} - \boldsymbol{E}^T \boldsymbol{D}] dV \tag{3.43}$$

$$\boldsymbol{p} = \frac{\partial \widehat{T}}{\partial \dot{\boldsymbol{u}}} = \rho_s \dot{\boldsymbol{u}} + \rho_p \dot{\boldsymbol{u}} \tag{3.44}$$

where $\dot{\boldsymbol{u}}$ is the velocity (time derivative of the displacement). The virtual work δW done by the external forces and applied surface charge (neglecting body forces) is

$$\delta W = \int_{S_1} \delta \boldsymbol{u}^T \boldsymbol{P}_s dS - \int_{S_2} \delta \boldsymbol{v}^T \boldsymbol{\sigma} dS \tag{3.45}$$

where $\boldsymbol{P}_s$ is the vector of applied forces, S_i is the surface area, $\boldsymbol{v}$ is the electric potential, $\boldsymbol{\sigma}$ is the surface charge.

3.5 The Variations

In order to derive the system electromechanical equations and mechanical/electrical boundary conditions of the structure, one needs to carry out variations with respect

to $\boldsymbol{u}$ and $\boldsymbol{v}$ in Eq. (3.40) and collect coefficients of similar terms. The variation of the kinetic energy is presented first, and followed by the variation of the potential energy (including strain and electric energies), and work of the external applied forces and electric charge $\boldsymbol{\sigma}$ (virtual work). A final variational equation is derived, which leads to all electromechanical system equations and boundary conditions. The variation operator δ is defined as interchangeable with the partial diffrentiation operator as outlined in [1] and [14].

3.5.1 Generalized Coordinates

The variation of the generalized coordinates $\boldsymbol{q}$ and $\boldsymbol{\phi}$ along with $\dot{\boldsymbol{q}}$ constitutes the basic variation upon which the next development is based. Using Eq. (3.23), (3.17), and (3.30), we get

$$\delta \boldsymbol{q} = \boldsymbol{A}\delta \boldsymbol{a}; \quad \delta \dot{\boldsymbol{q}} = \frac{1}{\theta}\boldsymbol{A}'\delta \boldsymbol{a}; \quad \delta \boldsymbol{\phi} = \boldsymbol{B}_v \delta \boldsymbol{v} \tag{3.46}$$

where the prime denotes differentiation with respect to non-dimensional time τ.

3.5.2 Kinetic Energy

From Eq. (3.7) we have

$$\dot{\boldsymbol{u}} = \boldsymbol{U}\dot{\boldsymbol{q}} \tag{3.47}$$

Substituting Eq. (3.47) into Eq. (3.42) results in

$$T = \int_{V_s} \frac{1}{2}\rho_s \dot{\boldsymbol{q}}^T \boldsymbol{U}^T \boldsymbol{U}\dot{\boldsymbol{q}} dV + \int_{V_p} \frac{1}{2}\rho_p \dot{\boldsymbol{q}}^T \boldsymbol{U}^T \boldsymbol{U}\dot{\boldsymbol{q}} dV \tag{3.48}$$

$$= \frac{1}{2}\dot{\boldsymbol{q}}^T (\boldsymbol{M}_s + \boldsymbol{M}_p)\dot{\boldsymbol{q}} \tag{3.49}$$

$$= \frac{1}{2}\dot{\boldsymbol{q}}^T \boldsymbol{M}\dot{\boldsymbol{q}} \tag{3.50}$$

where $\boldsymbol{M}_s$, $\boldsymbol{M}_p$, and $\boldsymbol{M}$ are the mass matrices given by

$$\boldsymbol{M}_s = \int_{V_s} \rho_s \boldsymbol{U}^T \boldsymbol{U} dV; \quad \boldsymbol{M}_p = \int_{V_p} \rho_p \boldsymbol{U}^T \boldsymbol{U} dV; \quad \boldsymbol{M} = \boldsymbol{M}_s + \boldsymbol{M}_p \tag{3.51}$$

from (3.50) and (3.46), the variation of the kinetic energy is given by

$$\delta T = \delta \dot{\boldsymbol{q}}^T \boldsymbol{M} \dot{\boldsymbol{q}} \tag{3.52}$$

Using

$$\frac{d}{dt}\left(\delta \boldsymbol{q}^T \boldsymbol{M} \dot{\boldsymbol{q}}\right) = \delta \dot{\boldsymbol{q}}^T \boldsymbol{M} \dot{\boldsymbol{q}} + \delta \boldsymbol{q}^T \boldsymbol{M} \ddot{\boldsymbol{q}} \tag{3.53}$$

we have

$$\delta \dot{\boldsymbol{q}}^T \boldsymbol{M} \dot{\boldsymbol{q}} = \frac{d}{dt}\left(\delta \boldsymbol{q}^T \boldsymbol{M} \dot{\boldsymbol{q}}\right) - \delta \boldsymbol{q}^T \boldsymbol{M} \ddot{\boldsymbol{q}} \tag{3.54}$$

in which

$$\delta \boldsymbol{q}^T \boldsymbol{M} \ddot{\boldsymbol{q}} = \delta \boldsymbol{a}^T \bar{\boldsymbol{M}} \ddot{\boldsymbol{a}} \tag{3.55}$$

where

$$\bar{\boldsymbol{M}} = \frac{1}{\theta^2} \bar{\boldsymbol{A}}^T \boldsymbol{M} \bar{\boldsymbol{A}}'' = \frac{1}{\theta^2} \begin{bmatrix} 0 & \boldsymbol{A}^{\mathbf{T}} \boldsymbol{M} \boldsymbol{A}'' \end{bmatrix} \tag{3.56}$$

3.5.3 Potential Energy

Using the constitutive equations of the elastic body and the piezoelectric material, the potential energy given by (3.43) can be further expanded into

$$U = \int_{V_s} \frac{1}{2} \boldsymbol{S}^T \boldsymbol{C}_s \boldsymbol{S} dV + \int_{V_p} \frac{1}{2} \left[\boldsymbol{S}^T \boldsymbol{C}_p \boldsymbol{S} - \boldsymbol{S}^T \boldsymbol{e}^T \boldsymbol{E} - \boldsymbol{E}^T \boldsymbol{e} \boldsymbol{S} - \boldsymbol{E}^T \boldsymbol{\varepsilon} \boldsymbol{E}\right] dV \tag{3.57}$$

The strains $\boldsymbol{S}$ are defined by the first derivative of the displacement vector $\boldsymbol{u}$ through the differential operator matrix $\boldsymbol{L}_u$ [16], and the electric field vector is defined by the electric potential $\boldsymbol{v}$ through the gradient operator $\boldsymbol{L}_\phi$

$$\boldsymbol{S} = \boldsymbol{B}_u \boldsymbol{q}; \quad \boldsymbol{E} = -\boldsymbol{B}_\phi \boldsymbol{\phi} \tag{3.58}$$

$$\boldsymbol{B}_u = \boldsymbol{L}_u \boldsymbol{U}; \quad \boldsymbol{B}_\phi = \boldsymbol{L}_\phi \boldsymbol{V} \tag{3.59}$$

Substituting Eq. (3.58) into Eq. (3.57) we obtain

$$U = \frac{1}{2}[\boldsymbol{q}^T(\boldsymbol{K}_{uus} + \boldsymbol{K}_{uup})\boldsymbol{q} + \boldsymbol{q}^T\boldsymbol{K}_{u\phi}\boldsymbol{\phi} + \boldsymbol{\phi}^T\boldsymbol{K}_{\phi u}\boldsymbol{q} - \boldsymbol{\phi}^T\boldsymbol{K}_{\phi\phi}\boldsymbol{\phi}] \quad (3.60)$$

$$= \frac{1}{2}[\boldsymbol{q}^T\boldsymbol{K}_{uu}\boldsymbol{q} + \boldsymbol{q}^T\boldsymbol{K}_{u\phi}\boldsymbol{\phi} + \boldsymbol{\phi}^T\boldsymbol{K}_{\phi u}\boldsymbol{q} - \boldsymbol{\phi}^T\boldsymbol{K}_{\phi\phi}\boldsymbol{\phi}] \quad (3.61)$$

in which

$$\boldsymbol{K}_{uus} = \int_{V_s} \boldsymbol{B}_u^T\boldsymbol{C}_s\boldsymbol{B}_u dV; \quad \boldsymbol{K}_{uup} = \int_{V_p} \boldsymbol{B}_u^T\boldsymbol{C}_p\boldsymbol{B}_u dV \quad (3.62)$$

$$\boldsymbol{K}_{u\phi} = \int_{V_p} \boldsymbol{B}_u^T\boldsymbol{e}^T\boldsymbol{B}_\phi dV; \quad \boldsymbol{K}_{\phi\phi} = \int_{V_p} \boldsymbol{B}_\phi^T\boldsymbol{\varepsilon}^T\boldsymbol{B}_\phi dV \quad (3.63)$$

$$\boldsymbol{K}_{uu} = \boldsymbol{K}_{uus} + \boldsymbol{K}_{uup}; \quad \boldsymbol{K}_{\phi u} = \boldsymbol{K}_{u\phi}^T \quad (3.64)$$

where $\boldsymbol{K}_{uus}$, $\boldsymbol{K}_{uup}$, and $\boldsymbol{K}_{uu}$ are the stiffness matrices $\boldsymbol{K}_{u\phi}$ is the electromechanical matrix of the piezoelectric part of the system, and $\boldsymbol{K}_{\phi\phi}$ is the piezoelectric (or capacitance) matrix.

Finally, the variation of the potential energy is readily obtained by using (3.46)

$$\delta U = \delta\boldsymbol{q}^T[\boldsymbol{K}_{uu}\boldsymbol{q} + \boldsymbol{K}_{u\phi}\boldsymbol{\phi}] + \delta\boldsymbol{\phi}^T[\boldsymbol{K}_{\phi u} - \boldsymbol{K}_{\phi\phi}] \quad (3.65)$$

$$= \delta\boldsymbol{a}^T[\bar{\boldsymbol{K}}_{uu}\bar{\boldsymbol{a}} + \bar{\boldsymbol{K}}_{u\phi}\boldsymbol{b}_v] + \delta\boldsymbol{b}_v^T[\bar{\boldsymbol{K}}_{\phi u}\bar{\boldsymbol{a}} - \boldsymbol{b}_v K_{\phi\phi}\boldsymbol{b}_v] \quad (3.66)$$

where

$$\bar{\boldsymbol{K}}_{uu} = \boldsymbol{A}^T\boldsymbol{K}_{uu}\bar{\boldsymbol{A}} = \begin{bmatrix}\boldsymbol{A}^T\boldsymbol{K}_{uu}\boldsymbol{A}_0 & \boldsymbol{A}^T\boldsymbol{K}_{uu}\boldsymbol{A}\end{bmatrix} \quad (3.67)$$

$$\bar{\boldsymbol{K}}_{u\phi} = \boldsymbol{A}^T\boldsymbol{K}_{u\phi}\boldsymbol{B}_v; \quad \bar{\boldsymbol{K}}_{\phi\phi} = \boldsymbol{B}^T\boldsymbol{K}_{\phi\phi}\boldsymbol{B}_v \quad (3.68)$$

3.5.4 Work done by External Forces

The work done by the externally applied forces and electric charges is expressed by

$$\delta W = \int_{S_1} \delta\boldsymbol{u}^T\boldsymbol{P}_s dS - \int_{S_2} \delta\boldsymbol{v}^T\boldsymbol{\sigma} dS \quad (3.69)$$

Upon substitution of Eqs. (3.34), and (3.35) into Eq. (3.69) one obtains

$$\delta W = \delta \boldsymbol{q}^T \boldsymbol{F} \boldsymbol{f} - \delta \boldsymbol{\phi}^T \boldsymbol{Q} \boldsymbol{\varphi} \tag{3.70}$$

$$= \delta \boldsymbol{a}^T \boldsymbol{B}_r \boldsymbol{b}_f - \delta \boldsymbol{b}_v^T \boldsymbol{B}_\sigma \boldsymbol{\beta} \tag{3.71}$$

where

$$\boldsymbol{F} = \int_{S_1} \boldsymbol{U}^T \boldsymbol{W} dS \tag{3.72}$$

$$\boldsymbol{Q} = \int_{S_2} \boldsymbol{V}^T \boldsymbol{V} dS \tag{3.73}$$

$$\boldsymbol{B}_r = \boldsymbol{A}^T \boldsymbol{F} \boldsymbol{B}_f \tag{3.74}$$

$$\boldsymbol{B}_\sigma = \boldsymbol{B}_v^T \boldsymbol{Q} \boldsymbol{B}_v \tag{3.75}$$

3.5.5 Boundary Terms

The boundary term in Hamilton's Law of Varying Action (HLVA) involving the generalized momentum in Eq. (3.38) namely $\delta \boldsymbol{q}^T \boldsymbol{p}$ evaluated at the limits of time period can be written as follows. Using Eqs. (3.44), (3.46), and (3.51), we get

$$\int_V \delta \boldsymbol{u}^T \boldsymbol{p} \Big|_{t_i}^{t_f} dv = \delta \boldsymbol{q}^T \boldsymbol{M} \dot{\boldsymbol{q}} \Big|_{t_i}^{t_f} \tag{3.76}$$

3.6 Algebraic Equations of Motion (AEM)

The algebraic equations of motions (AEM) are obtained through HLVA stated previously and given Eq. (3.40) in conjunction with the complete assumed mode model of Eq. (3.26). Upon substitution of the variational terms and collection of coefficients of similar terms, one can arrive at

$$\delta \boldsymbol{a}^T \left\{ \int_0^1 [(\bar{\boldsymbol{M}} + \bar{\boldsymbol{K}}_{uu}) \bar{\boldsymbol{a}} - \bar{\boldsymbol{K}}_{u\phi} \boldsymbol{b}_v - \boldsymbol{B}_r \boldsymbol{b}_f] d\tau \right\}$$

$$- \delta \boldsymbol{b}_v^T \left\{ \int_0^1 [\bar{\boldsymbol{K}}_{\phi u} \bar{\boldsymbol{a}} + \bar{\boldsymbol{K}}_{\phi\phi} \boldsymbol{b}_v - \boldsymbol{B}_\sigma \boldsymbol{\beta}] d\tau \right\} = \boldsymbol{0} \tag{3.77}$$

which leads to the following AEM,

$$\widetilde{G}\bar{a} = \widetilde{K}_{u\phi}b_v + \widetilde{B}_r b_f \tag{3.78}$$

$$\widetilde{K}_{\phi u}\bar{a} + \widetilde{K}_{\phi\phi}b_v = -\widetilde{B}_\sigma \beta \tag{3.79}$$

Eqs. (3.78), and (3.79) are usually referred to as the *actuator* equations, and *sensor* equations respectively, in which, the following notation is used

$$\widetilde{X} = \int_0^1 \bar{X} d\tau; \quad \text{and} \quad \bar{G} = \bar{M} + \bar{K}_{uu} \tag{3.80}$$

where $\bar{a}$ represents the coefficients of the system to be controlled, b_v is used to denote the coefficients of the control voltages, and b_f stands for the coefficient of the external control forces.

3.6.1 Actuator Equations

Eq. (3.78) can also be written as:

$$\widetilde{G}_r a + \widetilde{G}_0 a_0 = \widetilde{K}_{u\phi}b_v + \widetilde{B}_r b_f \tag{3.81}$$

$$\widetilde{G}_r a = \widetilde{K}_{u\phi}b_v + \widetilde{B}_r b_f - \widetilde{G}_0 a_0 \tag{3.82}$$

where $\widetilde{G}_r$ and $\widetilde{G}_0$ have dimensions $(m-1)r \times (m-1)r$ and $(m-1)r \times 2r$, respectively. As we can see the matrix $\widetilde{G}_r$ is square and its inverse will not be a major problem since both the mass and stiffness matrices are positive definite. The coupling matrix (forcing term) $\widetilde{K}_{u\phi}$ is of dimensions $(m-1)r \times K(l+1)$ and the forcing matrix $\widetilde{B}_r$ is of dimension $(m-1)r \times J(l+1)$ which makes them rectangular. The ranks of these matrices will play an important role in determining the mode controllability with respect to a set of inputs. Actuator placement for designing the deformable mirror will be consequently discussed using the rank of these matrices as will be seen

subsequently. Note also that $\widetilde{G}_0$ depends only on the stiffness matrix as

$$\widetilde{G}_0 = \int_0^1 A^T K_{uu} A_0 d\tau \tag{3.83}$$

Eq. (3.82) replaces the conventional linear state-space equations

$$\dot{X}(t) = A(t)X(t) + B(t)u(t) \tag{3.84}$$

where a and b_v and/or b_f are regarded as the state and control vectors respectively.

In particular, identification of a in AEM as the state vector in control context rests on justifiable grounds. In view of a typical simple power series expansion of an admissible $q_j(t)$ about t_i and comparing with Eq. (3.15), one can observe that the coefficients α_{ji} in Eq. (3.15) are directly proportional to the i^{th} order derivatives of the generalized coordinate $q_j(t)$. Of course, this reflects to a_{ji} in the nondimensional-time form of the expansion given by Eq. (3.18). This identification is consistent with the definition of state variables for a dependent variable in a differential equation setting which are typically chosen as the derivatives of the dependent variables. By necessity, in a differential equation setting only the displacement and velocity are identified as state variables. In contrast, in the expansion given by Eq. (3.15) or equivalently Eq. (3.18), higher order derivatives of q_j (including acceleration and jerk) also qualify as state variables. Accordingly the question of how many time modes in Eq. (3.18) should be included for a desired accuracy of the solution becomes tantamount to the question of how many generalized states should be included in the expansion.

3.6.2 Sensor Equations

This study is concerned only with the control design methodology using the dynamic model of the structure. One consequence of applying the variational principle to active piezoelectric structure is the resulting sensor equations. For completeness,

of this methodology, we only state the different sensing methods using the direct approach without any application pertaining to this study.

There are two types of sensing considered in this study, namely *voltage sensing* and *charge (or current) sensing.*

- **Voltage measurement sensor**

In the standard piezoelectric sensor application, the voltage at the piezoelectric electrodes is measured by a high impedance amplifier which allows no current flow to and from the electrodes. The electrodes are essentially open circuited and thus the applied charge is zero $\boldsymbol{\beta} = \mathbf{0}$, the measured voltage in this case is used to reconstruct the mechanical state using the sensor equation Eq. (3.79) from which we have,

$$\boldsymbol{b}_v = -\widetilde{\boldsymbol{K}}_{\phi\phi}^{-1}\widetilde{\boldsymbol{K}}_{\phi u}\bar{\boldsymbol{a}} \tag{3.85}$$

- **Charge measurement sensor**

Another important sensor application arises when a low impedance charge amplifier is attached to the piezoelectric. The electrodes are essentially shorted and thus the voltage is zero $\boldsymbol{b}_v = \mathbf{0}$. This type of sensor was examined by Lee in [56]. In this case the piezoelectric strain or strain rate can be found by measuring the charge or current flowing to the electrodes. The strain is proportional to the applied current, we thus get

$$\widetilde{\boldsymbol{B}}_\sigma\boldsymbol{\beta} = \widetilde{\boldsymbol{K}}_{\phi u}\bar{\boldsymbol{a}} \tag{3.86}$$

3.7 Generalized Coordinates Continuity Equations

Solutions of AEM for arbitrarily large intervals of time can be obtained by a time marching algorithm simply by providing continuity conditions of the generalized co-

ordinates tying subsequent transition intervals.

The continuity condition across two subsequent intervals (j) and $(j+1)$ for a time marching system has the form

$$\boldsymbol{a}_0^{(j+1)} = \boldsymbol{P}\boldsymbol{a}^{(j)} + \boldsymbol{P}_0\boldsymbol{a}_0^{(j)} \tag{3.87}$$

$\boldsymbol{P}$ and $\boldsymbol{P}_0$ can be identified from the continuity of time-modes expansion of generalized coordinates using the nondimensional form by writing

$$\boldsymbol{q}^{(j+1)}(0) = \boldsymbol{q}^{(j)}(1), \quad \boldsymbol{q}'^{(j+1)}(0) = \boldsymbol{q}'^{(j)}(1) \tag{3.88}$$

Using the non-dimensional expansion given by Eq. (3.13), these in turn define the initial conditions from each time subinterval in terms of the values already available from the previous one:

$$\boldsymbol{P}_0 = \begin{bmatrix} \boldsymbol{P}_{10} & \mathbf{0} & \dots & \mathbf{0} \\ \mathbf{0} & \boldsymbol{P}_{20} & \dots & \mathbf{0} \\ \vdots & \vdots & \dots & \vdots \\ \mathbf{0} & \mathbf{0} & \dots & \boldsymbol{P}_{r0} \end{bmatrix} \; ; \quad \boldsymbol{P} = \begin{bmatrix} \boldsymbol{P}_1 & \mathbf{0} & \dots & \mathbf{0} \\ \mathbf{0} & \boldsymbol{P}_2 & \dots & \mathbf{0} \\ \vdots & \vdots & \dots & \vdots \\ \mathbf{0} & \mathbf{0} & \dots & \boldsymbol{P}_r \end{bmatrix} \tag{3.89}$$

where

$$\boldsymbol{P}_{j0} = \begin{bmatrix} 1 & 1 \\ 0 & 1 \end{bmatrix}; \quad \boldsymbol{P}_j = \begin{bmatrix} 1 & 1 & \dots & 1 \\ 2 & 3 & \dots & m \end{bmatrix}; \tag{3.90}$$

It is worth noting that the continuity matrices $\boldsymbol{P}_0$ and $\boldsymbol{P}$ of dimensions $2r \times 2r$ and $2r \times (m-1)r$ respectively, depend only on the number of degrees of freedom and the degree of truncated power series for each degree of freedom; nothing else. As such, they remain unchanged throughout the total period of control time, regardless of whether the system dynamics are time varying or not. One consequence of this is an overwhelming simplicity in implementing the continuity, both analytically and computationally, without any compromise in return.

The number of terms to retain in the series expansion of the generalized coordinates has to do with the accuracy desired. This is also affected by the size of the time step $(t_i - t_f)$ and usually there is a trade off between this and the number of terms. Generally, one can determine an appropriate number of terms by solving the response problem first, in the absence of control inputs. For a given specific problem, a preliminary convergence check on the response solution can be made by starting with a small number of terms and increasing them gradually. Experience to date has shown that one does not need to go beyond single digits even for conceivably difficult problems, and in most cases six to eight terms in the series are sufficient [1, 8]. Convergence is also contingent upon the complexity of motion within the time interval $(t_i - t_f)$ [8]. Therefore θ should not be taken too large and it can be based on characteristic time of the system. In control applications with the same choice of θ, experience to date indicates that even fewer number of terms for the coordinates can be used without a noticeable compromise in accuracy, provided that the control effort is strong enough to damp the motion quickly [1]. However too much freedom should not be exercised in this respect, for otherwise this may lead to an unrealistic representation of the physical problem. On the other hand, one has complete freedom to choose the number of terms for the control inputs, since this is a matter of availability and/or capability of instrumentation to implement these inputs. Naturally, one might want to consider the simplest case, which would be only one term. This corresponds to a zero-order hold, a choice that would be very favorable for digital implementation. The number of terms used in the simulation examples of this study are given in the statements of these examples.

3.7.1 Hamilton's Law and Initial Value Problems

The first thing to be mentioned at this point is the clear distinction between what is commonly called Hamilton's principle and Hamilton's law of varying action. Hamilton's law given by Eq. (3.38) states

$$\int_{t_i}^{t_f} (\delta L + \delta W)dt - \int_V \delta \boldsymbol{u}^T \boldsymbol{p} \Big|_{t_i}^{t_f} = 0$$

If $\boldsymbol{u}$ is constrained to take on specified values at t_i and t_f then $\delta \boldsymbol{u}(t_i)$ and $\delta \boldsymbol{u}(t_f)$ vanish in Eq. (3.38) and the result is Hamilton's principle:

$$\delta \int_{t_i}^{t_f} \delta(L + W)dt = 0 \tag{3.91}$$

As pointed out by Simkins in [70], an observation to be made here is that Eq. (3.91) corresponds to a system of a boundary value problems -not initial value problem- since the boundary term can only vanish through boundary (end point) constraints either natural or imposed. Thus Eq. (3.91) cannot, with complete logic, be used to formulate any system of initial value problems of dynamics. The introduction of initial data has in fact always been the obstacle preventing the use of Hamilton's Principle for the variational formulation of initial valu problems. [70]

Since Hamilton's principle is a valid physical statement of mechanics only when the boundary constraints are such that the boundary term vanishes, it is really a "constrained variational principle," as opposed to Eq. (3.38), which are unconstrained variational laws of mechanics, suitable for the application of arbitrary constraint conditions.

Application of Hamilton's law to initial value problems has been demonstrated in many articles such as in [7, 8, 9, 10, 13, 70, 18, 1, 46].

3.8 Controllability

Theoretical aspects of controllability are well established in the linear system theory based on the traditional approach [24, 35]. The controllability concept is defined under the assumption that a complete knowledge of the linear differential state-space formulation are assumed to be known beforehand. Following the trend this concept (controllability) is only briefly discussed here, since a more detailed discussion is provided in [1] for discrete systems, the same concept applies for discrete systems and distributed parameter systems. But of course, they will be conveyed from the standpoint of direct algebraic formulation of dynamic equations presented in previous sections.

In the next sub-sections, first the definition of controllability is given, together with associated state-space equations. Then the corresponding algebraic equations are used to study it and to show how it fits the mainframe of the direct formulation. However, it is not the scope of this study to go in details of deriving the necessary and sufficient conditions of controllability as applied to AEM, rather we apply the already existing formalism of discrete systems developed in [1] to distributed parameter systems and study the conditions and terms under which the "modal" controllability is characterized. The controllability measure will be used in determining the controllable and uncontrollable modes for specific set of control inputs.

3.8.1 Controllability

Consider a linear differential state equations (LSE) for an r degrees of freedom time-varying discrete parameter linear dynamic system with R inputs given first by

$$\dot{\boldsymbol{X}}(t) = \boldsymbol{A}(t)\boldsymbol{X}(t) + \boldsymbol{B}(t)\boldsymbol{u}(t) \tag{3.92}$$

$\boldsymbol{X}$ is the state vector, $\boldsymbol{u}$ is the input vector, and $\boldsymbol{A}$ and $\boldsymbol{B}$ are respectively the state and input matrices whose entries are continuous functions of time over the total time interval I of study.

Definition

The state equation (LSE) is said to be *state controllable* at time $t_0 \in I$, if there exists a finite $t_1 \in I$ with $t_1 > t_0$ such that for any $\boldsymbol{X}(t_0)$ and $\boldsymbol{X}(t_1)$ in the state space, there exists an input $\boldsymbol{u}$ over $[t_0,\ t_1]$ that will transfer the state $\boldsymbol{X}(t_0)$ to the state $\boldsymbol{X}(t_1)$. Otherwise the state equation is said to be *uncontrollable* at time t_0.
In other words, this definition requires that the input $\boldsymbol{u}$ be capable of moving any state to any other state in a *finite* time. The trajectory that should take is not specified.

In terms of the algebraic state equation, rewriting the AEM,

$$\widetilde{G}_r \boldsymbol{a} = \widetilde{K}_{u\phi} \boldsymbol{b}_v + \widetilde{B}_r \boldsymbol{b}_f - \widetilde{G}_0 \boldsymbol{a}_0 \tag{3.93}$$

Controlled response of the system will be determined by the generalized state vector $\boldsymbol{a}$ through whatever input $\boldsymbol{b}_v$ or $\boldsymbol{b}_f$ it may call for a desired configuration. Generally speaking, the control $\boldsymbol{b}_v$ or $\boldsymbol{b}_f$ does not have to be in terms of $\boldsymbol{a}$. In particular, in the absence of the forcing term, the equation should yield the uncontrolled, unforced dynamic response of the system to arbitrary initial excitations. This means, one must be able to solve it for $\boldsymbol{a}$, and obtain

$$\boldsymbol{a} = -\widetilde{G}_r^{-1} \widetilde{G}_0 \boldsymbol{a}_0 \tag{3.94}$$

Therefore the matrix $\widetilde{G}_r$ must be invertible in the first place. Fortunately, given the structure of $\widetilde{G}_r$ which the sum of the square positive definite mass and stiffness matrices of the structure, this condition is already met. Hence, a necessary condition

for controllability is that the matrix $\widetilde{G}_r$ must be invertible.

The following analysis considers only structures with distributed actuators for simplicity and clarity of the matter, however the inclusion of structures with discrete actuators should be an obvious one. In what follows, to consider the discrete actuators case, one has to replace the control input b_v and the corresponding matrix $\widetilde{K}_{u\phi}$ with the inputs b_f and the matrix $\widetilde{B}_r$ respectively.

Considering a structure with distributed actuators (the case of bimorph mirrors), the control inputs are b_v ($b_f = 0$), using the controllability formalism of discrete systems given by Adiguzel [1], and defining the $2r \times K(l+1)$ C_L and $2r \times 2r$ Z_L as

$$\begin{aligned} C_L &= P\widetilde{G}_r^{-1}\widetilde{K}_{u\phi} \\ Z_L &= P\widetilde{G}_r^{-1}\widetilde{G}_0 + P_0 \end{aligned} \tag{3.95}$$

we can state

Local Controllability (for each time step)

- $\widetilde{G}_r^{-1}$ exists. (necessary condition)
- $rank\ C_L = K$ (Sufficient condition)

Global Controllability (for all steps up to the jth step)

- $\widetilde{G}_r^{-1}$ exists. (Necessary condition)
- $rank\ C_j = 2r$ (Sufficient condition)

where C_j of dimensions $2r \times jK(l+1)$ is given by

$$C_j = \left[C_L \; Z_L C_L \cdots Z_L^k C_L \cdots Z_L^{j-1} C_L\right] \tag{3.96}$$

The controllability conditions stated above will only lead to what we call a "Pseudo-controllable" system since the matrix C_L is rectangular. The pseudo-controllability is a consequence of the solution for the control inputs b_v using the algebraic equations of motion along with the continuity equations. The solution for control inputs b_v is given by

$$b_v = C_L^{\dagger}\{a_0^{j+1} - Z_L a_0^j\} \tag{3.97}$$

where $C_L^{\dagger}$ is the pseudo-inverse of C_L given by

$$C_L^{\dagger} = [C_L^T C_L]^{-1} C_L^T \tag{3.98}$$

Eq. (3.97) is the least square solution that minimizes

$$E = \|C_L b_v^j - a_0^{(j+1)} + Z_L a_0^{(j)}\| \tag{3.99}$$

or

$$C_L^{\dagger} = C_L^T [C_L C_L^T]^{-1} \tag{3.100}$$

which minimizes the control inputs (i.e. b_v) in the least square sense.

3.8.2 Trajectory Controllability

Controllability of algebraic system dynamics studied in the above section was strictly in the sense of *pointwise state controllability* so that the concept can be viewed from the same perspective as it is implied and done by the conventional (differential) state formulation. Accordingly, state trajectories are suppressed and so far it is considered

to be the capability to drive any $\boldsymbol{a}_0^{(1)}$ to any $\boldsymbol{a}_0^{(j)}$ with finite $j > 1$. By contrast, it may also be desirable to reach a particular trajectory from any $\boldsymbol{a}_0^1$ in a finite number of advances in time. The intention in this section is therefore to broaden the above mentioned perspective of controllability and extend it to search for trajectory specific inputs.

Response trajectory of the system during any step in time is determined by the generalized state vector $\boldsymbol{a}$ as per (AEM) and its continuity across the time steps maintained by the continuity equation. A desired trajectory on the other hand can be prescribed either analytically or as a set of point data. At any rate, it must be admissible and therefore, it can be curve fitted (step by step) by some suitable $\hat{\boldsymbol{a}}$ so that it implies with the associated (AEM) and the natural continuity constraints therein. Without further delay, using the same formalism as in [1] as applied to distributed parameter systems, the system is said to be *trajectory controllable* or $\boldsymbol{a}$*-controllable* when

Global $\boldsymbol{a}$-Controllability

- $\widetilde{\boldsymbol{G}}_r^{-1}$ exists. (Necessary condition)
- $rank\ \boldsymbol{C}_{\boldsymbol{a}_j} = rank\ \widetilde{\boldsymbol{K}}_{u\phi}$ (Sufficient condition)

where $\boldsymbol{C}_{\boldsymbol{a}_j}$ is given by

$$\boldsymbol{C}_{\boldsymbol{a}_j} = \left[\widetilde{\boldsymbol{K}}_{u\phi}\ \ \widetilde{\boldsymbol{G}}_0\boldsymbol{C}_L\ \ \widetilde{\boldsymbol{G}}_0\boldsymbol{Z}_L\boldsymbol{C}_L\ \ \widetilde{\boldsymbol{G}}_0\boldsymbol{Z}_L^2\boldsymbol{C}_L\ \cdots\ \widetilde{\boldsymbol{G}}_0\boldsymbol{Z}_L^{j-2}\boldsymbol{C}_L\right] \tag{3.101}$$

Chapter 4

Direct Optimal Control

In this chapter, the focus is on the development of a direct optimal control law for distributed parameter systems using the algebraic equations of motion obtained in previous chapters. In controlling the vibrations of a flexible structure using piezoelectric actuators, the control input is the voltage applied to the actuators of the flexible structure and the response is represented by the deflection of the surface, the variable w.

The following development is applied to distributed parameter systems with distributed actuators, for which the discrete actuators are considered inactive. Therefore, $\boldsymbol{b}_f = \mathbf{0}$.

An optimization problem consists generally of two major components; an objective function(or performance measure) and a set of constraint equations. In control applications, the former involves a certain performance measure criterion and the latter is usually the state space equations of the system. The objective is to determine the control input functions that minimize (or maximize as the case may be) the performance criterion while the constraints are simultaneously satisfied. In order to put

the proposed optimal control methodology in the right perspective, here, a widely used standard performance measure in the control theory is considered. Thus, that measure is chosen as

$$J = \frac{1}{2}\int_{t_i}^{t_f}\left\{\int_V \left[\boldsymbol{u}^T\boldsymbol{W}_u\boldsymbol{u} + \dot{\boldsymbol{u}}^T\boldsymbol{W}_{\dot{u}}\dot{\boldsymbol{u}} + \boldsymbol{v}^T\boldsymbol{R}\boldsymbol{v}\right] dV\right\} dt \tag{4.1}$$

which corresponds to a typical performance measure of classical linear quadratic regulator problems. In this selection Eq.(4.1), if one considers a general case involving all displacements in the x, y, and z directions, $\boldsymbol{W}_u$ and $\boldsymbol{W}_{\dot{u}}$ are 3×3 real, symmetric, positive definite weight matrices for $\boldsymbol{u}$ and $\dot{\boldsymbol{u}}$ respectively, $\boldsymbol{R}$ is a 3×3 real, symmetric, positive definite weight matrix for the control $\boldsymbol{v}$. However, for the special case studied herein these matrices would be reduced to a simple scalar coefficient since w is the only nonzero displacement. Naturally, it is also possible to account for some terminal measures and even cross coupling terms for $\boldsymbol{u}$ and $\dot{\boldsymbol{u}}$ in J. However such details are inconsequential from the perspective of the general methodology presented in this chapter.

4.1 Algebraic Performance Measure

To provide the statement of the direct (algebraic)optimal control problem, the performance measure given by Eq. (4.1) will be converted to an equivalent algebraic form. Non-dimensionalizing the time parameter t and substituting the assumed mode expansion of the displacement and electrical potential given by Eqs. (3.27) and (3.33) respectively into Eq. (4.1), the performance measure becomes

$$\begin{aligned} J[\bar{\boldsymbol{a}}, \boldsymbol{b}_v] &= \frac{\theta}{2}\int_0^1 [\boldsymbol{A}\boldsymbol{a} + \boldsymbol{A}_0\boldsymbol{a}_0]^T\boldsymbol{W}_q[\boldsymbol{A}\boldsymbol{a} + \boldsymbol{A}_0\boldsymbol{a}_0]d\tau \\ &+ \frac{\theta}{2}\int_0^1 [\frac{1}{\theta}\boldsymbol{A}'\boldsymbol{a} + \frac{1}{\theta}\boldsymbol{A}'_0\boldsymbol{a}_0]^T\boldsymbol{W}_{\dot{q}}[\frac{1}{\theta}\boldsymbol{A}'\boldsymbol{a} + \frac{1}{\theta}\boldsymbol{A}'_0\boldsymbol{a}_0]d\tau \\ &+ \frac{\theta}{2}\int_0^1 [\boldsymbol{B}\boldsymbol{b}_v]^T\boldsymbol{R}_v[\boldsymbol{B}\boldsymbol{b}_v]d\tau \end{aligned} \tag{4.2}$$

where ($'$) denotes nondimensional time derivative, and

$$\boldsymbol{W}_q = \int_V \boldsymbol{U}^T \boldsymbol{W}_u \boldsymbol{U} dV; \quad \boldsymbol{W}_{\dot{q}} = \int_V \boldsymbol{U}^T \boldsymbol{W}_{\dot{u}} \boldsymbol{U} dV; \quad \boldsymbol{R}_v = \int_V \boldsymbol{V}^T \boldsymbol{R} \boldsymbol{V} dV \tag{4.3}$$

which have dimensions $(r \times r)$, $(r \times r)$, and $(K \times K)$ respectively. Obviously, without loss of generality, the performance index could be defined differently using the weighting matrices $\boldsymbol{W}_q$, $\boldsymbol{W}_{\dot{q}}$ and $\boldsymbol{R}_v$ instead of the matrices $\boldsymbol{W}_u$, $\boldsymbol{W}_{\dot{u}}$, and $\boldsymbol{R}$. This choice will lead to allocating different weights to different modes, but the original definition of the performance index J has physical significance as it is related to energy of the system (kinetic energy, strain energy, etc...). The second choice may lead in some cases to better results but its physical significance is not obviously understood.

Performing the transposition and arranging terms, we obtain

$$\begin{aligned} J(\boldsymbol{a}, \boldsymbol{b}_v) &= \frac{\theta}{2} \boldsymbol{a}^T \left[\int_0^1 [\boldsymbol{A}^T \boldsymbol{W}_q \boldsymbol{A} + \frac{1}{\theta^2} \boldsymbol{A}'^T \boldsymbol{W}_{\dot{q}} \boldsymbol{A}'] d\tau \right] \boldsymbol{a} \\ &+ \theta \boldsymbol{a}^T \left[\int_0^1 [\boldsymbol{A}^T \boldsymbol{W}_q \boldsymbol{A}_0 + \frac{1}{\theta^2} \boldsymbol{A}'^T \boldsymbol{W}_{\dot{q}} \boldsymbol{A}'_0] d\tau \right] \boldsymbol{a}_0 \\ &+ \frac{\theta}{2} \boldsymbol{b}_v^T \left[\int_0^1 [\boldsymbol{B}^T \boldsymbol{R}_v \boldsymbol{B}] d\tau \right] \boldsymbol{a} \\ &+ \frac{\theta}{2} \boldsymbol{a}_0^T \left[\int_0^1 [\boldsymbol{A}_0^T \boldsymbol{W}_q \boldsymbol{A}_0 + \frac{1}{\theta^2} \boldsymbol{A}_0'^T \boldsymbol{W}_{\dot{q}} \boldsymbol{A}'_0] d\tau \right] \boldsymbol{a}_0 \end{aligned} \tag{4.4}$$

Defining

$$\widetilde{\boldsymbol{W}}_q = \int_0^1 [\boldsymbol{A}^T \boldsymbol{W}_q \boldsymbol{A}] d\tau; \quad \widetilde{\boldsymbol{W}}_{q0} = \int_0^1 [\boldsymbol{A}^T \boldsymbol{W}_q \boldsymbol{A}_0] d\tau \tag{4.5}$$

$$\widetilde{\boldsymbol{W}}_{\dot{q}} = \frac{1}{\theta^2} \int_0^1 [\boldsymbol{A}'^T \boldsymbol{W}_{\dot{q}} \boldsymbol{A}'] d\tau; \quad \widetilde{\boldsymbol{W}}_{\dot{q}0} = \frac{1}{\theta^2} \int_0^1 [\boldsymbol{A}'^T \boldsymbol{W}_{\dot{q}} \boldsymbol{A}'_0] d\tau \tag{4.6}$$

$$\widetilde{\boldsymbol{W}} = \widetilde{\boldsymbol{W}}_q + \widetilde{\boldsymbol{W}}_{\dot{q}}; \quad \widetilde{\boldsymbol{W}}_0 = \widetilde{\boldsymbol{W}}_{q0} + \widetilde{\boldsymbol{W}}_{\dot{q}0}; \quad \widetilde{\boldsymbol{R}}_v = \int_0^1 [\boldsymbol{B}^T \boldsymbol{R}_v \boldsymbol{B}] d\tau \tag{4.7}$$

$$J_0 = \frac{\theta}{2} \boldsymbol{a}_0^T \left[\int_0^1 [\boldsymbol{A}_0^T \boldsymbol{W}_q \boldsymbol{A}_0 + \frac{1}{\theta^2} \boldsymbol{A}_0'^T \boldsymbol{W}_{\dot{q}} \boldsymbol{A}'_0] d\tau \right] \boldsymbol{a}_0 \tag{4.8}$$

the objective function can be written as

$$J(\boldsymbol{a}, \boldsymbol{b}_v) = \frac{\theta}{2} \left\{ \boldsymbol{a}^T \widetilde{\boldsymbol{W}} \boldsymbol{a} + 2 \boldsymbol{a}^T \widetilde{\boldsymbol{W}}_0 \boldsymbol{a}_0 + \boldsymbol{b}_v^T \widetilde{\boldsymbol{R}}_v \boldsymbol{b}_v \right\} + J_0 \tag{4.9}$$

Hence, the linear quadratic regulator performance measure given by Eq. (4.1) in its typical functional form involving integral expressions is now converted to an equivalent algebraic form. Note that this result is achieved by introducing the complete assumed mode expansion given by Eqs. (3.27) and (3.33) into the performance measure, Eq. (4.1). Once the system is defined and the weight matrices are chosen, the integrations involved in the definition of $\widetilde{\boldsymbol{W}}_q$, $\widetilde{\boldsymbol{W}}_{q0}$, $\widetilde{\boldsymbol{W}}_{\dot{q}}$, $\widetilde{\boldsymbol{W}}_{\dot{q}0}$, and $\widetilde{\boldsymbol{R}}_v$ can easily be performed systematically; because the matrices $\boldsymbol{A}$, $\boldsymbol{A}'$, $\boldsymbol{A}_0$ and $\boldsymbol{B}$ possess a certain structure in their τ dependency by virtue of the time modes and $\boldsymbol{A}'_0$ is merely a constant matrix. Therefore, Eq. (4.9) is truly an algebraic expression. Note that the performance measure $J(\boldsymbol{a}, \boldsymbol{b}_v)$ is quadratic in the unknowns $\boldsymbol{a}$ and $\boldsymbol{b}_v$ and the last term J_0 is not function of $\boldsymbol{a}$ or $\boldsymbol{b}_v$.

4.2 Formulation of Constraints

The constraints of the optimal control problem consists of the state equations derived previously, from the AEM of the system under consideration. These are readily available in algebraic forms in terms of $\boldsymbol{a}$ and $\boldsymbol{b}_v$ from the linear algebraic state equations

$$\widetilde{\boldsymbol{G}}_r \boldsymbol{a} = \widetilde{\boldsymbol{K}}_{u\phi} \boldsymbol{b}_v - \widetilde{\boldsymbol{G}}_0 \boldsymbol{a}_0 \tag{4.10}$$

Simply, rearranging above equations, the constraint equations of the optimization problem are formed as:

$$\boldsymbol{C}(\boldsymbol{a}, \boldsymbol{b}_v) = \widetilde{\boldsymbol{G}}_r \boldsymbol{a} - \widetilde{\boldsymbol{K}}_{u\phi} \boldsymbol{b}_v + \widetilde{\boldsymbol{G}}_0 \boldsymbol{a}_0 \tag{4.11}$$

It is worth noting that the constraint equations thus obtained are the result of the direct substitution of the admissible functions forms (finite series expansion) of the

unknown states and inputs into Hamilton's law of varying action that governs the motion of the system.

4.3 Direct Optimal Control Statement

Developed above is the quadratic regulator performance measure converted to an equivalent algebraic performance measure along with the algebraic state equations written in the form of constraint equations. Hence, both components of the optimization problem are available in their algebraic form. Consequently, the linear optimal problem can now be stated as:

Linear Optimal Control Problem

- Minimizing $J(\boldsymbol{a}, \boldsymbol{b}_v) = \frac{\theta}{2}\left\{\boldsymbol{a}^T\widetilde{\boldsymbol{W}}\boldsymbol{a} + 2\boldsymbol{a}^T\widetilde{\boldsymbol{W}}_0\boldsymbol{a}_0 + \boldsymbol{b}_v^T\widetilde{\boldsymbol{R}}_v\boldsymbol{b}_v\right\} + J_0$
- Subject to $\boldsymbol{C}(\boldsymbol{a}, \boldsymbol{b}_v) = \widetilde{\boldsymbol{G}}_r\boldsymbol{a} - \widetilde{\boldsymbol{K}}_{u\phi}\boldsymbol{b}_v + \widetilde{\boldsymbol{G}}_0\boldsymbol{a}_0 = \boldsymbol{0}$

Assuming that the controllability and observability conditions are satisfied, a fixed final time t_f (corresponding to a fixed period of time θ) and free final states are considered. $\boldsymbol{a}$ and $\boldsymbol{b}_v$ constitute the unknown states and the unknown inputs respectively.

The equivalent problem in traditional control approach using differential equations would normally require a standard procedure for solution: Augment the objective function J by the differential state equations (constraints), after introducing a set of Lagrange multipliers (known as co-states); resort to techniques of calculus of variations to minimize the augmented objective function thereafter. It is well known that this conventional procedure leads to a set of nonlinear matrix differential equation

known as the Riccati Equations. By contrast, the direct optimal control problem involves only the algebraic equations. Two solution procedures are provided here. Both are straightforward and neither one leads to any differential equations. Instead, both procedures yield the optimal solution directly as shown below.

4.4 Optimal Solution

4.4.1 Optimal Solution via Direct Substitution

By noting the structure of the direct optimization problem emerged above, one recognizes that constraint equations $\boldsymbol{C}(\boldsymbol{a}, \boldsymbol{b}_v) = \boldsymbol{0}$ possess a bilinear form and, therefore, there is no need for a set of co-states. Furthermore, the algebraic character of the functional allows us to solve the problem by simple substitution rather than invoking any kind of calculus of variations.

From the constraint equations $\boldsymbol{C}(\boldsymbol{a}, \boldsymbol{b}_v) = \boldsymbol{0}$ we can readily obtain $\boldsymbol{a}$ in terms of $\boldsymbol{b}_v$:

$$\boldsymbol{a} = \widetilde{\boldsymbol{G}}_r^{-1}\widetilde{\boldsymbol{K}}_{u\phi}\boldsymbol{b}_v - \widetilde{\boldsymbol{G}}_r^{-1}\widetilde{\boldsymbol{G}}_0\boldsymbol{a}_0 \tag{4.12}$$

Substituting for $\boldsymbol{a}$ directly into the objective function, rearranging terms, one obtains

$$J(\boldsymbol{b}_v) = \frac{\theta}{2}\left\{\boldsymbol{b}_v^T[\boldsymbol{H} + \widetilde{\boldsymbol{R}}_v]\boldsymbol{b}_v + 2\boldsymbol{b}_v^T[\boldsymbol{H}_0\boldsymbol{a}_0]\right\} + \bar{J}_0(\boldsymbol{a}_0) \tag{4.13}$$

where

$$\boldsymbol{H} = [\widetilde{\boldsymbol{G}}_r^{-1}\widetilde{\boldsymbol{K}}_{u\phi}]^T\widetilde{\boldsymbol{W}}[\widetilde{\boldsymbol{G}}_r^{-1}\widetilde{\boldsymbol{K}}_{u\phi}] \tag{4.14}$$

$$\boldsymbol{H}_0 = [\widetilde{\boldsymbol{G}}_r^{-1}\widetilde{\boldsymbol{K}}_{u\phi}]^T[-\widetilde{\boldsymbol{W}}\widetilde{\boldsymbol{G}}_r^{-1}\widetilde{\boldsymbol{G}}_0 + \widetilde{\boldsymbol{W}}_0] \tag{4.15}$$

$$\bar{J}_0(\boldsymbol{a}_0) = J_0 + \frac{\theta}{2}\boldsymbol{a}_0^T[\widetilde{\boldsymbol{G}}_r^{-1}\widetilde{\boldsymbol{G}}_0]^T[\widetilde{\boldsymbol{W}}\widetilde{\boldsymbol{G}}_r^{-1}\widetilde{\boldsymbol{G}}_0 - 2\widetilde{\boldsymbol{W}}_0]\boldsymbol{a}_0 \tag{4.16}$$

Thus, the objective function is reduced to a simple quadratic form in $\boldsymbol{b}_v$. $\bar{J}_0(\boldsymbol{a}_0)$ represents the residual terms in $\boldsymbol{a}_0$ only and has no effect on the optimal solution. (mathematically, it is possible to construct a system of algebraic equations for which arbitrary eliminations may pose complications, this is not a concern in this study. since a natural separation of the controls and states takes place for the physical systems considered here through this study.)

• **Necessary Condition** to minimize $J(\boldsymbol{b}_v)$ is that

$$\frac{\partial J}{\partial \boldsymbol{b}_v} = 0 \tag{4.17}$$

which gives the optimal solution as:

$$\boldsymbol{b}_v^* = -[\boldsymbol{H} + \widetilde{\boldsymbol{R}}_v]^{-1}[\boldsymbol{H}_0\boldsymbol{a}_0] \tag{4.18}$$

• **Sufficient Condition** for $\boldsymbol{b}_v^*$ to correspond to a minimum is that the second partial derivative of $J(\boldsymbol{b}_v)$ with respect to $\boldsymbol{b}_v$ must be positive definite. From Eq. (4.13) we get

$$\frac{\partial^2 J}{\partial \boldsymbol{b}_v^2} = \theta[\boldsymbol{H} + \widetilde{\boldsymbol{R}}_v] \tag{4.19}$$

in which $\widetilde{\boldsymbol{R}}_v$ is positive definite since the weighting matrix $\boldsymbol{R}$ is positive semi definite. On the other hand, an inspection of Eq. (4.14) indicates the same for $\boldsymbol{H}$ too. Consequently, their sum is also positive definite. Therefore, $\frac{\partial^2 J}{\partial \boldsymbol{b}_v^2}$ is in fact positive definite. Hence, any concern on the existence of the inversion involved in obtaining $\boldsymbol{b}_v^*$ in Eq. (4.18) is removed.

4.4.2 Optimal Solution via Lagrange Multipliers

Another form of the optimal solution can be obtained directly by using *Lagrange Multipliers* associated with the constraint equations. To this end, we augment the

objective function and write

$$J_a(\boldsymbol{a}, \boldsymbol{b}_v) = J(\boldsymbol{a}, \boldsymbol{b}_v) + \theta \boldsymbol{\lambda}^T \boldsymbol{C}(\boldsymbol{a}, \boldsymbol{b}_v) \tag{4.20}$$

where $\boldsymbol{\lambda}$ is identified as an average Lagrange multiplier over $[t_0, t_f]$. Necessary conditions for optimality are:

$$\frac{\partial J_a}{\partial \boldsymbol{b}_v} = 0; \quad \frac{\partial J_a}{\partial \boldsymbol{a}} = 0; \quad \frac{\partial J_a}{\partial \boldsymbol{\lambda}} = 0 \tag{4.21}$$

Carrying out the required operations, the first and second conditions yield

$$\boldsymbol{b}_v = \widetilde{\boldsymbol{R}}_v^{-1} \widetilde{\boldsymbol{K}}_{u\phi}^T \boldsymbol{\lambda} \tag{4.22}$$

$$\boldsymbol{\lambda} = -\widetilde{\boldsymbol{G}}_r^{-T} [\widetilde{\boldsymbol{W}} \boldsymbol{a} + \widetilde{\boldsymbol{W}}_0 \boldsymbol{a}_0] \tag{4.23}$$

The last condition simply recovers the constraint equations. Substituting Eq. (4.23) into Eq. (4.22), the optimal solution is obtained:

$$\begin{aligned} \boldsymbol{b}_v^* &= -[\widetilde{\boldsymbol{R}}_v^{-1} \widetilde{\boldsymbol{K}}_{u\phi}^T \widetilde{\boldsymbol{G}}_r^{-T} \widetilde{\boldsymbol{W}}] \boldsymbol{a} - [\widetilde{\boldsymbol{R}}_v \widetilde{\boldsymbol{K}}_{u\phi}^T \widetilde{\boldsymbol{G}}_r^{-T} \widetilde{\boldsymbol{W}}_0] \boldsymbol{a}_0 \\ &= \boldsymbol{g} \boldsymbol{a} + \boldsymbol{g}_0 \boldsymbol{a}_0 \end{aligned} \tag{4.24}$$

Since $\widetilde{\boldsymbol{R}}_v$ is positive definite, the sufficient condition for $\boldsymbol{b}_v^*$ to be a minimum is assured. The difference between the forms of optimal control in Eq. (4.18) and Eq. (4.24) is one of algebraic operations. Eq. (4.24) clearly shows the full state feedback form of the optimal direct control, however the alternate form Eq. (4.18) being in terms of feedback of initial states only will prove to be much more practical in simulating the closed loop system and implementation of the control law.

4.4.3 Optimal Gains and Physical Controls

Obviously the optimal control solution $\boldsymbol{b}_v^*$ is not the actual physical optimal control to be implemented. These latter are simply obtained using the time assumed-modes

expansion. Using Eq. (4.18) or (4.24) the physical control (ie. voltage) is given by

$$\phi^*(\tau) = B(\tau)b_v^* \tag{4.25}$$

Looking at the form of b_v^* in Eq. (4.18) and Eq. (4.24) we can easily identify optimal feedback gain matrices g_0, g_1 and $\bar{g}$ by writing

$$b_{v1}^* = g_1 a_0 \tag{4.26}$$

$$b_{v2}^* = \bar{g}\bar{a} \tag{4.27}$$

where

$$g_1 = -[H + \widetilde{R}_v]^{-1} H_0 \tag{4.28}$$

$$\bar{g} = [g_0\ g] \tag{4.29}$$

Note that these gain matrices are constants and need to be computed only once during the period $[t_i, t_f]$. Their physical counterparts can be readily obtained as

$$K_1(\tau) = B(\tau)g_1; \quad \bar{K}(\tau) = B(\tau)\bar{g} \tag{4.30}$$

4.5 Closed Loop System

As stated previously, the algebraic equations of motion derived in the preceding chapter take on the role of the differential state space equations of conventional control theory for the same dynamic system. Both representations describe the open loop system dynamics. Similar to the conventional approach, the feedback controls either in Eq.(4.26) or Eq.(4.27) can be introduced into the state space equations to arrive at the closed loop system. However, since the simulation of the closed-loop dynamics is desired, the form of state feedback given by Eq. (4.26) would be more useful to this end. Accordingly, substituting Eq. (4.26) into Eq. (4.10) we obtain

$$a = [\widetilde{G}_r^{-1}\widetilde{K}_{u\phi}g_1 - \widetilde{G}_r^{-1}\widetilde{G}_0]a_0 \tag{4.31}$$

which is in the form of

$$\boldsymbol{a} = \boldsymbol{\Phi a}_0 \tag{4.32}$$

$$\boldsymbol{\Phi} = [\widetilde{\boldsymbol{G}}_r^{-1}\widetilde{\boldsymbol{K}}_{u\phi}\boldsymbol{g}_1 - \widetilde{\boldsymbol{G}}_r^{-1}\widetilde{\boldsymbol{G}}_0] \tag{4.33}$$

The matrix $\boldsymbol{\Phi}$ can now be identified as the closed loop system dynamic matrix, similar to the transition matrix of the conventional state-space control theory. With the aid of natural continuity conditions across each time step, Eq. (4.32) relates the closed loop dynamics in any time step to the initial values at any previous step and for that matter to the original initial conditions of the dynamic problem. Using the continuity condition given by Eq. (3.87) one can write

$$\begin{aligned} \boldsymbol{a}_0^{j+1} &= \boldsymbol{P\Phi a}_0^j + \boldsymbol{P}_0\boldsymbol{a}_0^j \\ &= (\boldsymbol{P\Phi} + \boldsymbol{P}_0)\boldsymbol{a}_0^j \end{aligned} \tag{4.34}$$

where $\boldsymbol{P}$ and $\boldsymbol{P}_0$ are given by Eq. (3.89). According to Eq. (4.32) we have

$$\boldsymbol{a}^{j+1} = \boldsymbol{\Phi a}_0^{j+1} \tag{4.35}$$

Hence, with Eq. (4.34) and Eq. (4.35) the dynamic response can easily be computed for any period of time. Noting also, that the simplicity both analytically and computationally of the proposed methodology as applied to linear optimal control problem under discussion should be more obvious now.

It is important to note that the methodology thus far developed is not restricted to structures with distributed actuators only. For that matter, for example if we consider discrete actuators instead of distributed ones, the optimal control inputs $\boldsymbol{b}_f^*$ corresponding to $\boldsymbol{b}_v^*$ as given by Eq. (4.24) along with the closed loop dynamic matrix $\boldsymbol{\Phi}$ would be

$$\boldsymbol{b}_f^* = -[\widetilde{\boldsymbol{R}}_v^{-1}\widetilde{\boldsymbol{B}}_r^T\widetilde{\boldsymbol{G}}_r^{-T}\widetilde{\boldsymbol{W}}]\boldsymbol{a} - [\widetilde{\boldsymbol{R}}_v\widetilde{\boldsymbol{B}}_r^T\widetilde{\boldsymbol{G}}_r^{-T}\widetilde{\boldsymbol{W}}_0]\boldsymbol{a}_0$$

$$= \boldsymbol{g}\boldsymbol{a} + \boldsymbol{g}_0\boldsymbol{a}_0 \tag{4.36}$$

$$\boldsymbol{\Phi} = [\widetilde{\boldsymbol{G}}_r^{-1}\widetilde{\boldsymbol{B}}_r\boldsymbol{g}_1 - \widetilde{\boldsymbol{G}}_r^{-1}\widetilde{\boldsymbol{G}}_0] \tag{4.37}$$

4.6 Active Vibration Control of a Plate

In most practical applications, the thickness of a plate is small in comparison with its smallest lateral dimension, and hence Kirchhoff's hypothesis may be assumed to be valid. That is, tractions on surfaces parallel to the reference plane are negligibly small as compared with the inplane stresses, and inplane displacements are linear functions of z. The transverse shear deformations and rotary inertia are neglected. The transverse shear strains are also neglected i.e. $S_{31} = S_5 = 0$ and $S_{32} = S_4 = 0$. Under this assumption the inplane displacements u and v and the transverse deflection w at an arbitrary point of the plate in the x, y and z directions may be approximated by

$$\begin{aligned} u(x,y,z,t) &= -z\frac{\partial w}{\partial x} \\ v(x,y,z,t) &= -z\frac{\partial w}{\partial y} \\ w(x,y,z,t) &= w(x,y,t) \end{aligned} \tag{4.38}$$

The strains are related to the displacement field as:

$$S_1 = \frac{\partial u}{\partial x}; \quad S_2 = \frac{\partial v}{\partial y}; \quad S_6 = \frac{\partial u}{\partial y} + \frac{\partial v}{\partial x} \tag{4.39}$$

which gives

$$S_1 = -z\frac{\partial^2 w}{\partial x^2}; \quad S_2 = -z\frac{\partial^2 w}{\partial y^2}; \quad S_6 = -2z\frac{\partial^2 w}{\partial y \partial x} \tag{4.40}$$

and

$$S_3 = S_4 = S_5 = 0 \tag{4.41}$$

so, the strain vector is reduced to

$$\boldsymbol{S} = [S_1 \; S_2 \; S_6]^T \tag{4.42}$$

and hence the matrix $\boldsymbol{B}_u$ is given by for Cartesian coordinate as,

$$\boldsymbol{B}_u = \boldsymbol{L}_u \boldsymbol{U} = - \begin{bmatrix} \frac{\partial^2}{\partial x^2} \\ \frac{\partial^2}{\partial y^2} \\ 2\frac{\partial^2}{\partial x \partial y} \end{bmatrix} \boldsymbol{U}(x,y) \tag{4.43}$$

and in polar coordinates it is expressed as

$$\boldsymbol{B}_u = - \begin{bmatrix} \frac{\partial^2}{\partial r^2} \\ \frac{1}{r}\frac{\partial}{\partial r} + \frac{1}{r^2}\frac{\partial^2}{\partial \theta^2} \\ 2\left(\frac{1}{r}\frac{\partial^2}{\partial r \partial \theta} - \frac{1}{r^2}\frac{\partial}{\partial \theta}\right) \end{bmatrix} \boldsymbol{U}(r,\theta) \tag{4.44}$$

and the corresponding material elasticity matrix $\boldsymbol{C}$ after integrating over the thickness, along with the piezoelectric matrix $\boldsymbol{e}$ are given by

$$\boldsymbol{C} = \frac{Yh^3}{12(1-\nu^2)} \begin{bmatrix} 1 & \nu & 0 \\ \nu & 1 & 0 \\ 0 & 0 & \frac{1-\nu}{2} \end{bmatrix} ; \quad \boldsymbol{e}^T = \begin{bmatrix} 0 & 0 & e_{31} \\ 0 & 0 & e_{32} \\ 0 & 0 & 0 \end{bmatrix} \tag{4.45}$$

where Y is Young's modulus, ν is Poisson's ratio, h thickness of the plate. The potential operator $\boldsymbol{B}_\phi$ is given by

$$\boldsymbol{B}_\phi = \begin{bmatrix} 0 \\ 0 \\ \frac{\partial}{\partial z} \end{bmatrix} \boldsymbol{V} \tag{4.46}$$

At this point, the designer must decide upon the shapes of the assumed displacement field w and electrical potential $\boldsymbol{v}$.

In an adaptive optics system, a tip-tilt mirror is a fast steering mirror which corrects for wavefront gradient of the incoming light beam. The surface of the mirror

Property	Plexiglas	Piezo. Ceramics (PZT G1195)	Units
ρ	1.19×10^3	7.6×10^3	kg/m^3
Y	3.10×10^9	63.0×10^9	N/m^2
h	1.60×10^{-3}	100.0×10^{-6}	m
ν	0.35	0.28	
d_{31}		180×10^{-12}	m/V
d_{32}		180×10^{-12}	m/V

Table 4.1: Material Properties

has to be constantly flat. But because of the induced vibrations in the mirror's motion, some vibration mode shapes come to exist which degrade the performance of the mirror. The optimal control methodology developed previously for the regulator problem is applied for such a case.

A plexiglas square plate sandwiched between two thin piezoelectric polymers is used in the analysis. It is assumed that all four edges of the plate are simply supported. The top piezoelectric layer is divided into quarters, giving four equally segmented actuators. Figure 4.1 illustrates the plate model. Note that the separation is infinitesimally small so that it is continuously elastic, but is open-circuit electrically. It is assumed that the plate has a dimension of $0.2 \times 0.2 \times 1.6 \times 10^{-3} m^3$ and it is made of plexiglas. The piezoelectric actuator layer is made of piezoelectric polyvinylidene fluoride (PVDF) polymer with a thickness of $100 \mu m$. All material properties are summerized in Table 4.1.

Case I: Controller performance

In this case we consider the uncontrolled and the controlled response of the plate. No damping is included (be it natural or Rayleigh type). The four patches represent the actuators with four control inputs. The time-series expansion of the each single

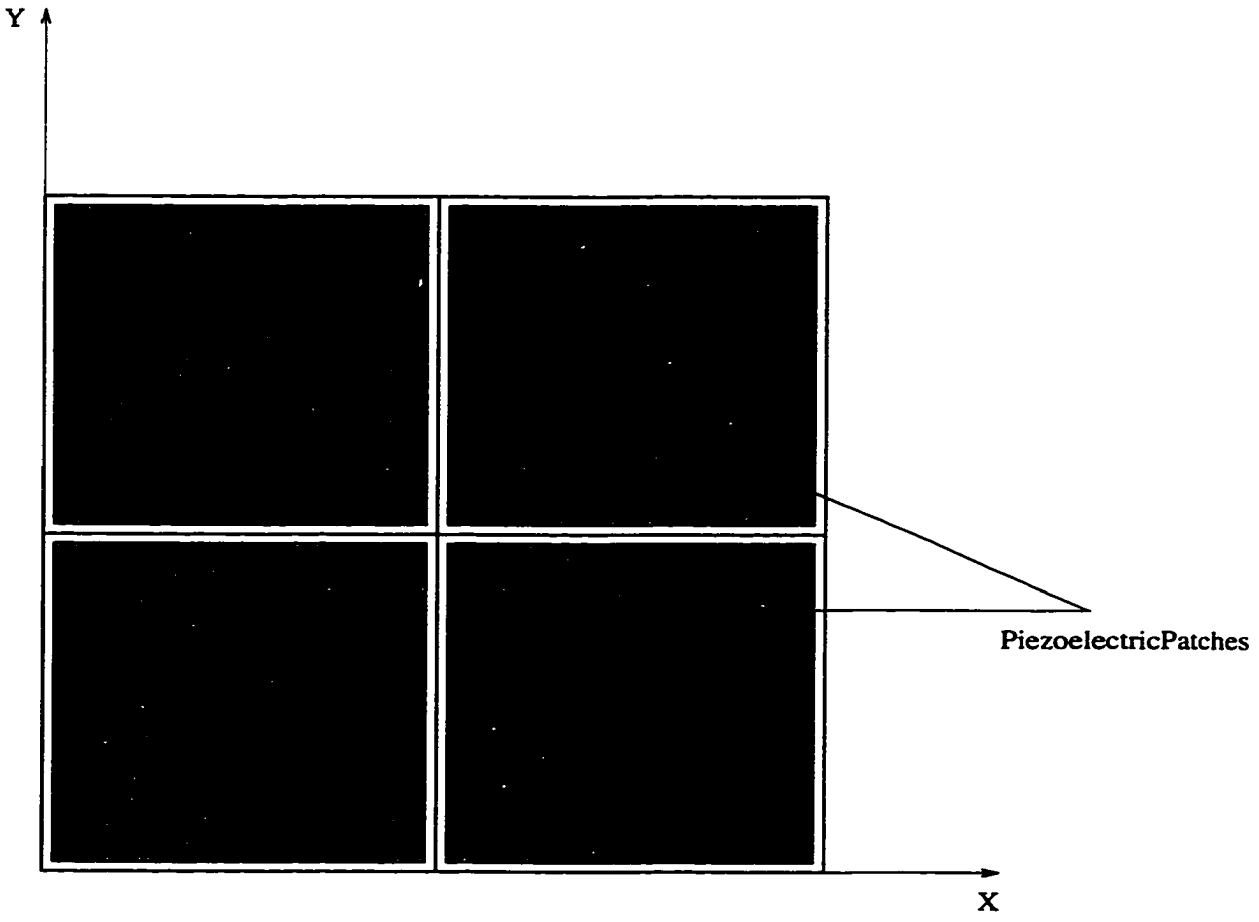

Figure 4.1: Geometry of the square plate with piezoelectrics

input is restrained to the zeroth order term in the series. Thus the simplest possible form of expansion of the inputs is chosen. With this choice, the control variable $\bar{v}$ is identified as the physical control input and by definition it is an unknown constant to be found optimally over the control period $t_0 \leq t \leq t_1$. Hence it is assumed that the control input will remain constant at its value at the beginning of each control interval. This corresponds to a zero-order hold on the physical input over a control period, a choice which would be very attractive for digital implementation.
The system matrices can be obtained following step by step the procedure given throughout this chapter.

For this case, the mode shapes for a simply supported square plate are given by

$$U_{pq} = \sin(\frac{p\pi x}{a}) \sin(\frac{q\pi y}{a}); \quad p = 1,2,3; \quad q = 1,2 \tag{4.47}$$

which is equivalent to $r = 6$ natural modes. Obviously, one can include as many modes as possible to ensure a more precise analysis of the plate vibration. However, the goal here is to study the performance of the controller designed using the direct optimal methodology, therefore, the six first modes already represent the six natural modes, further analysis was not deemed necessary.

For the generalized coordinates $\boldsymbol{q}_i$, the time-series expansion was limited to $m = 4$ equivalent to a third order fitting polynomial. The plate was given an initial disturbance (initial velocity is zero) where all the natural modes were excited with different amplitudes. For the controller, the weighting factors were chosen to be $\boldsymbol{W}_u = 1 \times 10^2$, $\boldsymbol{W}_{\dot{u}} = 2 \times 10^2$, and $\boldsymbol{R} = 1$. The sampling period was chosen to be 20 ms. With these choices, the feedback gain $\boldsymbol{g}_1$ of Eq. (4.28) was readily computed using the definitions of matrices involved via Eqs. (4.14, 4.15). We could also compute the full state feedback gain matrix $\bar{\boldsymbol{g}}$ defined by Eq.(4.29) which is for this case a 4×24 gain matrix. However, by considering the closed loop system, the 4×12 gain matrix $\boldsymbol{g}$ is

eliminated to yield an effective 4×12 gain matrix $\boldsymbol{g}_1$ for the feedback of initial states only.

Unlike the discrete system case, the gain matrix in distributed parameter systems, is not a feedback matrix of physical displacements and velocities. However, the optimal control methodology does yield a linear state feedback control in the common form after conversion of different matrices to their physical counterparts.

Figure(4.2) shows the uncontrolled and controlled responses at a specified location ($x = y = 5cm$ from the (0,0) corner) on the plate along with the control voltages time history of the four actuators.

The shape of the plate at specified time frames is shown in Figure (4.3), where we can see clearly how the controller acts to damp out the higher modes at first, dealing later with only the first modes to bring the whole structure to zero displacement at the final time. This is confirmed by the fact that the decay of any modal oscillation depends mainly on the frequency content of the mode considered. Hence, even if we have the same active damping gain (equivalent to damping ratio), the higher modes decay faster.

Case II: Effect of the initial disturbance

In this case, we study the effect of the initial condition (disturbance) on the performance of the controller leaving the weighting factors $\boldsymbol{W}_u$, $\boldsymbol{W}_{\dot{u}}$, and $\boldsymbol{R}$ the same as in the previous case (case I). For this case only one mode, namely mode (1,1) is considered.

The results of the uncontrolled and controlled responses at the center of the plate, and the time history of the input control voltages are depicted in Figure (4.4). The results show that the control effort to damp out the oscillations are lower than for the previous case, this can be explained by the fact that the oscillation amplitude has

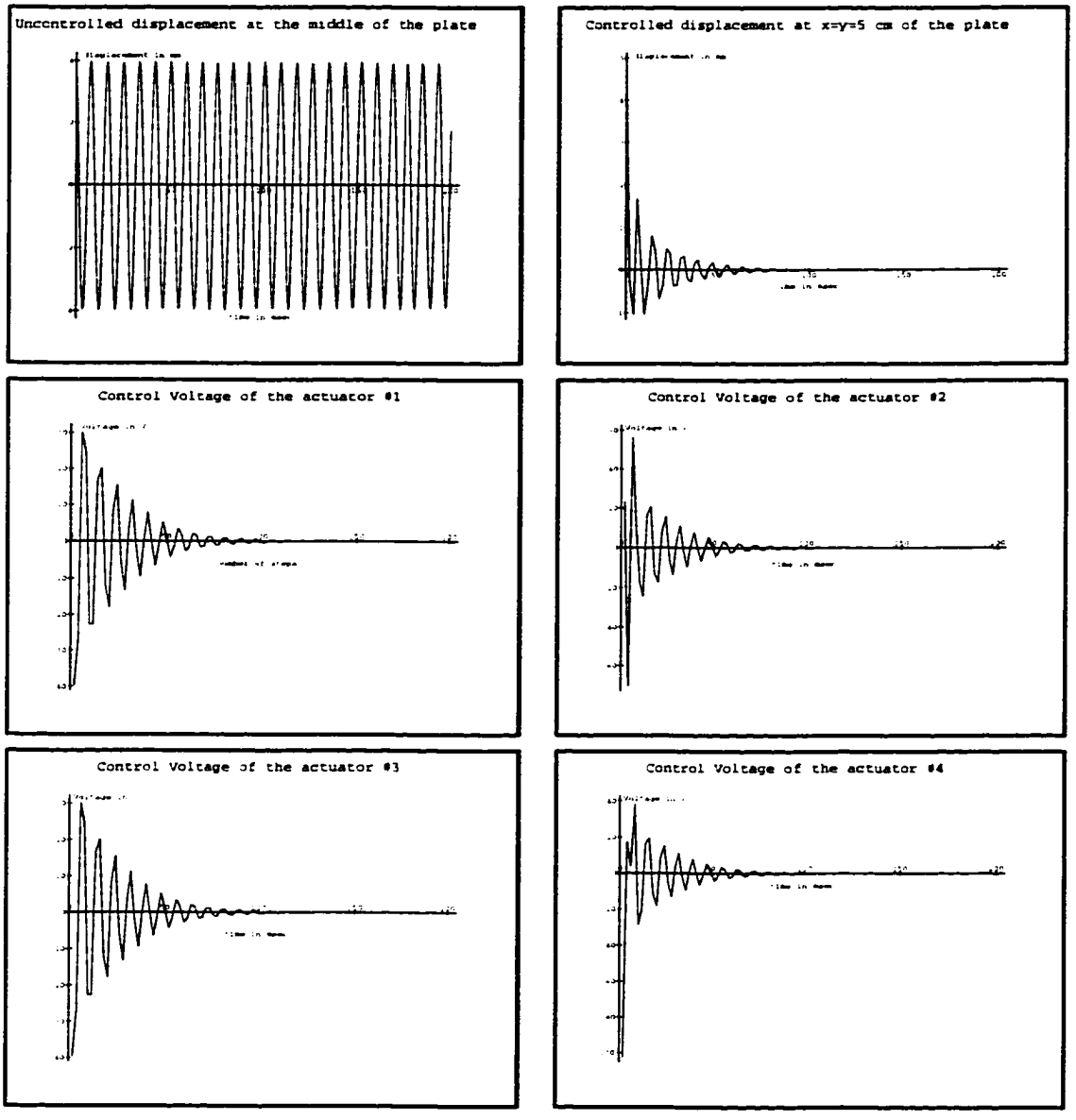

Figure 4.2: Controlled and Uncontrolled responses at point (5,5)cm of the plate, and the control voltages of the four piezoelectric patches for the controlled response; Case I

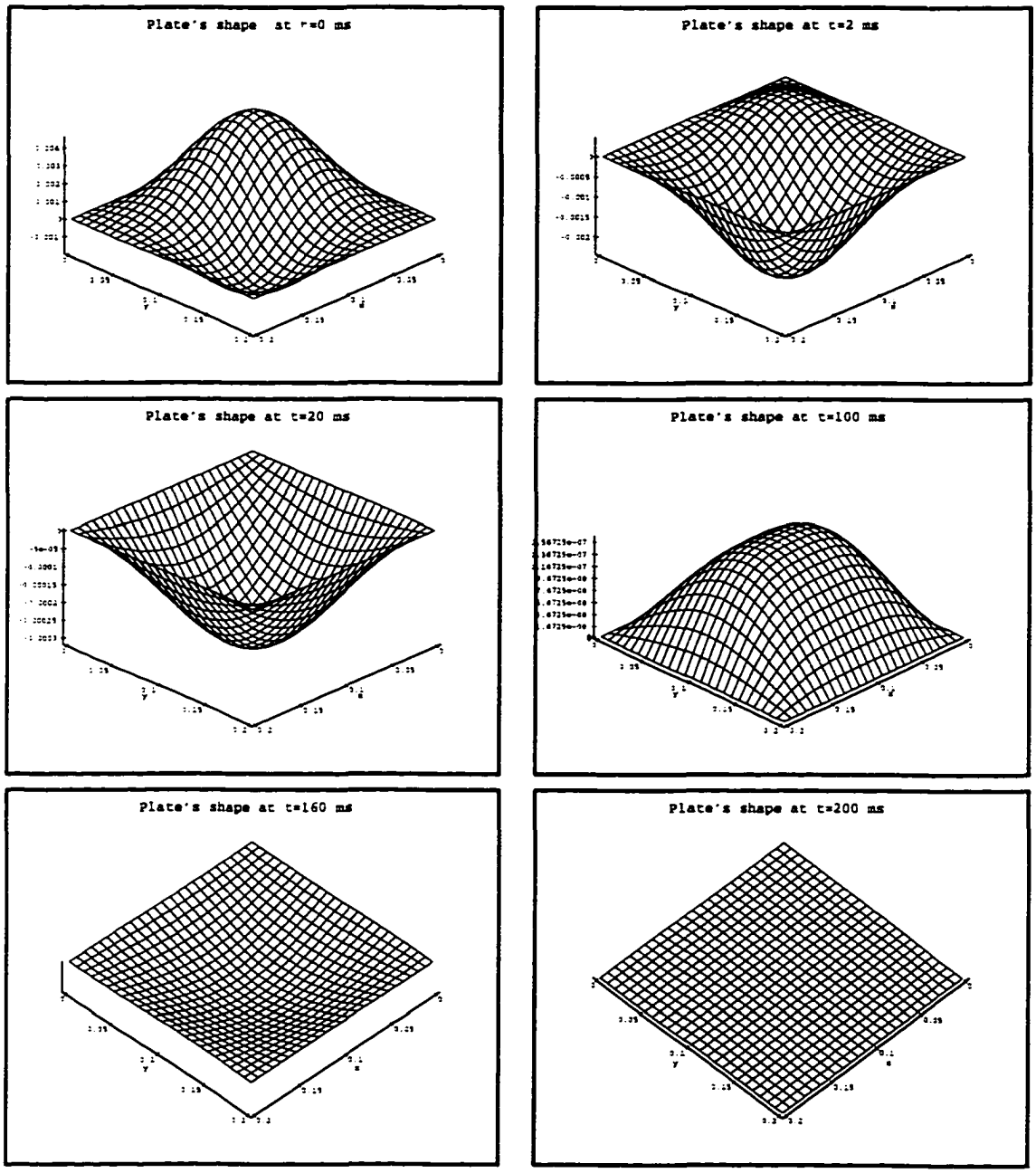

Figure 4.3: Shape of the plate at different time frames

diminished due to the absence of higher modes.

Also to be noticed, is the uniform behavior of the four actuators to act as one single actuator for such a case, this due to the single mode excitation. Clearly, this shows how the controller is trying to optimally distribute the control effort among the four actuators, leading to lower demand in input control voltages.

Case III: Effect of the weighting factors

In this case, we study the effect of the weighting factors $\boldsymbol{W}_u$, $\boldsymbol{W}_{\dot{u}}$, and $\boldsymbol{R}$ on the performance of the controller. First, only $\boldsymbol{W}_{\dot{u}}$ was set to a higher value than in the previous case, $\boldsymbol{W}_{\dot{u}} = 2 \times 10^3$, whereas $\boldsymbol{W}_u$ and $\boldsymbol{R}$ remain the same as in case I. Figure (4.5) shows the uncontrolled and the controlled responses at the center of the plate, along with the time history of the control voltages of the four actuators.

In this case, the oscillations are damped very quickly as compared to case I, but the price to pay for that results in higher voltages to drive the actuators to such performance of the controller. In another attempt -not shown here- to study the effect of $\boldsymbol{W}_u$ on the performance of the controller, it was noticed that, the factor $\boldsymbol{W}_{\dot{u}}$ has a predominant effect on the controller performance. This is due to the fact that the control efforts (moments) induced in the segmented distributed actuator counteract the motion of one half and augment the motion in the other half of the displacement feedback control cycle. However, the control efforts (moments) always counteract the oscillation in the velocity feedback control. Furthermore, higher gains give better control effects. However, in practice, the total feedback voltage is restricted by a breakdown voltage, usually $10 - 30V/\mu m$ (d.c./a.c. voltage), for piezoelectric PVDF polymers. Besides, a sudden change of high voltages resulting from higher control gains could cause unstable oscillations.

Case IV: Effect of the actuator area size

In this example, the actuators area is changed from covering the total palate's area Ω to $\frac{\Omega}{2}$, $\frac{\Omega}{3}$, and $\frac{\Omega}{4}$. Figure (4.6) shows the controlled response at the center of the plate with the input control voltage of actuator # 1 only, since only one mode is in effect. The weighting factors $\boldsymbol{W}_u$, $\boldsymbol{W}_{\dot{u}}$, and $\boldsymbol{R}$ remain unchanged throughout each area case.

It is observed that the control effect decreases as the effective actuator area shrinks. This is due to the effective control line moments reduces as the effective area becomes smaller.

4.7 Concluding Remarks

The optimal control law introduced here represents a global optimum for the the time interval $(t_0,\ t_1)$. In a time-marching solution for an arbitrary length of time, it localizes to the time slice $(t_0,\ t_1)$. Certainly one may be concerned that the control policy generated for an arbitrary period by time-marching of local controls may not be globally optimal. Such concerns should be overridden by simplicity and computational efficiency with which locally optimal direct controls can be obtained by the method proposed in this chapter. Furthermore, the global optimality of solutions of the linear quadratic regulator theory for arbitrary control periods is only subjective and not necessarily desirable for all control tasks and the traditional theory merely serves as an elegant mathematical means of generating control laws. It is this latter feature that makes it more valuable to the control designer rather than its global optimality. From this perspective, the feedback control gain matrix $\bar{\boldsymbol{g}}$ of the direct method obtained as a non-algorithmic solution to the control problem should be an attractive alternative to traditional indirect approach which uses differential equations and culminates in Riccati equations.

To recapitulate, a direct method of optimal feedback control via Hamilton's law is developed and illustrated. The method yields closed form solutions for feedback control gains by optimizing a quadratic regulator performance measure. The novel feature of the method is that the control and response problems are cast in the form of algebraic equations instead of traditional differential equations. Consequently, the technique developed here has the potential to yield solutions to control problems in a general, yet simple, straightforward, computationally efficient manner. The case in point is the subject of this chapter: The form of the solution we developed is equally applicable to both time-variant and time-invariant linear distributed parameter systems, and furthermore, in the proposed method no Riccati equations -or alike- were encountered.

Applied to active vibration control, the direct methodology offers an alternative method of analysis and simulation of stuctural dynamics. For the example studied, it was found that the control effect decreases as the weighting factors decrease. The control effect also decreases as the actuator effective area is reduced.

Since the lower modes are more important than the higher modes in structural monitoring and control, only lower modes are considered in this study.

Higher feedback gains generally lead to better control effects. However, in practice, the highest feedback voltage is restricted by a breakdown voltage, around $10 - 30\ V/\mu m$ (d.c./a.c. voltage) for piezoelectric PVDF polymers. In addition, an abrupt change of feedback control resulting from high feedback gains could introduce unstable oscillations.

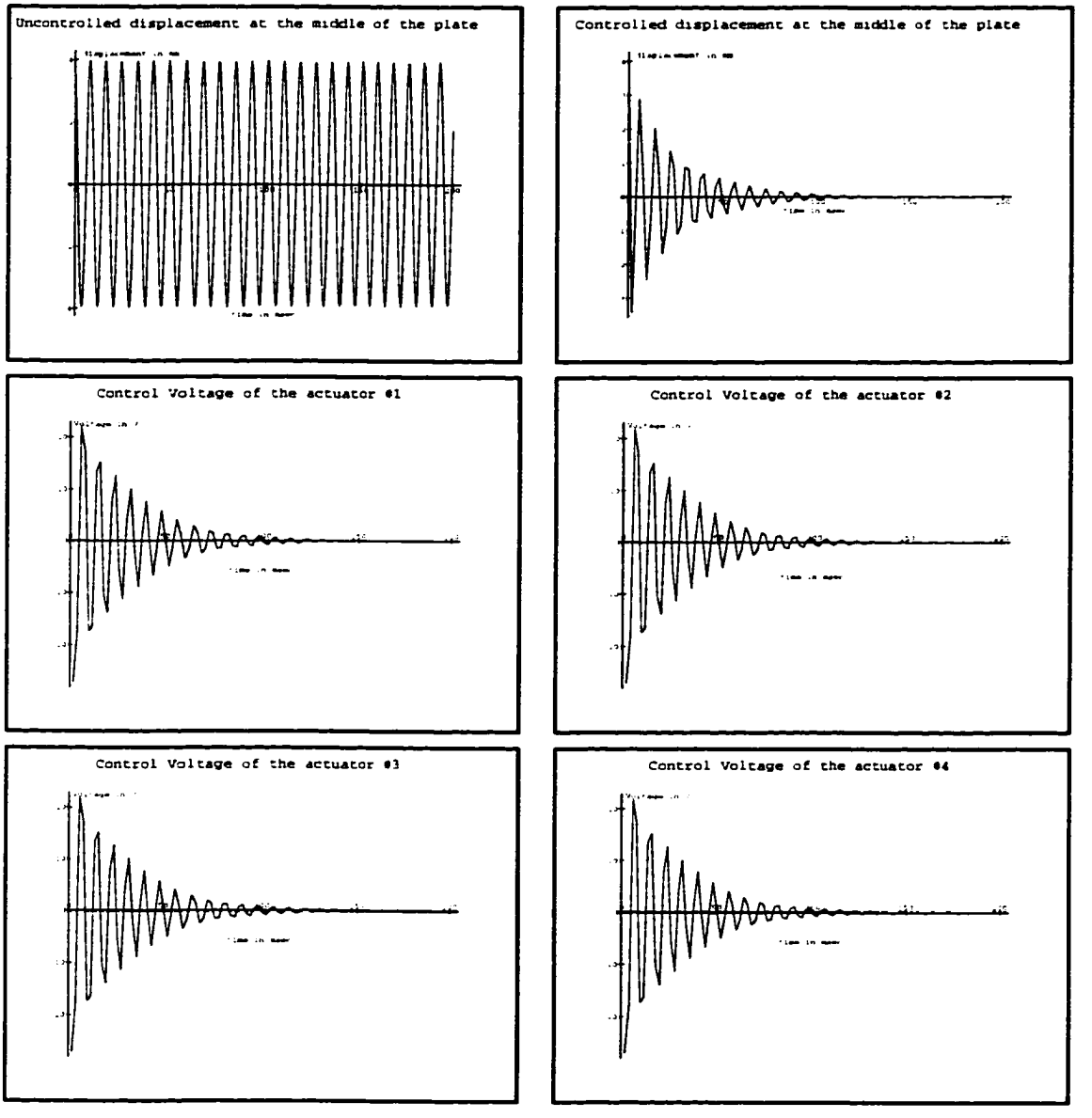

Figure 4.4: Controlled and Uncontrolled Displacements at the middle of the plate, and the control voltages of the four actuators; Case II

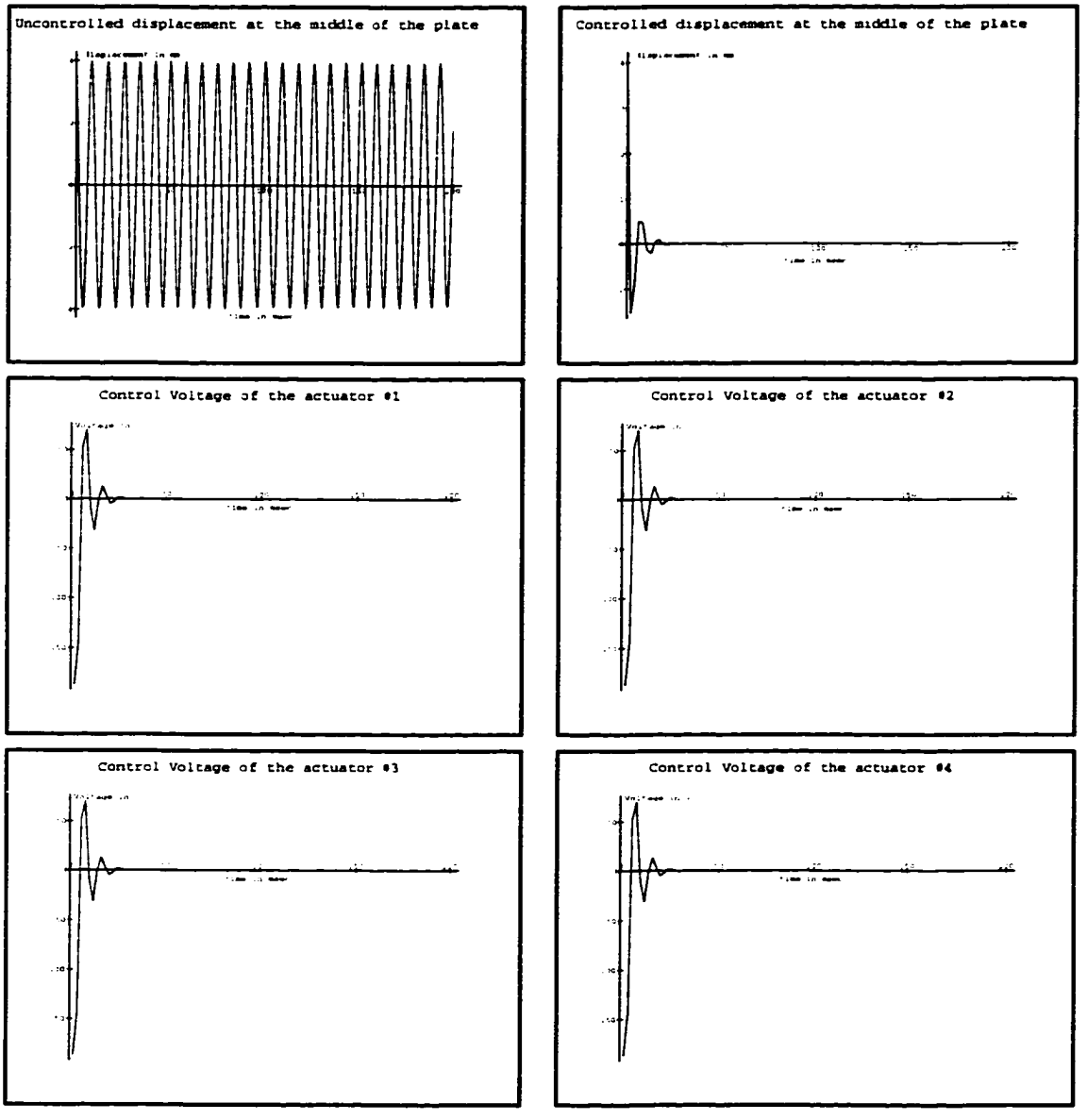

Figure 4.5: Controlled and Uncontrolled Displacements at the middle of the plate, and the control voltages of the four actuators; Case III

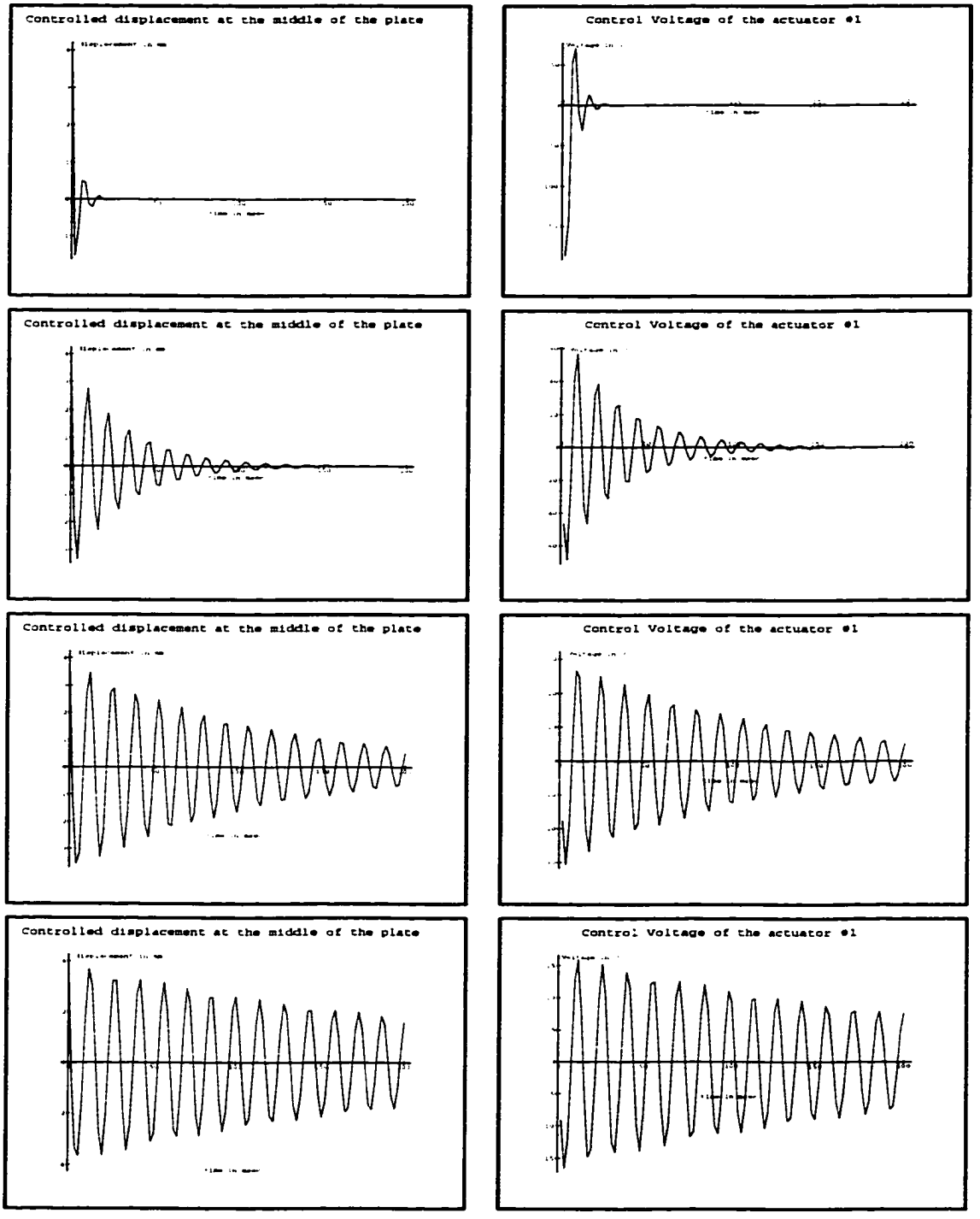

Figure 4.6: Controlled Displacement at the center of the plate, and the control voltages; Case IV

Chapter 5

Direct Optimal Shape Control

5.1 Direct Optimal Tracking Control

In this chapter, the tracking control problem is envisaged, particularly, the focus is on finding an optimal control law for configurating a surface to a desired shape in time and space. The main application of this control law is to control a deformable mirror used in adaptive optics where the surface of the mirror has to be configured to the shape of the light wavefront. The problem considered is: Given the shape of the wavefront in time and space, find the optimal control law to configure the surface of the deformable mirror to the desired surface (wavefront shape).

The direct optimal regulator problem was presented in the preceding chapter, for which the optimal solution was obtained given the algebraic state equations. For targeting a surface configuration in space and time, the previous formulation need to be reconsidered and modified as necessary. Hence the general tracking problem is considered.

In a similar manner as previously symbolised, the performance measure for linear

optimality problems we consider is given by

$$J = \frac{1}{2}\int_{t_i}^{t_f}\left\{\int_V \left[(\boldsymbol{u}-\hat{\boldsymbol{u}})^T\boldsymbol{W}_u(\boldsymbol{u}-\hat{\boldsymbol{u}}) + (\dot{\boldsymbol{u}}-\dot{\hat{\boldsymbol{u}}})^T\boldsymbol{W}_{\dot{u}}(\dot{\boldsymbol{u}}-\dot{\hat{\boldsymbol{u}}}) + \boldsymbol{v}^T\boldsymbol{R}\boldsymbol{v}\right] dV\right\} dt \quad (5.1)$$

where $\hat{\boldsymbol{u}}$ denotes the prescribed configuration in space and time (or simply the prescribed trajectory) for the generalized displacement vector $\boldsymbol{u}$. $\boldsymbol{W}_u$ and $\boldsymbol{W}_{\dot{u}}$ are real, symmetric, positive definite weight matrices for $\boldsymbol{u}$ and $\dot{\boldsymbol{u}}$ respectively, $\boldsymbol{R}$ is a real, symmetric, positive semidefinite weight matrix for the control $\boldsymbol{v}$. The subscript t of J_t in Eq. (5.1) designates that the integrand is in terms of the actual time variable t.

5.2 Prescribed Trajectories

The prescribed vector of desired trajectories for tracking is given by

$$\hat{\boldsymbol{u}} = [\hat{u}\ \hat{v}\ \hat{w}]^T \quad (5.2)$$

these trajectories can be prescribed either analytically or as set of point data. Either way, they can be curve fitted and represented by modal expansion. More specifically, for a period of time $[t_i\ t_f]$ corresponding to a nondimensional time period [0 1] where the nondimensional time variable is τ we can write

$$\hat{\boldsymbol{u}} = \widehat{\boldsymbol{U}}(x,y,z)[\widehat{\boldsymbol{A}}(\tau)\hat{\boldsymbol{a}} + \widehat{\boldsymbol{A}}_0(\tau)\hat{\boldsymbol{a}}_0] \quad (5.3)$$

The form of the prescribed trajectory is inspired from the modal expansion (assumed modes) method presented in chapter 3. In the curve fitting process, the space and time functions could be chosen arbitrarily as long as the boundary conditions are respected. Among the choices, we can always choose $\widehat{\boldsymbol{U}}$ and $\widehat{\boldsymbol{A}}$ as

$$\widehat{\boldsymbol{U}} = \boldsymbol{U} \quad (5.4)$$

$$\widehat{\boldsymbol{A}} = \boldsymbol{A} \quad (5.5)$$

for $\widehat{A}_0$ is equal to A_0 by virtue of initial conditions. The expressions of $\widehat{U}$ and $\widehat{A}$ given by Eq. (5.4) and (5.5) will be used through out this chapter. Other choices could be used without altering the generality of the proposed method.

5.3 Objective Function

The objective function to be minimized is given by the performance measure of Eq. (5.1). To make it easier to follow, the performance measure is written in terms of nondimensional time τ and decomposed into three components as follows

$$J_t = J_u + J_{\dot{u}} + J_v \tag{5.6}$$

where each component is given by

$$J_u = \frac{\theta}{2}\int_0^1 \int_V (\boldsymbol{u}-\hat{\boldsymbol{u}})^T \boldsymbol{W}_u (\boldsymbol{u}-\hat{\boldsymbol{u}}) dV d\tau \tag{5.7}$$

$$J_{\dot{u}} = \frac{\theta}{2}\int_0^1 \int_V (\dot{\boldsymbol{u}}-\dot{\hat{\boldsymbol{u}}})^T \boldsymbol{W}_{\dot{u}} (\dot{\boldsymbol{u}}-\dot{\hat{\boldsymbol{u}}}) dV d\tau \tag{5.8}$$

$$J_v = \frac{\theta}{2}\int_0^1 \int_V \boldsymbol{v}^T \boldsymbol{R}\boldsymbol{v} dV d\tau \tag{5.9}$$

Using Eq. (5.3) and Eq. (3.26) we get

$$\boldsymbol{u}-\hat{\boldsymbol{u}} = \boldsymbol{U}[\boldsymbol{A}(\boldsymbol{a}-\hat{\boldsymbol{a}}) + \boldsymbol{A}_0(\boldsymbol{a}_0-\hat{\boldsymbol{a}}_0)] \tag{5.10}$$

$$\dot{\boldsymbol{u}}-\dot{\hat{\boldsymbol{u}}} = \boldsymbol{U}[\boldsymbol{A}'(\boldsymbol{a}-\hat{\boldsymbol{a}}) + \boldsymbol{A}'_0(\boldsymbol{a}_0-\hat{\boldsymbol{a}}_0)] \tag{5.11}$$

Substituting into Eq. (5.7), transposing, and rearranging terms, yields

$$\begin{aligned} J_u = & \frac{\theta}{2}\int_0^1 \int_V (\boldsymbol{a}-\hat{\boldsymbol{a}})^T \boldsymbol{A}^T \boldsymbol{U}^T \boldsymbol{W}_u \boldsymbol{A}(\boldsymbol{a}-\hat{\boldsymbol{a}}) dV d\tau \\ & + \frac{\theta}{2}\int_0^1 \int_V 2(\boldsymbol{a}-\hat{\boldsymbol{a}})^T \boldsymbol{A}^T \boldsymbol{U}^T \boldsymbol{W}_u \boldsymbol{U}[\boldsymbol{A}_0(\boldsymbol{a}_0-\hat{\boldsymbol{a}}_0) dV d\tau \\ & + \frac{\theta}{2}\int_0^1 \int_V (\boldsymbol{a}_0-\hat{\boldsymbol{a}}_0)^T \boldsymbol{A}_0^T \boldsymbol{U}^T \boldsymbol{W}_u \boldsymbol{A}_0(\boldsymbol{a}_0-\hat{\boldsymbol{a}}_0) dV d\tau \end{aligned} \tag{5.12}$$

Using Eq. (4.3) we can write the component J_u of the performance index J as

$$\begin{aligned} J_u &= \frac{\theta}{2}\int_0^1 [(\boldsymbol{a}-\hat{\boldsymbol{a}})^T \boldsymbol{A}^T \boldsymbol{W}_q \boldsymbol{A}(\boldsymbol{a}-\hat{\boldsymbol{a}}) + 2(\boldsymbol{a}-\hat{\boldsymbol{a}})^T \boldsymbol{A}^T \boldsymbol{W}_q \boldsymbol{A}_0(\boldsymbol{a}_0-\hat{\boldsymbol{a}}_0) \\ &+ (\boldsymbol{a}_0-\hat{\boldsymbol{a}}_0)^T \boldsymbol{A}_0^T \boldsymbol{W}_q \boldsymbol{A}_0(\boldsymbol{a}_0-\hat{\boldsymbol{a}}_0)]d\tau \end{aligned} \tag{5.13}$$

Similarly, $J_{\dot{u}}$ is written as

$$\begin{aligned} J_{\dot{u}} &= \frac{\theta}{2}\int_0^1 [(\boldsymbol{a}-\hat{\boldsymbol{a}})^T \boldsymbol{A}'^T \boldsymbol{W}_{\dot{q}} \boldsymbol{A}'(\boldsymbol{a}-\hat{\boldsymbol{a}}) + 2(\boldsymbol{a}-\hat{\boldsymbol{a}})^T \boldsymbol{A}'^T \boldsymbol{W}_{\dot{q}} \boldsymbol{A}'_0(\boldsymbol{a}_0-\hat{\boldsymbol{a}}_0) \\ &+ (\boldsymbol{a}_0-\hat{\boldsymbol{a}}_0)^T \boldsymbol{A}_0'^T \boldsymbol{W}_{\dot{q}} \boldsymbol{A}'_0(\boldsymbol{a}_0-\hat{\boldsymbol{a}}_0)]d\tau \end{aligned} \tag{5.14}$$

and

$$J_v = \frac{\theta}{2}\int_0^1 \boldsymbol{b}_v^T \boldsymbol{B}^T \boldsymbol{R}_v \boldsymbol{B} \boldsymbol{b}_v d\tau \tag{5.15}$$

Using the notation given by Eqs. (4.5), (4.6, and (4.7), we finally obtain J in the form

$$J(\boldsymbol{a}, \boldsymbol{b}_v) = \frac{\theta}{2}\left\{(\boldsymbol{a}-\hat{\boldsymbol{a}})^T \widetilde{\boldsymbol{W}}(\boldsymbol{a}-\hat{\boldsymbol{a}}) + 2(\boldsymbol{a}-\hat{\boldsymbol{a}})^T \widetilde{\boldsymbol{W}}_0(\boldsymbol{a}_0-\hat{\boldsymbol{a}}_0) + \boldsymbol{b}_v^T \widetilde{\boldsymbol{R}}_v \boldsymbol{b}_v\right\} + J_0 \tag{5.16}$$

where

$$\begin{aligned} J_0 &= \frac{\theta}{2}\int_0^1 (\boldsymbol{a}_0-\hat{\boldsymbol{a}}_0)^T \boldsymbol{A}_0'^T \boldsymbol{W}_{\dot{q}} \boldsymbol{A}'_0(\boldsymbol{a}_0-\hat{\boldsymbol{a}}_0)d\tau \\ &+ \frac{\theta}{2}\int_0^1 (\boldsymbol{a}_0-\hat{\boldsymbol{a}}_0)^T \boldsymbol{A}_0'^T \boldsymbol{W}_{\dot{q}} \boldsymbol{A}'_0(\boldsymbol{a}_0-\hat{\boldsymbol{a}}_0)d\tau \end{aligned} \tag{5.17}$$

5.4 Direct Optimal Tracking Control Statement

Given the constraint equations Eq. (4.11) along with the objective function represented by Eq. (5.16), one can state the direct optimal tracking problem formulation as follows

Direct Optimal Tracking Problem

- Minimizing: $J(\boldsymbol{a}, \boldsymbol{b}_v) = \frac{\theta}{2}\Big\{(\boldsymbol{a}-\hat{\boldsymbol{a}})^T\widetilde{\boldsymbol{W}}(\boldsymbol{a}-\hat{\boldsymbol{a}}) + 2(\boldsymbol{a}-\hat{\boldsymbol{a}})^T\widetilde{\boldsymbol{W}}_0(\boldsymbol{a}_0-\hat{\boldsymbol{a}}_0) + \boldsymbol{b}_v^T\widetilde{\boldsymbol{R}}_v\boldsymbol{b}_v\Big\} + J_0$

- Subject to : $\boldsymbol{C}(\boldsymbol{a}, \boldsymbol{b}_v) = \widetilde{\boldsymbol{G}}_r\boldsymbol{a} - \widetilde{\boldsymbol{K}}_{u\phi}\boldsymbol{b}_v + \widetilde{\boldsymbol{G}}_0\boldsymbol{a}_0 = \boldsymbol{0}$

5.5 Optimal Solution

Before proceeding into the solution, it would be useful for us to rewrite the objective function in a suitable form to facilitate the algebraic operations subsequently. For this we write

$$J = \frac{\theta}{2}[\boldsymbol{a}^T\widetilde{\boldsymbol{W}}\boldsymbol{a} + 2\boldsymbol{a}^T\widetilde{\boldsymbol{W}}_0\boldsymbol{a}_0 + \boldsymbol{b}_v^T\widetilde{\boldsymbol{R}}_v\boldsymbol{b}_v] - \theta[\boldsymbol{a}^T\widetilde{\boldsymbol{W}}\hat{\boldsymbol{a}} + \boldsymbol{a}^T\widetilde{\boldsymbol{W}}_0\boldsymbol{a}_0] + \hat{J}(\boldsymbol{a}_0, \hat{\boldsymbol{a}}, \hat{\boldsymbol{a}}_0) \quad (5.18)$$

where

$$\hat{J} = \frac{\theta}{2}[\hat{\boldsymbol{a}}^T\widetilde{\boldsymbol{W}}\hat{\boldsymbol{a}} + 2\hat{\boldsymbol{a}}^T\widetilde{\boldsymbol{W}}_0\hat{\boldsymbol{a}}_0 - 2\hat{\boldsymbol{a}}^T\widetilde{\boldsymbol{W}}_0\boldsymbol{a}_0] + J_0 \quad (5.19)$$

By inspection of Eq. (5.18), we note that the major difference between this and the corresponding optimal regulator problem is the presence of the middle term in the expression of Eq. (5.18). Therefore, the procedure for solution will be almost the same as before taking into account the differences between the two formulations.

5.5.1 Optimal Solution via Direct Substitution

Method of direct substitution introduced in chapter 3 is examined first, which uses the constraint equation Eq. (4.11) to write $\boldsymbol{a}$ as function of $\boldsymbol{b}_v$ and then injecting it

into the expression of the objective function. Hence $\boldsymbol{a}$ is eliminated from J and the resulting expression is

$$J(\boldsymbol{b}_v) = \frac{\theta}{2}\left\{\boldsymbol{b}_v^T[\boldsymbol{H}+\widetilde{\boldsymbol{R}}_v]\boldsymbol{b}_v + 2\boldsymbol{b}_v^T[\boldsymbol{H}_0\boldsymbol{a}_0]\right\} - \theta\boldsymbol{b}_v^T[\widetilde{\boldsymbol{G}}_r^{-1}\widetilde{\boldsymbol{K}}_{u\phi}]^T(\widetilde{\boldsymbol{W}}\hat{\boldsymbol{a}} + \widetilde{\boldsymbol{W}}_0\hat{\boldsymbol{a}}_0) + \bar{J}_0(\boldsymbol{a}_0, \hat{\boldsymbol{a}}, \hat{\boldsymbol{a}}_0) \tag{5.20}$$

where $\bar{J}_0(\boldsymbol{a}_0, \hat{\boldsymbol{a}}, \hat{\boldsymbol{a}}_0)$ represents all the residual terms in $\boldsymbol{a}_0$, $\hat{\boldsymbol{a}}$, and $\hat{\boldsymbol{a}}_0$, and has no effect on the optimal solution, and the objective function is reduced to a quadratic form in $\boldsymbol{b}_v$

• **Necessary Condition** to minimize $J(\boldsymbol{b}_v)$ is that

$$\frac{\partial J}{\partial \boldsymbol{b}_v} = 0$$

This gives immediately the optimal solution as

$$\hat{\boldsymbol{b}}_v^* = [\boldsymbol{H}+\widetilde{\boldsymbol{R}}_v]^{-1}\left\{[\widetilde{\boldsymbol{G}}_r^{-1}\widetilde{\boldsymbol{K}}_{u\phi}]^T(\widetilde{\boldsymbol{W}}\hat{\boldsymbol{a}} + \widetilde{\boldsymbol{W}}_0\hat{\boldsymbol{a}}_0) - \boldsymbol{H}_0\boldsymbol{a}_0\right\} \tag{5.21}$$

• **Sufficient Condition** for $\hat{\boldsymbol{b}}^*$ to correspond to a minimum is that the second partial derivative of $J(\boldsymbol{b}_v)$ with respect to $\boldsymbol{b}_v$ must be positive definite. From Eq. (4.13) we get

$$\frac{\partial^2 J}{\partial \boldsymbol{b}_v^2} = \theta[\boldsymbol{H}+\widetilde{\boldsymbol{R}}_v] \tag{5.22}$$

in which $\widetilde{\boldsymbol{R}}_v$ is positive definite since the weight matrix $\boldsymbol{R}$ is by definition. On the other hand, an inspection of Eq. (4.14) indicate the same for $\boldsymbol{H}$ too. Consequently, their sum is also positive definite. Therefore, $\frac{\partial^2 J}{\partial \boldsymbol{b}_v^2}$ is in fact positive definite. Which should clarify the existence of the inverse involved in obtaining $\hat{\boldsymbol{b}}^*$.

The optimal solution $\hat{\boldsymbol{b}}^*$ could also be written as

$$\hat{\boldsymbol{b}}_v^* = \boldsymbol{g}_1\boldsymbol{a}_0 + \hat{\boldsymbol{b}}_{v0} \tag{5.23}$$

where

$$g_1 = -[H + \widetilde{R}_v]^{-1} H_0 \tag{5.24}$$

$$\hat{b}_{v0} = [H + \widetilde{R}_v]^{-1} [\widetilde{G}_r^{-1} \widetilde{K}_{u\phi}]^T (\widetilde{W}\hat{a} + \widetilde{W}_0 \hat{a}_0) \tag{5.25}$$

A simple inspection of Eq. (5.23) reveals that in the optimal tracking solution is imbeded the optimal regulator solution. That is the first term in Eq. (5.23) corresponds to the optimal solution of the regulator problem, the second term involves contribution from both disturbance and tracking components. Note also that the gain matrix G_0 is the same as the one without tracking. The term $\hat{b}_0$ can be viewed as a reference input imposed by the prescribed trajectories and input disturbances at every interval $[t_0\ t_f]$. The gain matrix is systematically determined as soon as the system is defined and the weighting matrices are chosen. Moreover, it is computed once throughtout the total period of control time as well as the matrices of $\hat{a}$ and $\hat{a}_0$ defining the reference input.

5.5.2 Optimal Solution via Lagrange Multipliers

A different method for obtaining the optimal solution of the tracking problem, is the one in which Lagrange multipliers are used. To this end, the objective function given by Eq. (5.16) is augmeted by a the constraint equation associated with Lagrange multipliers. Lagrange multiplier vector λ is averaged over the period of time $[t_0\ t_f]$. Thus the extended objective function is written as

$$J_a(a, b_v) = J(a, b_v) + \theta \lambda^T C(a, b_v) \tag{5.26}$$

Necessary conditions for optimality are:

$$\frac{\partial J_a}{\partial b_v} = 0; \quad \frac{\partial J_a}{\partial a} = 0; \quad \frac{\partial J_a}{\partial \lambda} = 0 \tag{5.27}$$

Carrying out the required operations, the first and second conditions yield

$$\boldsymbol{b}_v = \widetilde{\boldsymbol{R}}_v^{-1}\widetilde{\boldsymbol{K}}_{u\phi}^T\boldsymbol{\lambda} \tag{5.28}$$

$$\boldsymbol{\lambda} = -\widetilde{\boldsymbol{G}}_r^{-T}[\widetilde{\boldsymbol{W}}(\boldsymbol{a}-\hat{\boldsymbol{a}}) + \widetilde{\boldsymbol{W}}_0(\boldsymbol{a}_0-\hat{\boldsymbol{a}}_0)] \tag{5.29}$$

The last condition simply recovers the constraint equations. Substituting Eq. (5.29) into Eq. (5.28), the optimal solution is obtained:

$$\begin{aligned}\hat{\boldsymbol{b}}_v^* &= -[\widetilde{\boldsymbol{R}}_v^{-1}\widetilde{\boldsymbol{K}}_{u\phi}^T\widetilde{\boldsymbol{G}}_r^{-T}]\left\{\widetilde{\boldsymbol{W}}(\boldsymbol{a}-\hat{\boldsymbol{a}}) + \widetilde{\boldsymbol{W}}_0(\boldsymbol{a}_0-\hat{\boldsymbol{a}}_0)\right\} \\ &= \boldsymbol{g}(\boldsymbol{a}-\hat{\boldsymbol{a}}) + \boldsymbol{g}_0(\boldsymbol{a}_0-\hat{\boldsymbol{a}}_0)\end{aligned} \tag{5.30}$$

The positive definitness of $\widetilde{\boldsymbol{G}}_r$ insures for $\hat{\boldsymbol{b}}^*$ to be minimum. The form of the optimal solution thus obtained which is of linear state feedback form, is different from the one obtained by direct substitution. This difference is merely one of an algebraic operation. However, using Eq. (5.21) will prove to be much more practical in simulating the closed loop system and implementation of the control law since it is function of the initial states only.

5.5.3 Optimal Gains and Physical Controls

The physical controls can be obtained in the same way as prviously done for the case of optimal regulator problem. Reconsidering the physical control voltages given by Eq. (5.31)

$$\boldsymbol{\phi}^*(\tau) = \boldsymbol{B}_v(\tau)\hat{\boldsymbol{b}}^*$$

along with Eqs. (5.23), (5.30) restated as

$$\begin{aligned}\hat{\boldsymbol{b}}_{v1}^* &= \boldsymbol{g}_1\boldsymbol{a}_0 + \hat{\boldsymbol{b}}_0 \\ \hat{\boldsymbol{b}}_{v2}^* &= \boldsymbol{g}(\boldsymbol{a}-\hat{\boldsymbol{a}}) + \boldsymbol{g}_0(\boldsymbol{a}_0-\hat{\boldsymbol{a}}_0)\end{aligned}$$

the physical controls can be obtained as

$$\phi(\tau) = \bar{K}(\bar{a} - \bar{\tilde{a}}); \quad \phi(\tau) = K_1 a_0 \tag{5.31}$$

which gives

$$K_1(\tau) = B_v(\tau) g_1; \quad \bar{K}(\tau) = B_v(\tau)\bar{g} \tag{5.32}$$

with

$$\bar{g} = [g_0 \; g] \tag{5.33}$$

$\bar{K}$ and K_1 are the actual feedback matrices which will be time dependent if B_v is τ dependent. Note that the possible time dependency of the feedback gains $\bar{K}$ (or K_1) is implicit through the assumed-time modes, however the actual gain computations are done only for the matrix g_1 (or $\bar{g}$). The optimal control law Eqs. (5.31), (5.31) represent a global optimium for the time interval $[t_i \; t_f]$. In a time-marching solution for an arbitrary length of time, it localizes to the time slice $(t_f - t_i)$. One may be concerned that the control policy generated for an aribtrary period by time-marching of local controls may not be globally optimal. However, the simplicity and computational efficiency here should override such concerns. Moreover, noting that the feedback control gain matrix G of the direct approach is obtained as non-algorithmic solution to the optimal control problem, it should be an attractive alternative to traditional indirect approach which culminates in Riccati equations.

5.5.4 Concluding Remarks

As was done with the optimal regulator problem, the optimal tracking problem is not restricted only to stuctures having distributed actuators. For a structure with discrete actuators the optimal solution, and consequently optimal gains can be obtained by

simple substitution of the matrix $\widetilde{B}_r$ in lieu of $\widetilde{K}_{u\phi}$ for different gain calculation as in the optimal solution given by Eq. (5.30) we can get

$$\begin{aligned} \hat{b}_f^* &= -[\widetilde{R}_v^{-1}\widetilde{B}_r^T\widetilde{G}_r^{-T}]\left\{\widetilde{W}(a-\hat{a})+\widetilde{W}_0(a_0-\hat{a}_0)\right\} \\ &= g(a-\hat{a})+g_0(a_0-\hat{a}_0) \end{aligned} \tag{5.34}$$

Another important point pertaining to the actuator placement index. Given the optimal control gain matrix g_1 (or $\bar{g}$), one can always check the singular values of this matrix to exclude the corresponding mode from the model, leading to computationally more efficient control system.

5.6 Tracking Control of a Deformable Mirror

A circular bimorph deformable mirror is considered in this study. The mirror's diameter is 60 mm, however the optically active area has a diameter of 30 mm. The total mirror's thickness is 1 mm. The mirror is considred simply supported at the edge (i.e at its r=30 mm) and has six electrodes in the back, one central electrode and five peripheral ones, see Figure (5.1). In this study, Zernike polynomials up to ten modes with different amplitudes are chosen to be the desired shape of the mirror. Outside the optically active area, the mode shapes considered satisfy the simply supported boundary condition of the mirror, these mode shapes are also enforced with continuity conditions at the interface, these include displacement, slope and moment continuities at $r = 15\ mm$.

The displacement field w, within an optically active area is also represented by Zernike polynomials. However the total area of the mirror goes beyond this optically active area. It is important to choose the optically active area of the deformable mirror within normalized dimensions less than unity. This choice is necessary to

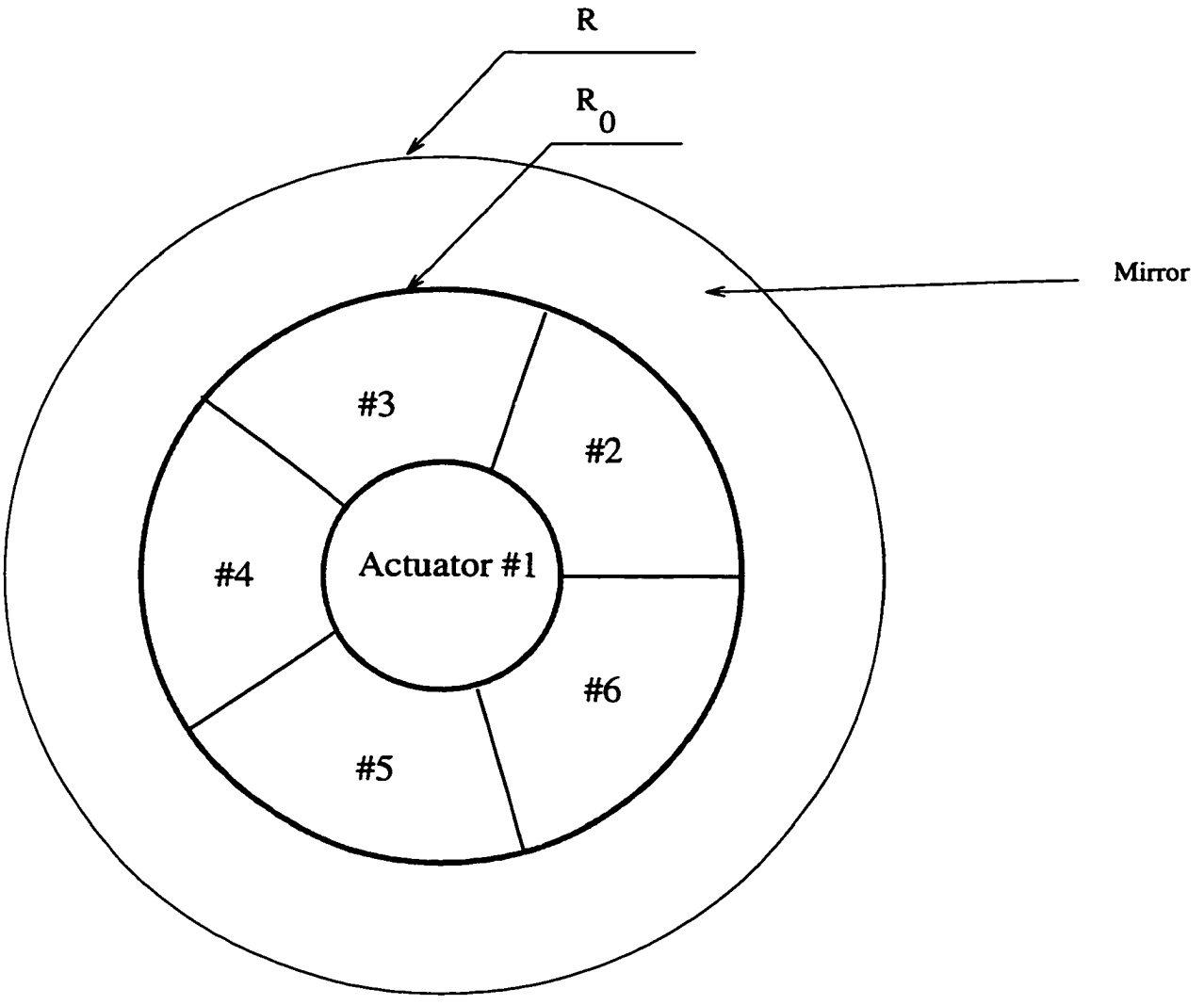

Figure 5.1: Bimorph mirror with sixe electrodes

accommodate the Zernike polynomials, which generally have nonzero or spatially varying values at the edge and at the same time account for the boundary conditions at the support points of the mirror. Therefore for circular mirror with a radius R, we have

$$w(r,\theta,t) = \begin{cases} w_1(r,\theta) = \boldsymbol{U}_1(r,\theta)\boldsymbol{q}(t); & \text{inside the aperture} \\ w_2(r,\theta) = \boldsymbol{U}_2(r,\theta)\boldsymbol{\eta}(t); & \text{outside the aperture} \end{cases} \tag{5.35}$$

$U_{1i} = Z_i$ and $\boldsymbol{q}$ represents the Zernike coefficients, and U_{2i} are given;

$$U_{21} = ln\left(\frac{r}{R}\right) \tag{5.36}$$

$$U_{22} = 1 - \left(\frac{r}{R}\right)^2 \tag{5.37}$$

$$U_{23} = \left(\frac{r}{R}\right)^2 \left[1 - \left(\frac{r}{R}\right)^2\right] \tag{5.38}$$

In addition to the specified displacements boundary conditions, the displacements, w_1 and w_2, must satisfy the natural continuity conditions at the aperture boundaries . i.e at $r = R_0$.

$$w_1(R_0,\theta,t) = w_2(R_0,\theta,t) \tag{5.39}$$

$$\left.\frac{\partial w_1}{\partial r}\right|_{R_0} = \left.\frac{\partial w_2}{\partial r}\right|_{R_0} \tag{5.40}$$

$$\left.\frac{\partial^2 w_1}{\partial r^2}\right|_{R_0} = \left.\frac{\partial^2 w_2}{\partial r^2}\right|_{R_0} \tag{5.41}$$

Similarly, the potential field within the piezoceramic can be represented in terms of the voltage at the electrodes of each patch. For a K patches the potential function is approximated by

$$\boldsymbol{v} = [V_1\ V_2 \cdots\ V_K]\boldsymbol{\phi} \tag{5.42}$$

where

$$V_i = \begin{cases} (\frac{z}{h})^2 - 1; & \theta_{i1} < \theta < \theta_{i2};\ \ r_{i1} < r < r_{i2} \\ 0 & otherwise \end{cases} \tag{5.43}$$

where θ_{i1} and θ_{i2} are the angular limits of the i^{th} electrode, and r_{i1} and r_{i2} are the lower and upper radial limits of the i^{th} electrode. This shape function gives a potential function that is grounded on both surfaces of a bimorph mirror. (i.e at $z = \pm h$).

Case I: Tracking control of an environment disturbance

In this example, it is assumed that the atmosphere changes suddenly, and can be represented by a tracking trajectory -labeled trajectory # 1- (desired generalized coordinate) of the form:

$$\hat{q}_i = \exp(-\alpha\omega t)\sin(\beta\omega t) \tag{5.44}$$

where α and β are positive constants. The tracking path was sampled at a 5 ms time step, and curve fitted to a 3^{rd} order polynomial. The desired trajectory can be regarded as a set of data points through which a polynomial curve fitting will be done over each local time sub interval of length θ. The control inputs were chosen to be a zero-order hold on the physical input as in the previous chapter. Another trajectory is considered in this case where the atmosphere changes randomly in time.

For the tracking controller the weighting factors were shosen to be $\boldsymbol{W}_u = 1 \times 10^2$, $\boldsymbol{W}_{\dot{u}} = 1 \times 10^5$, and $\boldsymbol{R} = 8$. Figure (5.2) shows the prescribed trajectories and the controlled responses at the center of the mirror. The input control voltages time histories for both trajectories are depicted in Figures (5.3), (5.4). The results suggest, that wether the trajectory is a predefined time function or a randomly generated one over a period of time, the controller is still able to track it within the specified limits of the hardware used, such as input voltage limitations, and/or Digital Signal Processor limitations in terms of speed and number of bits used for quantization of the incomming signal in the process of curve fitting.

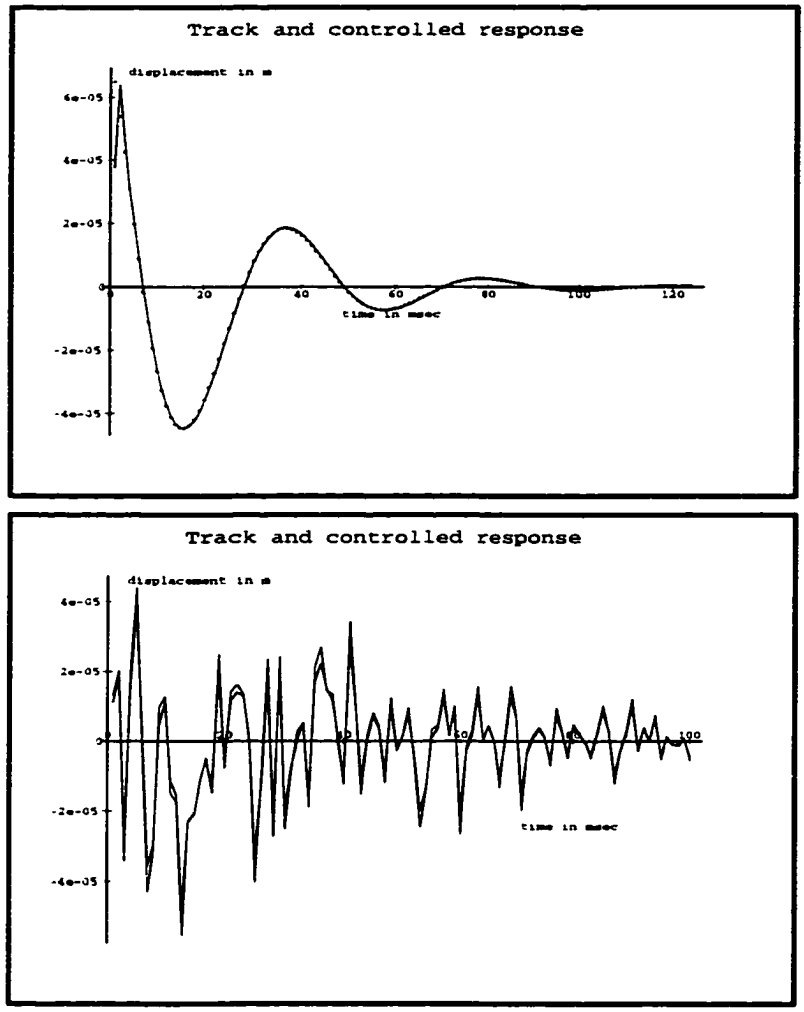

Figure 5.2: Tracking and response at the center of the mirror for two different trajectories

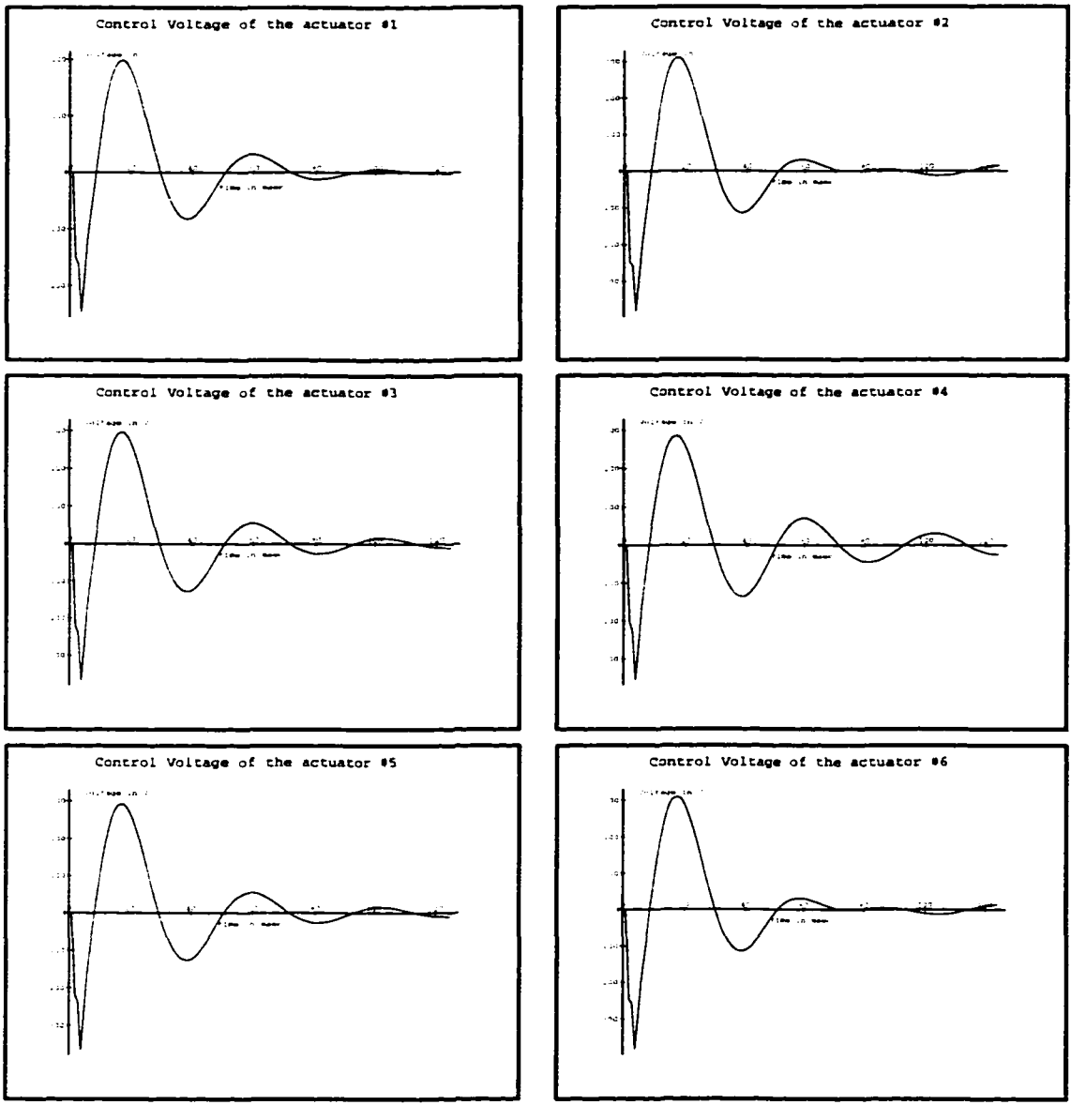

Figure 5.3: Control voltages corresponding to trajectory #1

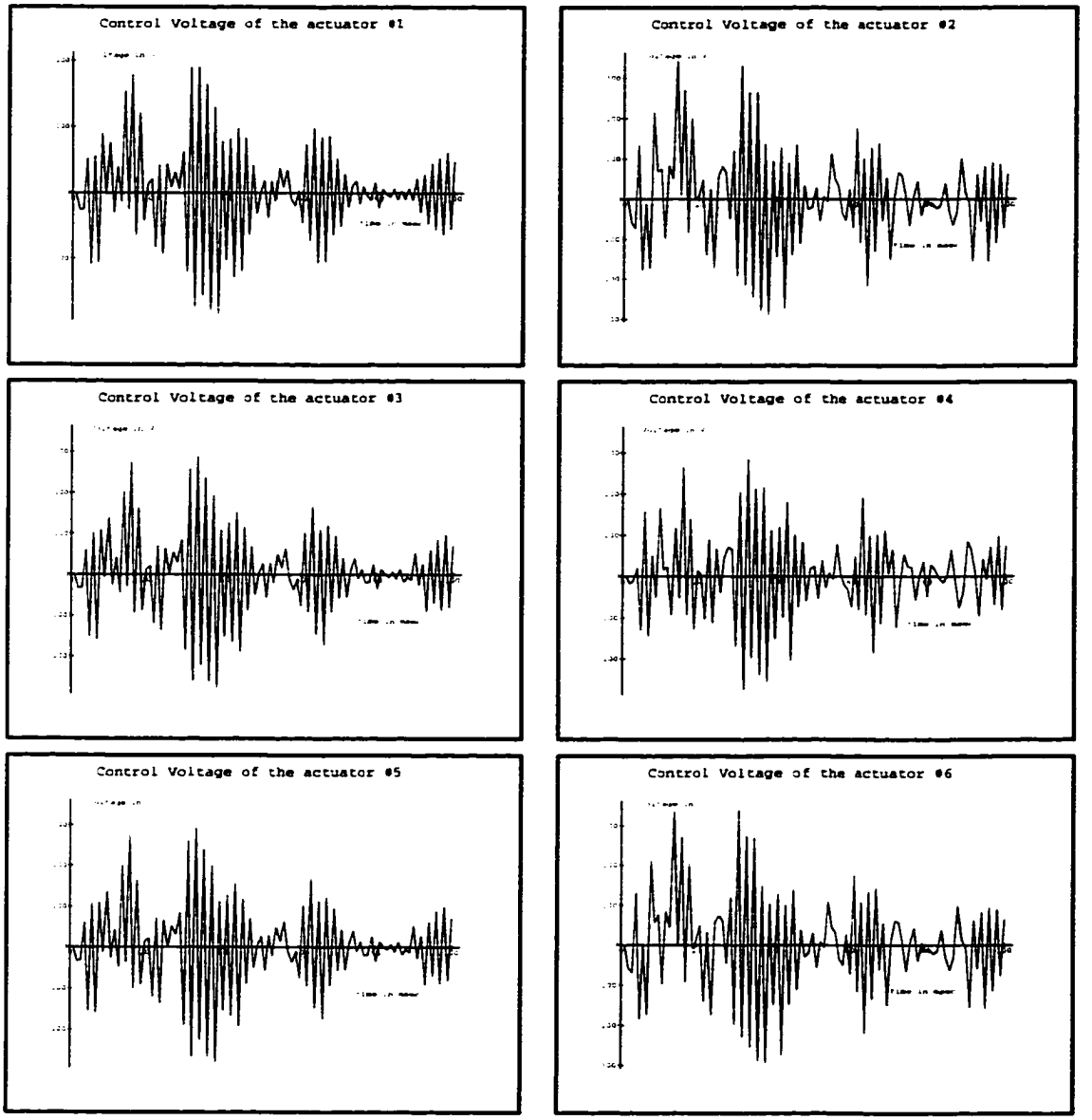

Figure 5.4: Control voltages for the randomly generated trajectory

Case II: Effect of the number of electrodes

In this case we study the effect of the number of electrodes on the number of Zernike modes to be controlled. We compared the results of two designs, in the first one we consider six (6) electrodes over the optically active area, in the second design there are seventeen (17) electrodes over the same optically active area. For both designs, we want to control ten (10) Zernike modes. Figure (5.5) shows a contour plot of the mirror's surface at different time frames for the six electrodes case. Figure (5.6) shows the contour plots of the mirror's surface at the same time frames for the seventeen (17) electrodes case.

By analysing these results, it becomes obvious that the more electrodes used the better is the accuracy of the controlled surface to match the number of Zernike modes. This can be seen from the fact that at $t = 70\ ms$ frame, the six electrodes mirror is able to control only four (4) Zernike modes, whereas the seventeen (17) electrodes one presents six (6) Zernike modes. This lead us to ask the fundamental question, how much is each mode controllable? or in other words, we need to have a controllability measure rather than asserting only if the system is controllable or not. This question, although pertaining to this study is the subject of a wide broad area in control systems of flexible structures. A controllability measure will be defined to answer this question subsequently.

The choice of the number of electrodes for each case was motivated by two effects. For the six electrode case, the number of Zernike modes to control was higher than the number of available input control voltages, in this case we are dealing with an under-determined system. For the seventeen electrodes case, we have more electrodes than modes, the system is overdetermined. In both cases, the control input is calculated

to minimize in the least square error between the desired and the controlled response for each time period. Note also, that the choice of an optimal methodology (be it direct or indirect) allows us to calculate the input control voltages without resort to pseudoinverse of the matrix $\widetilde{K}_{u\phi}$ which -as it is known- is not an exact inverse of the same matrix.

The controllability test allowed us in each simulation case to see whether the system is controllable or not. The degree of controllability of each mode was not possible using the same test procedure, namely checking the rank of the matrix $C_L = P\widetilde{G}_r^{-1}\widetilde{K}_{u\phi}$.

Controllability measure:

A controllability measure was developed using the direct methodology. The measure is represented by the condition number of the matrix Σ given by

$$\Sigma = \widetilde{G}_r^{-1}\left[\widetilde{K}_{u\phi}g_1 - \widetilde{G}_0\right] \tag{5.45}$$

The condition number by definition is the ratio of the largest singular value over the lowest singular value of the matrix Σ. This measures how far is the largest singular value to the lowest one, an indication how well is the system conditioned. It is obvious that a well conditioned system is a system which has the minimal condition number. Analyzing both 6 and 17-electrode mirrors cases, the condition number of each case was found to be 8044 for 6-electrode mirror, and 2823 for 17-electrode one. This explains well why for the latter case we have more controlled Zernike modes than the former case.

This suggests that the less controllable modes corresponding to the lowest singular values can be deleted from the model without affecting much the performance of the system. This would reduce further the system and speed up the matrices computation procedure involved in the computation of the feedback gain.

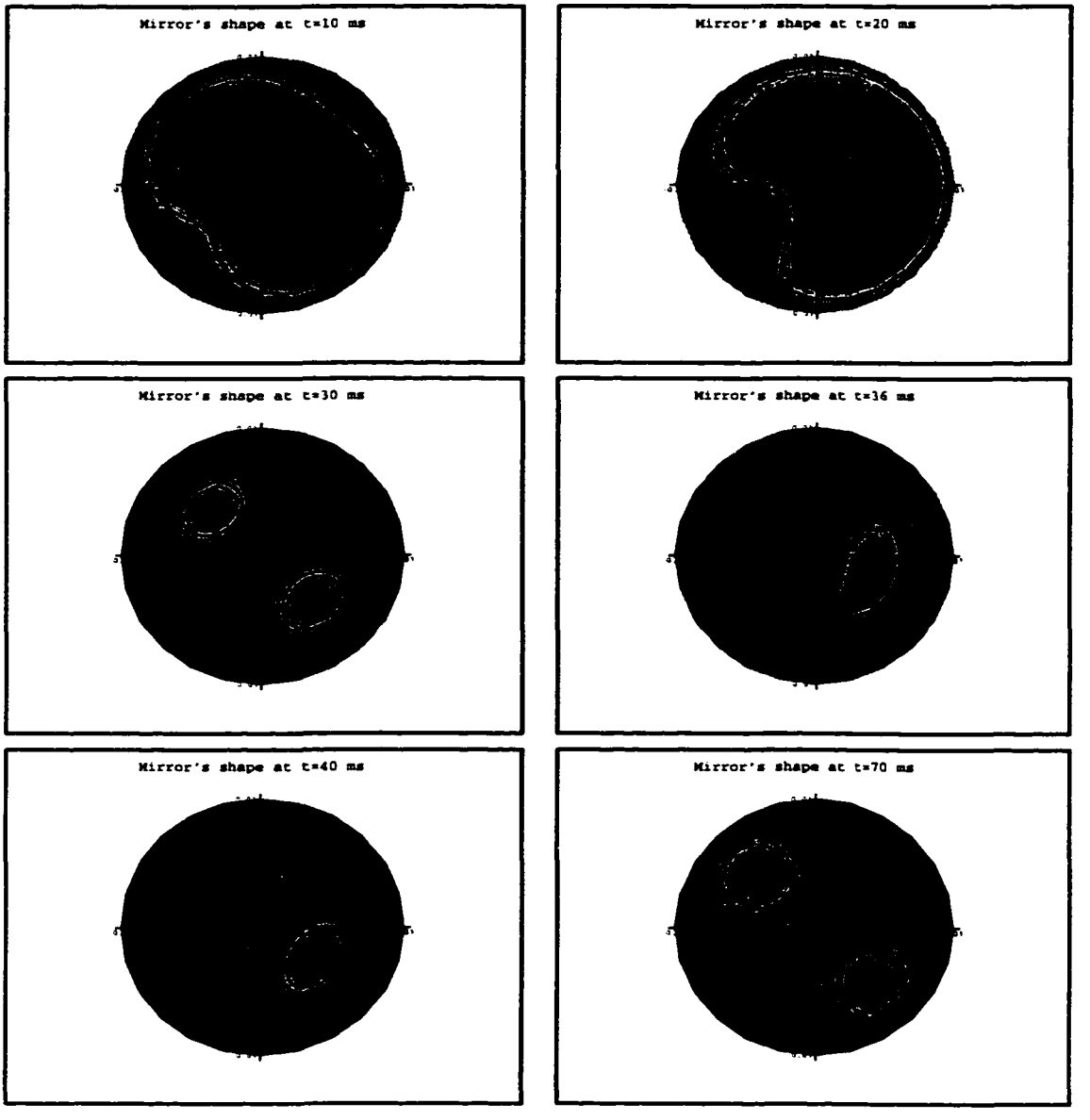

Figure 5.5: Surface shape of the mirror for 10 modes and 6 electrodes

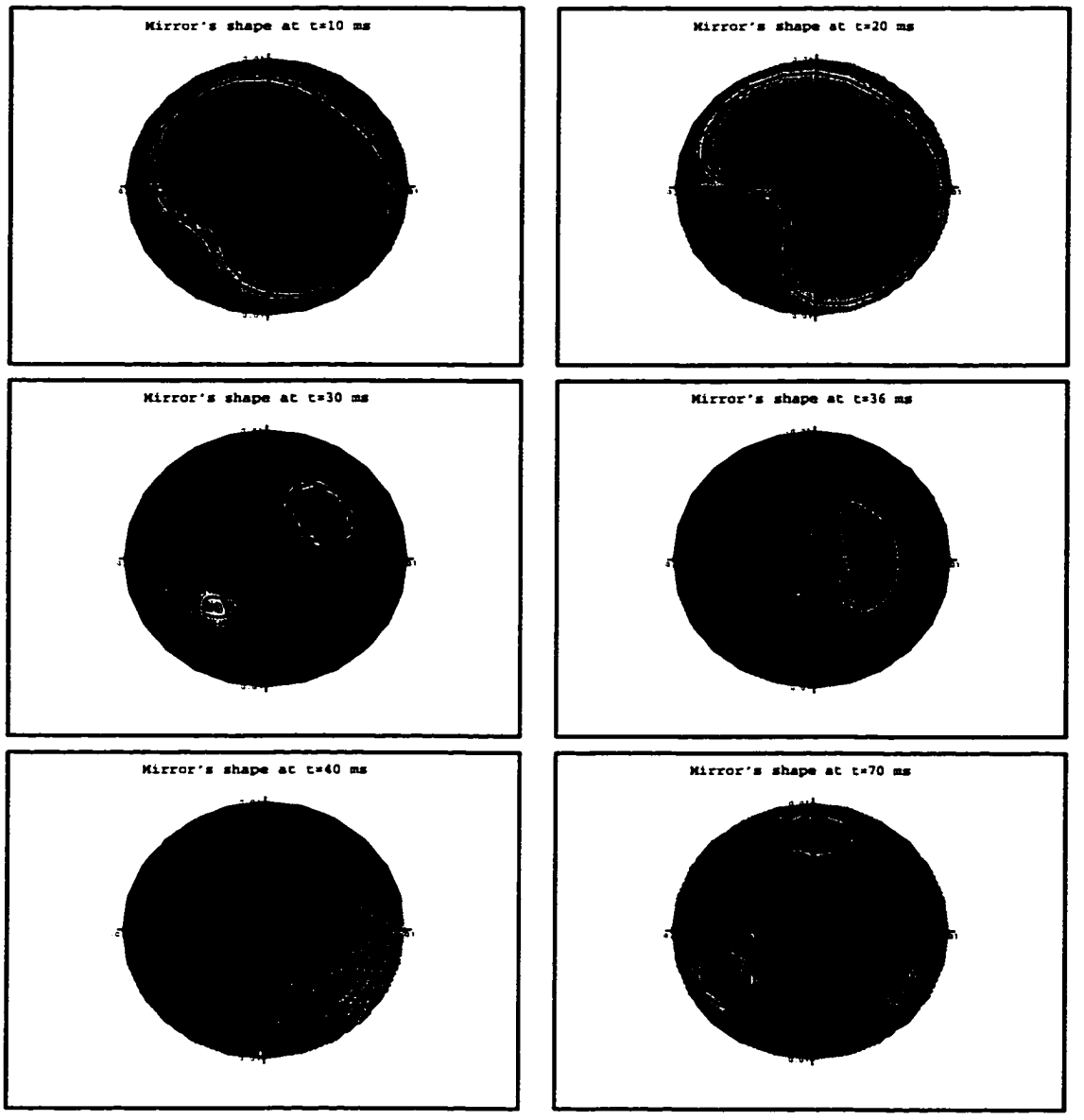

Figure 5.6: Surface shape of the mirror for 10 modes and 17 electrodes

5.7 Concluding Remarks

In this chapter, direct methodology for optimal active shape control (optimal tracking) of distributed parameter system is presented. It is seen that the representation of prescribed trajectories for coordinates in the form of polynomial curve fitting simplifies the algebra considerably. As a result, the procedures to obtain the optimal policies here are essentially the same as in the case without tracking, since the constraint equations remain the same. Hence, specific contributions of tracking to the optimal solutions can readily be identified when compared to nontracking counterparts. The tracking effect has the appearance of a reference input to the nontracking solution. Since the method reduces the optimality problem to an algebraic one, the feedback gains are obtained in a closed form, readily applicable to simulate the closed-loop system. Furthermore, the form of the solutions is equally applicable to time varying cases. The optimal tracking control laws derived here represent a global optimum for the time interval $[t_i\ t_f]$. In a time marching solution for an arbitrary length of time, they localize to the time slice $(t_i - t_f)$. One may be concerned that the control policy generated for an arbitrary period by time-marching of local controls may not be globally optimal. But the simplicity with which locally optimal direct controls can be obtained by the method proposed here has the potential to overcome such concerns in practice.

From this perspective, the feedback control gain matrices of the direct method obtained as non-algorithmic solution to the control problem may serve as an attractive alternative to the traditional indirect approaches that use differential equations and culminate in Riccati equations.

Applied to shape control of a deformable mirror, as part of an adaptive optics system, the direct methodology allowed us to simulate and have a good understanding

about the behavior of the deformable mirror in presence of different atmospheric conditions which affect the the light wavefront distortions.

The wavefront distortions were represented by Zernike polynomials where the time dependent coefficient of each mode represents the desired trajectory in time. Two cases were considered in this study, the first case simulate an abrupt change of the atmosphere, the second is totally a random trajectory. The optimal tracking controller designed using the direct methodology showed high performance in presence of any type of disturbance.

The number of electrodes controlling the bimorph mirror is an important parameter to consider in the design of such a device. It was found that, increasing number of electrodes would improve the accuracy of the desired shape, in that matter large number of electrodes allow wide spectrum of Zernike modes to be controlled.

A controllability measure was set to assess the controllability of each mode for a given mirror's design. This controllability measure is simple, straightforward and offers a new alternative to the design of deformable mirrors in terms of modal controllability.

Chapter 6

Space-Time Finite Element Formulation

In order to gain an insight to the proposed optimal control methodology, an alternative method in analyzing and evaluating the control system of distributed parameter systems which is in the same line of thought, is investigated herein.

In this chapter, instead of using modal expansion in space and time of the mechanical and electrical coordinates, a finite element discretization in both space and time is considered, from which the optimal control law is derived. The steps undertaken are the same as for the modal expansion method, precisely, first, the variables are discretized in time and space. After substitution of the discretized variables into Hamilton's Law, we derive the algebraic equations of motion. Then these equations are put in a discrete state-space from for which the optimal control law can be obtained. At the end of the chapter the case studies considered previously with the assumed mode technique are repeated here for comparison purposes.

6.1 Variational Equations

To derive the equations of motion, we use Hamilton's law of varying action (HLVA) given in chapter 3 by Eq.(3.38). All the terms included in Eq.(3.38) are given in chapter 3, so, to avoid repeating the same statements, only the final variational equation is given below.

Substituting all strain, electric displacement, virtual work terms in HLVA and taking the variation, one can derive

$$\begin{aligned}
&\int_{t_1}^{t_2} \left\{ \int_V \rho \delta \dot{\boldsymbol{u}}^T \dot{\boldsymbol{u}} dV - \int_V \left[\delta \boldsymbol{S}^T \boldsymbol{C} \boldsymbol{S} + \delta \boldsymbol{S}^T \boldsymbol{e} \boldsymbol{E} - \delta \boldsymbol{E}^T \boldsymbol{e} \boldsymbol{S} - \delta \boldsymbol{E}^T \boldsymbol{\epsilon} \boldsymbol{E} \right] dV \right. \\
&\left. - \int_V \delta \boldsymbol{u}^T \boldsymbol{P}_b dV + \int_{S_1} \delta \boldsymbol{u}^T \boldsymbol{P}_s dS - \int_{S_2} \delta \boldsymbol{\phi}^T \boldsymbol{q} dS \right\} dt \\
&= \int_V \delta \boldsymbol{u}^T \boldsymbol{p} dV \Big|_{t_1}^{t_2}
\end{aligned} \tag{6.1}$$

6.2 Finite Element Discretization

The discretization is done in both space and time domains. The domain of solution in each time step contains a set of elements in space direction and m elements in the time direction ($\Delta\tau = \tau^{(2)} - \tau^{(1)}$ is the temporal element length). The displacement $\boldsymbol{u}$, velocity $\dot{\boldsymbol{u}}$ and the applied voltage $\boldsymbol{\phi}$ are defined within the element and the momentum $\boldsymbol{p}$ is defined on the element temporal boundaries. It should be noted that the discretization of displacements and the momenta are independent. This fact ensures that there is no loss of accuracy due to the temporal differentiation. Thus,

we have the following discretization scheme.

$$\begin{aligned}
\boldsymbol{u} &= \boldsymbol{\Phi}(x,y,z)\boldsymbol{\Psi}(t)\boldsymbol{u}_s \quad ; \quad \delta\boldsymbol{u} = \boldsymbol{\Phi}(x,y,z)\boldsymbol{\Psi}(t)\delta\boldsymbol{u}_s \\
\dot{\boldsymbol{u}} &= \boldsymbol{\Phi}(x,y,z)\dot{\boldsymbol{\Psi}}(t)\boldsymbol{u}_s \quad ; \quad \delta\dot{\boldsymbol{u}} = \boldsymbol{\Phi}(x,y,z)\dot{\boldsymbol{\Psi}}(t)\delta\boldsymbol{u}_s \\
\boldsymbol{\phi} &= \boldsymbol{\Omega}(x,y,z)\boldsymbol{\Gamma}(t)\boldsymbol{\phi}_s \quad : \quad \delta\boldsymbol{\phi} = \boldsymbol{\Omega}(x,y,z)\boldsymbol{\Gamma}(t)\delta\boldsymbol{\phi}_s \\
\boldsymbol{q} &= \boldsymbol{\Theta}(x,y)\boldsymbol{\Gamma}(t)\boldsymbol{q}_s \quad ; \quad \boldsymbol{p} = \boldsymbol{\Phi}(x,y,z)\boldsymbol{p}_s \\
& \qquad\qquad ; \quad \boldsymbol{P}_s = \boldsymbol{\omega}(x,y)\boldsymbol{\gamma}(t)\boldsymbol{f}_s
\end{aligned} \tag{6.2}$$

where $\boldsymbol{\Phi}$, $\boldsymbol{\Omega}$, $\boldsymbol{\omega}$, and $\boldsymbol{\Theta}$ are matrices of spatial shape functions, and $\boldsymbol{\Psi}$, $\boldsymbol{\Gamma}$ and $\boldsymbol{\gamma}$ are matrices of temporal shape functions, $\boldsymbol{u}_s$, $\boldsymbol{\phi}_s$, $\boldsymbol{q}_s$, $\boldsymbol{P}_{cs}$, $\boldsymbol{P}_{ss}$, and $\boldsymbol{p}_s$ are vectors of the nodal variables of the structure.

Denoting u_i^j, v_i^j, and w_i^j the displacements in x, y, and z directions respectively of node i at time level j, for a structure of n space-wise nodes, the displacement vector $\boldsymbol{u}_s^j$ at time level j, and the total displacement vector $\boldsymbol{u}_s$ are as follows:

$$\boldsymbol{u}_s^j = [u_1^j, v_1^j, w_1^j, \cdots, u_n^j, v_n^j, w_n^j]^T \tag{6.3}$$

$$\boldsymbol{u}_s = [\boldsymbol{u}_s^1, \cdots \boldsymbol{u}_s^m]^T \tag{6.4}$$

where m is the number of time-wise nodes.

The strains $\boldsymbol{S}$ are defined by the first derivative of the displacement vector $\boldsymbol{u}$ through the differential operator matrix $\boldsymbol{L}_u$ [16]. The electric field vector is defined by the electric potential $\boldsymbol{\phi}$ through the gradient operator $\boldsymbol{L}_\phi$ as follows

$$\begin{aligned}
\boldsymbol{S} &= \boldsymbol{B}_u\boldsymbol{\Psi}\boldsymbol{u}_s \qquad \boldsymbol{E} = -\boldsymbol{B}_\phi\boldsymbol{\Gamma}\boldsymbol{\phi}_s \\
\boldsymbol{B}_u &= \boldsymbol{L}_u\boldsymbol{\Phi} \qquad \boldsymbol{B}_\phi = \boldsymbol{L}_\phi\boldsymbol{\Omega}
\end{aligned} \tag{6.5}$$

For a hexahedron isoparametric piezoelectric solid element with eight space-wise nodes, we have

$$\boldsymbol{B}_u = [\boldsymbol{B}_{u_1}, \ldots, \boldsymbol{B}_{u_8}] \tag{6.6}$$

$$\boldsymbol{B}_\phi = [\boldsymbol{B}_{\phi_1}, \ldots, \boldsymbol{B}_{\phi_8}] \tag{6.7}$$

Where

$$\boldsymbol{B}_{u_i} = \begin{bmatrix} \frac{\partial \Phi_i}{\partial x} & 0 & 0 \\ 0 & \frac{\partial \Phi_i}{\partial y} & 0 \\ 0 & 0 & \frac{\partial \Phi_i}{\partial z} \\ 0 & \frac{\partial \Phi_i}{\partial z} & \frac{\partial \Phi_i}{\partial y} \\ \frac{\partial \Phi_i}{\partial z} & 0 & \frac{\partial \Phi_i}{\partial x} \\ \frac{\partial \Phi_i}{\partial y} & \frac{\partial \Phi_i}{\partial x} & 0 \end{bmatrix}; \qquad \boldsymbol{B}_{\phi_i} = \begin{bmatrix} \frac{\partial \Omega_i}{\partial x} \\ \frac{\partial \Omega_i}{\partial y} \\ \frac{\partial \Omega_i}{\partial z} \end{bmatrix} \tag{6.8}$$

6.3 Equations of Motion

Using Eqs. (6.1),(6.2), and (6.5), considering the coefficients of $\delta \boldsymbol{u}^T$ and $\delta \boldsymbol{\phi}^T$ results in the system's (structure) equations of motion

$$\left(\bar{\boldsymbol{M}} - \bar{\boldsymbol{K}}_{uu}\right) \boldsymbol{u}_s - \bar{\boldsymbol{K}}_{u\phi} \boldsymbol{\phi}_s = \bar{\boldsymbol{F}}_s \boldsymbol{f}_s + \bar{\boldsymbol{G}} \boldsymbol{p}_s \tag{6.9}$$

$$\bar{\boldsymbol{K}}_{\phi\phi} \boldsymbol{\phi}_s - \bar{\boldsymbol{K}}_{u\phi}^T \boldsymbol{u}_s = \bar{\boldsymbol{Q}} \boldsymbol{q}_s \tag{6.10}$$

where the matrices present in the formulation are as follows:

$$\bar{\boldsymbol{M}} = \int_{t_1}^{t_2} \dot{\boldsymbol{\Psi}}^T \left[\sum_{Nel} \int_{V_e} \rho \boldsymbol{\Phi}^T \boldsymbol{\Phi} dV \right] \dot{\boldsymbol{\Psi}} dt = \int_{t_1}^{t_2} \dot{\boldsymbol{\Psi}}^T \boldsymbol{M} \dot{\boldsymbol{\Psi}} dt \tag{6.11}$$

$$\bar{\boldsymbol{K}}_{uu} = \int_{t_1}^{t_2} \boldsymbol{\Psi}^T \left[\sum_{Nel} \int_{V_e} \boldsymbol{B}_u^T \boldsymbol{C} \boldsymbol{B}_u dV \right] \boldsymbol{\Psi} dt = \int_{t_1}^{t_2} \boldsymbol{\Psi}^T \boldsymbol{K}_{uu} \boldsymbol{\Psi} dt \tag{6.12}$$

$$\bar{\boldsymbol{K}}_{u\phi} = \int_{t_1}^{t_2} \boldsymbol{\Psi}^T \left[\sum_{Nel} \int_{V_e} \boldsymbol{B}_u^T \boldsymbol{e}^T \boldsymbol{B}_\phi dV \right] \boldsymbol{\Gamma} dt = \int_{t_1}^{t_2} \boldsymbol{\Psi}^T \boldsymbol{K}_{u\phi} \boldsymbol{\Gamma} dt \tag{6.13}$$

$$\bar{\boldsymbol{K}}_{\phi\phi} = \int_{t_1}^{t_2} \boldsymbol{\Gamma}^T \left[\sum_{Nel} \int_{V_e} \boldsymbol{B}_\phi^T \boldsymbol{\epsilon} \boldsymbol{B}_\phi dV \right] \boldsymbol{\Gamma} dt = \int_{t_1}^{t_2} \boldsymbol{\Gamma}^T \boldsymbol{K}_{\phi\phi} \boldsymbol{\Gamma} dt \tag{6.14}$$

$$\bar{\boldsymbol{F}}_s = -\int_{t_1}^{t_2} \boldsymbol{\Psi}^T \left[\sum_{Nel} \int_{S_1} \boldsymbol{\Phi} \boldsymbol{\omega} \, dS \right] \boldsymbol{\gamma} dt \tag{6.15}$$

$$\bar{\boldsymbol{G}} = \boldsymbol{\Psi}^T \Big|_{t_1}^{t_2} \left[\sum_{Nel} \int_{V_e} \boldsymbol{\Phi}^T \boldsymbol{\Phi} dV \right] \tag{6.16}$$

$$\bar{\boldsymbol{Q}} = \int_{t_1}^{t_2} \boldsymbol{\Gamma}^T \left[\sum_{Nel} \int_{S_2} \boldsymbol{\Omega}^T \boldsymbol{\Theta} \, dS \right] \boldsymbol{\Gamma} dt \tag{6.17}$$

In Eq. (6.11-6.17) V_e is the element's volume, Nel is the number of elements in the structure, and $\bar{M}$, $\bar{K}_{uu}$, $\bar{K}_{u\phi}$, $\bar{K}_{\phi\phi}$ are respectively the mass, stiffness, electromechanical coupling, and piezoelectric capacitance matrices, and the momenta matrices of the assembled system which are written as

$$\bar{M} = \begin{bmatrix} \int_{t_1}^{t_2} \dot{\Psi}_1^T M \dot{\Psi}_1 dt & \dots & \int_{t_1}^{t_2} \dot{\Psi}_1^T M \dot{\Psi}_m dt \\ \vdots & \dots & \vdots \\ \int_{t_1}^{t_2} \dot{\Psi}_m^T M \dot{\Psi}_1 dt & \dots & \int_{t_1}^{t_2} \dot{\Psi}_m^T M \dot{\Psi}_m dt \end{bmatrix} \tag{6.18}$$

$$\bar{K}_{uu} = \begin{bmatrix} \int_{t_1}^{t_2} \Psi_1^T K_{uu} \Psi_1 dt & \dots & \int_{t_1}^{t_2} \Psi_1^T K_{uu} \Psi_m dt \\ \vdots & \dots & \vdots \\ \int_{t_1}^{t_2} \Psi_m^T K_{uu} \Psi_1 dt & \dots & \int_{t_1}^{t_2} \Psi_m^T K_{uu} \Psi_m dt \end{bmatrix} \tag{6.19}$$

$$\bar{K}_{u\phi} = \begin{bmatrix} \int_{t_1}^{t_2} \Psi_1^T K_{u\phi} \Gamma_1 dt & \dots & \int_{t_1}^{t_2} \Psi_1^T K_{u\phi} \Gamma_m dt \\ \vdots & \dots & \vdots \\ \int_{t_1}^{t_2} \Psi_m^T K_{u\phi} \Gamma_1 dt & \dots & \int_{t_1}^{t_2} \Psi_m^T K_{u\phi} \Gamma_m dt \end{bmatrix} \tag{6.20}$$

$$\bar{K}_{\phi\phi} = \begin{bmatrix} \int_{t_1}^{t_2} \Gamma_1^T K_{\phi\phi} \Gamma_1 dt & \dots & \int_{t_1}^{t_2} \Gamma_1^T K_{\phi\phi} \Gamma_m dt \\ \vdots & \dots & \vdots \\ \int_{t_1}^{t_2} \Gamma_m^T K_{\phi\phi} \Gamma_1 dt & \dots & \int_{t_1}^{t_2} \Gamma_m^T K_{\phi\phi} \Gamma_m dt \end{bmatrix} \tag{6.21}$$

$$\bar{Q} = \begin{bmatrix} \int_{t_1}^{t_2} \Gamma_1^T Q \Gamma_1 dt & \dots & \int_{t_1}^{t_2} \Gamma_1^T Q \Gamma_m dt \\ \vdots & \dots & \vdots \\ \int_{t_1}^{t_2} \Gamma_m^T Q \Gamma_1 dt & \dots & \int_{t_1}^{t_2} \Gamma_m^T Q \Gamma_m dt \end{bmatrix} \tag{6.22}$$

$$\bar{G} = \begin{bmatrix} G & \dots & 0 \\ \vdots & \dots & \vdots \\ 0 & \dots & G \end{bmatrix} = \frac{1}{\rho} \begin{bmatrix} M & \dots & 0 \\ \vdots & \dots & \vdots \\ 0 & \dots & M \end{bmatrix} \tag{6.23}$$

where M, K_{uu}, $K_{u\phi}$, $K_{\phi\phi}$, and G are the usual mass, stiffness, electromechanical coupling, and piezoelectric capacitance matrices, and the momenta matrices of the assembled system respectively. The mass matrix M and stiffness matrix K_{uu} include

both the elastic part as well as the piezoelectric part of the whole structure. The structure's matrices are defined as

$$M = \sum_{Nel} \int_{V_e} \rho \Phi^T \Phi dV \tag{6.24}$$

$$K_{uu} = \sum_{Nel} \int_{V_e} B_u^T C B_u dV \tag{6.25}$$

$$K_{u\phi} = \sum_{Nel} \int_{V_e} B_u^T e^T B_\phi dV \tag{6.26}$$

$$K_{\phi\phi} = \sum_{Nel} \int_{V_e} B_\phi^T \epsilon B_\phi dV \tag{6.27}$$

$$Q = \sum_{Nel} \int_{S_e} \Omega^T \Theta dS \tag{6.28}$$

6.3.1 Actuator Equations

The equations of motion thus obtained represent as in the assumed mode model, the actuator equation and sensor equation. Since we are merely concerned with the actuator equation in this study, this latter is analyzed more thoroughly.

The actuator equation (6.9), can be written in a more compact form as:

$$\begin{bmatrix} B_{11} & \dots & B_{1m} \\ \vdots & \dots & \vdots \\ B_{m1} & \dots & B_{mm} \end{bmatrix} \begin{Bmatrix} u_s^1 \\ \vdots \\ u_s^m \end{Bmatrix} = \begin{Bmatrix} -\mathcal{P}^1 \\ 0 \\ \mathcal{P}^m \end{Bmatrix} + \begin{Bmatrix} h^1 \\ \vdots \\ h^m \end{Bmatrix} \tag{6.29}$$

$$\begin{Bmatrix} -\mathcal{P}^1 \\ 0 \\ \mathcal{P}^m \end{Bmatrix} = \begin{bmatrix} G & \dots & 0 \\ \vdots & \dots & \vdots \\ 0 & \dots & G \end{bmatrix} \begin{Bmatrix} -p_s^1 \\ \vdots \\ p_s^m \end{Bmatrix} \tag{6.30}$$

where

$$B_{ij} = \bar{M}_{ij} - \left(\bar{K}_{uu}\right)_{ij} \tag{6.31}$$

$$h = [h^1 \dots h^m]^T = \bar{K}_{u\phi}\phi_s + \bar{F}_s f_s \tag{6.32}$$

6.3.2 Sensor Equations

The sensing procedure considered in this section deals with the determination (measurement) of the resultant voltage subject to a prescribed displacement. There are two different cases to explore, namely: *i*) when a structure is used a simultaneous sensor/actuator transducer, and *ii*) the structure is used only as a sensor.

In a general case the voltage generated as a consequence of a prescribed displacement and an applied charge is given by:

$$\boldsymbol{\phi}_s = \bar{\boldsymbol{K}}_{\phi\phi}^{-1}\left[\bar{\boldsymbol{K}}_{u\phi}^{T}\boldsymbol{u}_s + \bar{\boldsymbol{Q}}\boldsymbol{q}_s\right] \tag{6.33}$$

or in an elaborate form:

$$\begin{Bmatrix} \boldsymbol{\phi}_s^1 \\ \vdots \\ \boldsymbol{\phi}_s^m \end{Bmatrix} = \begin{bmatrix} \boldsymbol{L}_{11} & \dots & \boldsymbol{L}_{1m} \\ \vdots & \dots & \vdots \\ \boldsymbol{L}_{m1} & \dots & \boldsymbol{L}_{mm} \end{bmatrix} \begin{Bmatrix} \boldsymbol{u}_s^1 \\ \vdots \\ \boldsymbol{u}_s^m \end{Bmatrix} + \begin{bmatrix} \boldsymbol{N}_{11} & \dots & \boldsymbol{N}_{1m} \\ \vdots & \dots & \vdots \\ \boldsymbol{N}_{m1} & \dots & \boldsymbol{N}_{mm} \end{bmatrix} \begin{Bmatrix} \boldsymbol{q}_s^1 \\ \vdots \\ \boldsymbol{q}_s^m \end{Bmatrix} \tag{6.34}$$

- **Voltage measurement sensor**

In the standard piezoelectric sensor application, the voltage at the piezoelectric electrodes is measured by a high impedance amplifier which allows no current flow to and from the electrodes. The electrodes are essentially open circuited and thus the applied charge is zero $\boldsymbol{q}_s = \boldsymbol{0}$, the measured voltage in this case is used to reconstruct the mechanical state using the sensor equation Eq. (6.33)

$$\boldsymbol{\phi}_s = \bar{\boldsymbol{K}}_{\phi\phi}^{-1}\bar{\boldsymbol{K}}_{u\phi}^{T}\boldsymbol{u}_s \tag{6.35}$$

- **Charge measurement sensor**

Another important sensor application arises when a low impedance charge amplifier is attached to the piezoelectric. The electrodes are essentially shorted and thus the

voltage is zero $\boldsymbol{\phi}_s = \mathbf{0}$. This type of sensor was examined in [56]. In this case the piezoelectric strain or strain rate can be found by measuring the charge or current flowing to the electrodes. The strain is proportional to the applied current

$$\boldsymbol{q}_s = -\bar{\boldsymbol{Q}}^{-1}\bar{\boldsymbol{K}}_{u\phi}^{T}\boldsymbol{u}_s \tag{6.36}$$

6.4 Two Nodes Time Element

We consider a structure of n space-wise nodes and 2 time-wise nodes ($m = 2$),and linear polynomial in time direction, for which, the equations of motion are written as:

$$\begin{bmatrix} \boldsymbol{B}_{11} & \boldsymbol{B}_{12} \\ \boldsymbol{B}_{21} & \boldsymbol{B}_{22} \end{bmatrix} \begin{Bmatrix} \boldsymbol{u}_s^1 \\ \boldsymbol{u}_s^2 \end{Bmatrix} = \begin{Bmatrix} -\boldsymbol{\mathcal{P}}_s^1 \\ \boldsymbol{\mathcal{P}}_s^2 \end{Bmatrix} + \begin{Bmatrix} \boldsymbol{h}^1 \\ \boldsymbol{h}^2 \end{Bmatrix} \tag{6.37}$$

$$\begin{Bmatrix} -\boldsymbol{\mathcal{P}}^1 \\ \boldsymbol{\mathcal{P}}^2 \end{Bmatrix} = \frac{1}{\rho}\begin{bmatrix} \boldsymbol{M} & \mathbf{0} \\ \mathbf{0} & \boldsymbol{M} \end{bmatrix} \begin{Bmatrix} -\boldsymbol{p}_s^1 \\ \boldsymbol{p}_s^m \end{Bmatrix} \tag{6.38}$$

Transforming Eq. (6.37) into

$$\boldsymbol{x}^2 = \boldsymbol{\mathcal{H}}\boldsymbol{x}^1 + \bar{\boldsymbol{h}} \tag{6.39}$$

where

$$\begin{aligned} \boldsymbol{x}^j &= \begin{bmatrix} \boldsymbol{u}_s^j & \boldsymbol{\mathcal{P}}_s^j \end{bmatrix}^T \\ \boldsymbol{\mathcal{H}} &= \begin{bmatrix} -\boldsymbol{B}_{12}^{-1}\boldsymbol{B}_{11} & \boldsymbol{B}_{12}^{-1} \\ \boldsymbol{B}_{22}\boldsymbol{B}_{12}^{-1}\boldsymbol{B}_{11} - \boldsymbol{B}_{21} & -\boldsymbol{B}_{22}\boldsymbol{B}_{12}^{-1} \end{bmatrix} \\ \bar{\boldsymbol{h}} &= \begin{bmatrix} \boldsymbol{B}_{12}^{-1}\boldsymbol{h}^1 \\ +\boldsymbol{B}_{22}\boldsymbol{B}_{12}^{-1}\boldsymbol{h}^1 - \boldsymbol{h}^2 \end{bmatrix} \end{aligned} \tag{6.40}$$

Given the forcing terms $\boldsymbol{h}$, and knowing the generalized displacement and momenta at the initial stage $\boldsymbol{x}^1$, $\boldsymbol{x}^2$ can be obtained and the solution is evaluated step-by-step.

Note that the numerical computation of the matrices $\mathcal{H}$ and $\bar{h}$ needs to be done only once during the solution. Computationally, the inversion of B_{12} is the most intensive step during this solution procedure.

For linear polynomials in the time direction the temporal shape functions are given by

$$\tau = \frac{t - t_i}{t_f - t_i} \quad ; \quad \Delta t = t_f - t_i \tag{6.41}$$

$$\Psi_1 = \Gamma_1 = (1 - \tau) I_n; \quad \Psi_2 = \Gamma_2 = \tau I_n \tag{6.42}$$

$$\dot{\Psi}_1 = \dot{\Gamma}_1 = -\tfrac{1}{\Delta t} I_n; \quad \dot{\Psi}_2 = \dot{\Gamma}_2 = \frac{1}{\Delta t} I_n \tag{6.43}$$

The matrix B and its constituents are thus obtained by direct time integration of Eqs. (6.18 - 6.21) where $t_i \leq t \leq t_f$,

$$\bar{M} = \frac{1}{\Delta t} \begin{bmatrix} M & -M \\ -M & M \end{bmatrix}; \quad \bar{K}_{uu} = \frac{\Delta t}{3} \begin{bmatrix} K_{uu} & \frac{1}{2} K_{uu} \\ \frac{1}{2} K_{uu} & K_{uu} \end{bmatrix} \tag{6.44}$$

$$\bar{K}_{u\phi} = \frac{\Delta t}{3} \begin{bmatrix} K_{u\phi} & \frac{1}{2} K_{u\phi} \\ \frac{1}{2} K_{u\phi} & K_{u\phi} \end{bmatrix}; \quad \bar{K}_{\phi\phi} = \frac{\Delta t}{3} \begin{bmatrix} K_{\phi\phi} & \frac{1}{2} K_{\phi\phi} \\ \frac{1}{2} K_{\phi\phi} & K_{\phi\phi} \end{bmatrix} \tag{6.45}$$

where M and K_{uu} are the usual global mass and stiffness matrices of the structure respectively. The submatrices B_{ij} of B in Eq. (6.37) are then given by

$$B_{11} = B_{22} = \frac{1}{\Delta t} M - \frac{\Delta t}{3} K_{uu} \tag{6.46}$$

$$B_{12} = B_{21} = -\frac{1}{\Delta t} M - \frac{\Delta t}{6} K_{uu} \tag{6.47}$$

6.5 Optimal Control Formulation

In this section, the optimal regulator control problem is introduced first using the dynamic model obtained through the finite element discretization scheme. The ob-

jective is to control the shape of the flexible structure (mirror) so that the resulting shape is as close to the desired configuration as possible. This is done by defining an objective function (performance index) to be minimized. The performance index can be viewed as weighted sum of the mechanical energy accumulated in the system during the operation and the control effort. Particularly using the same performance index J introduced in Chapter 4, namely:

$$J = \frac{1}{2}\int_{t_i}^{t_f}\left\{\int_V \left[\boldsymbol{u}^T\boldsymbol{W}_u\boldsymbol{u} + \dot{\boldsymbol{u}}^T\boldsymbol{W}_{\dot{u}}\dot{\boldsymbol{u}} + \boldsymbol{\phi}^T\boldsymbol{R}\boldsymbol{\phi}\right] dV\right\} dt \tag{6.48}$$

where all the matrices involved are given in Chapter 4.

Using the space-time finite element approach, and considering the two nodes time element model, the control input $\boldsymbol{\phi}$ or $\boldsymbol{P}_s$ is approximated by a constant within the element which is equivalent to introducing of a *zero order holder* into the control loop. The forcing term $\bar{\boldsymbol{h}}$ is then expressed as (with $\boldsymbol{f}_s = \boldsymbol{0}$)

$$\bar{\boldsymbol{h}} = \boldsymbol{\mathcal{B}}\boldsymbol{\phi}_s = \frac{\Delta t}{2}\begin{bmatrix} \boldsymbol{B}_{12}^{-1}\boldsymbol{K}_{u\phi} \\ (\boldsymbol{B}_{22}\boldsymbol{B}_{12}^{-1} - \boldsymbol{I})\boldsymbol{K}_{u\phi} \end{bmatrix}\boldsymbol{\phi}_s \tag{6.49}$$

The resulting dynamic model is written in a discrete state space form as

$$\boldsymbol{x}^{(2)} = \boldsymbol{\mathcal{H}}\boldsymbol{x}^{(1)} + \boldsymbol{\mathcal{B}}\boldsymbol{\phi}_s \tag{6.50}$$

where the matrix $\boldsymbol{\mathcal{B}}$ is given by Eq. (6.49)

Thus, a descretized performance index can then be written as -the control inputs being $\boldsymbol{\phi}_s$-

$$J = \frac{1}{2}\sum_{j=1}^{m}\left[(\boldsymbol{x}^j)^T\boldsymbol{Q}^j\boldsymbol{x}^j + \boldsymbol{\phi}_s^T\boldsymbol{R}\boldsymbol{\phi}_s\right] \tag{6.51}$$

or in the case the control forces being $\boldsymbol{P}_s$ we get

$$J = \frac{1}{2}\sum_{j=1}^{m}\left[(\boldsymbol{x}^j)^T\boldsymbol{Q}^j\boldsymbol{x}^j + \boldsymbol{f}_s^T\boldsymbol{R}\boldsymbol{f}_s\right] \tag{6.52}$$

System Model:

$$\boldsymbol{x}_{k+1} = \boldsymbol{\mathcal{H}}\boldsymbol{x}_k + \boldsymbol{\mathcal{B}}\boldsymbol{u}_k \quad k > i$$

Performance Index:

$$J_i = \frac{1}{2}\sum_{k=i}^{m}(\boldsymbol{x}_k^T\boldsymbol{Q}_k\boldsymbol{x}_k + \boldsymbol{u}_k^T\boldsymbol{R}_k\boldsymbol{u}_k) \quad \boldsymbol{Q}_k \geq \boldsymbol{0},\ \boldsymbol{R}_k > \boldsymbol{0} \text{ and symmetric}$$

Optimal Feedback Control:

$$\boldsymbol{S}_k = \boldsymbol{\mathcal{H}}^T\left[\boldsymbol{S}_{k+1} - \boldsymbol{S}_{k+1}\boldsymbol{\mathcal{B}}(\boldsymbol{\mathcal{B}}^T\boldsymbol{S}_{k+1}\boldsymbol{\mathcal{B}} + \boldsymbol{R}_k)^{-1}\boldsymbol{\mathcal{B}}^T\boldsymbol{S}_{k+1}\right]\boldsymbol{\mathcal{H}} + \boldsymbol{Q}_k \quad \boldsymbol{S}_m = \boldsymbol{0}$$

$$\boldsymbol{K}_k = (\boldsymbol{\mathcal{B}}^T\boldsymbol{S}_{k+1}\boldsymbol{\mathcal{B}} + \boldsymbol{R}_k)^{-1}\boldsymbol{\mathcal{B}}^T\boldsymbol{S}_{k+1}\boldsymbol{\mathcal{H}}, \quad k < m$$

$$\boldsymbol{u}_k = -\boldsymbol{K}_k\boldsymbol{x}_k, \quad k < m$$

Table 6.1: Optimal Regulator Control Problem with free End State

The form of the performance index J is similar to the one usually used for Discrete Linear Quadratic Regulator with final state free. Following the same procedure as explained in [57], the optimal solution is obtained through the algorithm given in table (6.1).

Note that the optimization problem defined above is over a *finite* number of parameters (the nodal values of the control voltage, or the nodal forces)

6.6 Active vibration control of a plate

The same example as in section (4.6) is reconsidered here, the purpose is to confirm the performance of the direct optimal control methodology presented in the previous chapters, by studying an equivalent but different control design of distributed param-

eter systems. For this reason, only the regulator problem will be considered in this study, extension of the same method to tracking problem can be easily done following the steps of the algorithm thus described.
In this case the plate is modeled using finite element software developed by (ANSYS Inc.). A 3-D solid element is used for space discretization, the plate has four elements, and each actuator is represented by one piezoelectric element, giving eight elements in total for the whole structure. The structure was given an initial disturbance at the center of the plate and the optimal controller was activated. Since only one mode is disturbed (mainly the central node), the four actuators have the same behavior, which gives the same input control voltages time histories. For clarity, the results of one actuator are shown here.

Figure (6.1) shows the controlled response and the input control voltages of each actuator for two different weighting matrices. As it is shown, the behavior of the controller using this method is very similar to the one designed using the direct methodology. It can be seen that there exist small high frequency residual oscillations after complete damping. These could be the result of temporal truncation errors interference. They can be considerably reduced by applying small temporal steps or using some high feedback gains.

6.7 Optimal Tracking Control

For the optimal tracking problem, the optimal tracking control law is obtained through the algorithm given in Table (6.2). The tracking controller, is designed to track the trajectory of the mirror's surface, rather than the Zernike mode's trajectory. This is a major difference between the tracking optimal controller designed using the direct methodology and the one using space-time finite elements method. In this case we

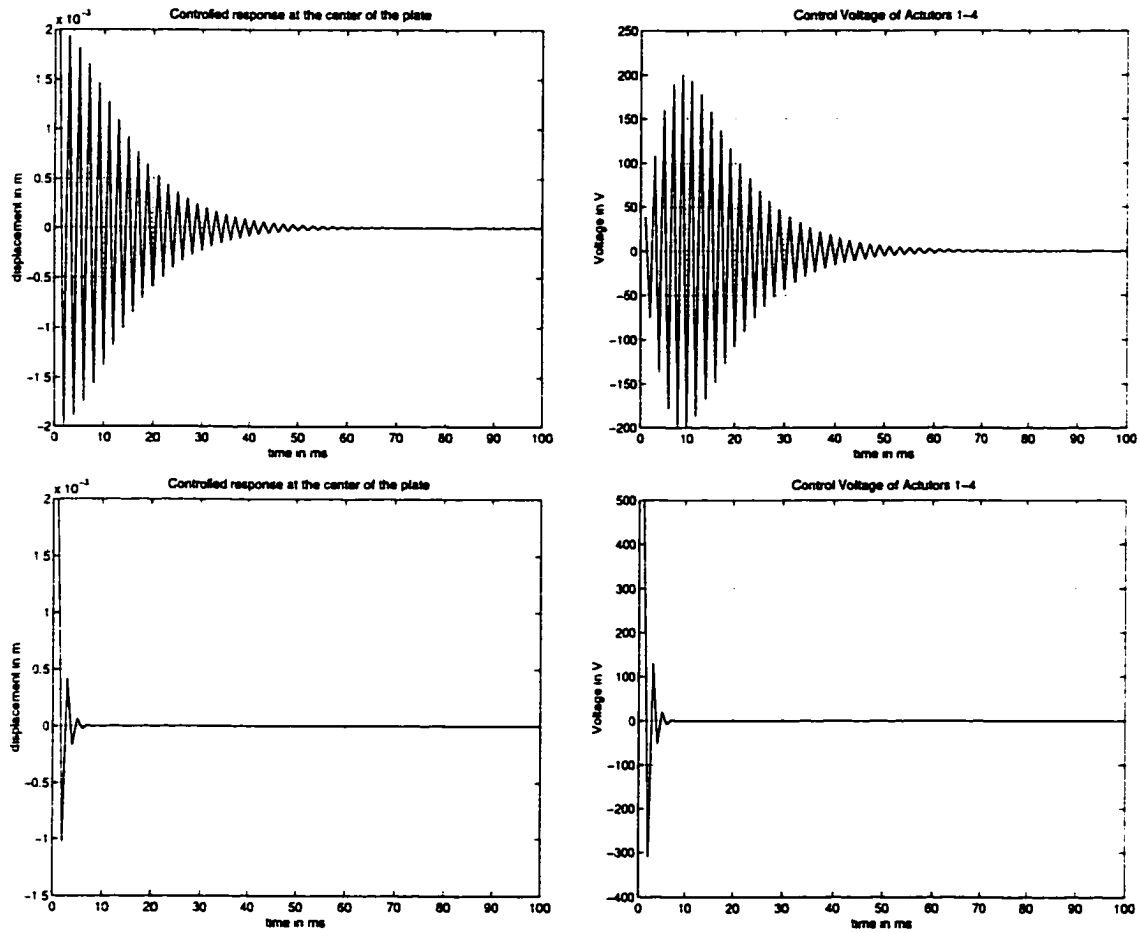

Figure 6.1: Displacement at the center of the plate, and the control voltages

System Model:

$$\boldsymbol{x}_{k+1} = \mathcal{H}\boldsymbol{x}_k + \mathcal{B}\boldsymbol{u}_k$$
$$\boldsymbol{y}_k = \mathcal{C}\boldsymbol{x}_k$$

Performance Index:

$$J_i = \frac{1}{2}\sum_{k=i}^{m}[(\boldsymbol{y}_k - \boldsymbol{r}_k)^T\boldsymbol{Q}_k(\boldsymbol{y}_k - \boldsymbol{r}_k) + \boldsymbol{u}_k^T\boldsymbol{R}_k\boldsymbol{u}_k] \quad \boldsymbol{Q}_k \geq \boldsymbol{0}, \boldsymbol{R}_k > \boldsymbol{0}$$

Optimal Affine Control:

$$\boldsymbol{K}_k = (\mathcal{B}^T\boldsymbol{S}_{k+1}\mathcal{B} + \boldsymbol{R}_k)^{-1}\mathcal{B}^T\boldsymbol{S}_{k+1}\mathcal{H}; \quad \boldsymbol{S}_m = \boldsymbol{0}$$

$$\boldsymbol{S}_k = \mathcal{H}^T\boldsymbol{S}_{k+1}(\mathcal{H} - \mathcal{B}\boldsymbol{K}_k) + \mathcal{C}^T\boldsymbol{Q}_k\mathcal{C}$$

$$\boldsymbol{V}_k = (\mathcal{H} - \mathcal{B}\boldsymbol{K}_k)^T\boldsymbol{V}_{k+1} + \mathcal{C}^T\boldsymbol{Q}_k\boldsymbol{r}_k \quad \boldsymbol{V}_m = \boldsymbol{0}$$

$$\boldsymbol{K}_k^v = (\mathcal{B}^T\boldsymbol{S}_{k+1}\mathcal{B} + \boldsymbol{R}_k)^{-1}\mathcal{B}^T$$

$$\boldsymbol{u}_k = -\boldsymbol{K}_k\boldsymbol{x}_k + \boldsymbol{K}_k^v\boldsymbol{V}_{k+1}$$

Table 6.2: Optimal Linear Quadratic Tracker

can only control (track) the shape of the mirror after fitting it to a desired shape for each time step, which affects considerably the response time of the controller. Furthermore, the structural matrices are larger compared to the assumed modes ones. Adding to that, the feedback control gain is obtained in an algorithmic procedure rather than in a closed form such in the case of direct methodology. For this reason the tracking optimal control using space-time finite elements is presented here without any example due to the non-relevance of the comparison.

6.8 Concluding Remarks

In this chapter, a space-time finite element formulation for the optimal control design was developed. It is a new computational approach for modelling and control of flexible structures. Finite element method is used for both spatial and temporal discretization and creates the appropriate framework for simultaneous control and structural model design iterations. This approach can be successfully applied in areas like active vibration damping. It has the advantage of being a general method for such applications with no need to find the structural model modes. However, for applications like in adaptive optics where a flexible structure -deformable mirror- has to be controlled to track a modal shape in space, this method needs an additional step -curve fitting- to complete the task, which puts it in a lower performance rank with respect to the direct optimal methodology.

The model matrices are generally larger than their counterpart in the direct methodology approach.

Chapter 7

Closing Comments

The mission of this dissertation was to investigate and develop a methodology which allowed to the control of any flexible structure in an optimal way and was simple to implement and computationally efficient. An emphasis placed on application to adaptive optics systems.
The Direct methodology presented and developed in this study offers many advantages for such applications compared to traditional approaches.

First, using space-time mode expansion technique, derivations of the algebraic equations of motion for a distributed parameter system were developed -for the first time- in chapter 3, this lead to the extension of the concept of controllability from discrete systems and its adaptation to distributed parameter systems. The modal expansion was the basis for the introduction of the direct optimal control methodology. Applied successfully for active vibration control of plates, this set the way to the design of an optimal shape controller for an adaptive optics system. Finally an alternative method was developed to assess the direct methodology in terms of its performance.

To recapitulate here it would appropriate to review the outline of this presentation and state explicitly what was planned and accomplished.

To begin with, a background exposition was provided, this was subdivided into two main issues, namely the issue of the direct methodology, and the issue of the adaptive optics control system. The sources of inspiration and the motives to pursue this study were presented; its scope and purposes were spelled out and a layout of the manuscript was given. Accordingly then, a broad picture about adaptive optics systems was presented along with the different systems which constitute an adaptive optics system, the functionality of each component and its limitations.

Hamilton's law of varying action was stated; the dynamic systems under consideration were defined, the mode shapes were chosen to satisfy the boundary conditions of a vibrating structure, and the Zernike modes were chosen to shape a deformable mirror, the generalized coordinates -mechanical and electrical- and the input functions were written as simple series expansions in time; these were directly substituted into Hamilton's law; time variable was integrated out and hence the algebraic equations of motion were derived. The unknown expansion coefficients of the time series (assumed time-modes) for the generalized coordinates were recognized as the states and those of the input functions were recognized as the controls. These algebraic equations were so formed that it enabled both the response and control problems to be addressed.

Next, controllability properties pertaining to these equations were investigated. This was followed by an account of optimal control problems. To this effect, the stage was set with a typical quadratic regulator performance measure in its familiar function form involving integral expressions, widely used in optimal control theory. Then, the time modes expansions were introduced into the performance measure, time was integrated out and hence the equivalent algebraic performance measure was obtained. This, together with the algebraic state equations, instantly transformed the usual

variational optimal control problem to an equivalent algebraic problem. Subsequently, optimal feedback gains were obtained in closed form, ready to simulate the associated closed-loop systems. This lead to the development of a newly designed controllability measure where the condition number of a coefficient matrix was taken as a reference. Thus a direct optimal control methodology was developed for distributed parameter systems and demonstrated.

The method was extended to tracking problems and optimal tracking policies were obtained. This revealed the usefulness of the method to control directly Zernike modes without resorting to an additional step for surface fitting. Finally an equivalent but different approach was developed and simulated where space and time were descretized in finite elements. This approach proved to be useful for structural modelling and control design within the same framework, where the structural and control design are carried out in parallel.

Without any resort to differential state equations, some control problems were studied directly via algebraic state equations, derived and cast here for general spatially continuous mechanical systems. The direct methodology proved to be simple and general. The direct methodology presented here is proposed as an alternative choice. It has proven to be very suitable to application such as adaptive optics control system design.

Many issues still remain to be addressed, namely:

- Implementation of a direct methodology constitute an interesting subject to investigate.
- Possible implications and/or interpretation towards frequency domain techniques can be looked into.

- Estimation and filtering techniques constitute an attractive research domain using the direct methodology especially when considered with control design.
- Different assumed mode forms can also be studied and a comparison study would be appropriate.
- a Direct time optimal control problems deserves closer attention since the time is integrated out. Adaptive control and systems identification using the direct methodology constitute another avenue for researchers to explore.

References

[1] E. Adiguzel. *"A New Treatise of Dynamic Systems via Algebraic State Equations"*. PhD thesis, The Ohio State University, 1994.

[2] D. M. Alloin and J. M. Marriotti, editors. *Adative Optics for Astronomy.* Kluwer Academic Publishers, Netherlands, 1994.

[3] A. R. Atilgan and D. H. Hodges. "Space-Time Mixed Finite Elements for Rods". *Journal of Sound and Vibration.* 192(3):731–739, 1996.

[4] J. N. Aubrun, K. R. Lorell, T. S. Mast, and J. E. Nelson. "Dynamic Analysis of the Actively Controlled Segemented Mirror of the W. M. Keck Ten Meter Telescope". *IEEE Control Magazine*, December 1987.

[5] H. W. Babcock. "The possibility of compensating Astronomical Seeing". *Publ. Astronomical Society Pac.*, 65, 1953.

[6] H. W. Babcock. "Adaptive Optics Revisited". *Science*, 249, July 1990.

[7] C. D. Bailey. "Vibration of Thermally Stressed Plates with Various Boundary Conditions". *AIAA journal*, 11(1):14–19, January 1973.

[8] C. D. Bailey. "A New Look at Hamilton's Principle". *Foundation of Physics*, 5:433–451, 1975.

[9] C. D. Bailey. "Application of Hamilton's Law of Varying Action". *AIAA journal*. 13:1154–1157, 1975.

[10] C. D. Bailey. "Exact and Direct Analytical Solutions to Vibrating Systems With Discontinuities". *Journal fo Sound and Vibration*, 44(1):15–25, 1976.

[11] C. D. Bailey. "Hamilton, Ritz and Elastodynamics". *ASME Journal of Applied Mechanics*, 43:684–688, 1976.

[12] C. D. Bailey. "The Method of Ritz Applied to the Equation of Hamilton". *Computer Methods in Applied Mechanics and Engineering*, 7:235–247, 1976.

[13] C. D. Bailey. "Direct analytical solutions to nonuniform beam problems". *Journal of Sound and Vibration*, 56:501–507, 1978.

[14] C. D. Bailey. "Further Remarks on the Law of Varying Action and the Symbol δ". *Journal of Sound and Vibration*, 131:331–344, 1989.

[15] P. Z. Bar-Yoseph, D. Fisher, and O. Gottlieb. "Spectral Element Methods for Nonlinear Temporal Dynamical Systems". *Computational Mechanics*, 18:302–313, 1996.

[16] K. J. Bathe. *Finite Element Procedure*. Prentice Hall, 1996.

[17] J. M. Beckers. "Adaptive Optics for Astronomy:Principles, Performance, and Applications.". *Annu. Rev. Astron. Astrophysics*, 31:13–62, 1993.

[18] A. Ben-Tal and P. Bar-Yoseph. "Space-time Spectral Element Method For Optimal Slewing of a Flexible Beam". *International Journal for Numerical Methods in Engineering*, 39:3101–3121, 1996.

[19] M. A. V. Bokern, R. N. Pascahll, and B.M. Welsh. "modal control for an adaptive optics system using lqg compensation". *Computers & Electrical Engineering*, 18:421–434, 1992.

[20] M. Born and E. Wolf. *Principles of Optics*. Pergamont Press, Oxford, 5th edition, 1975.

[21] M. Borri, G. L. Ghiringhelli, M. Lanz, P. Mantegazza, and T. Merlini. "Dynamic Response of Mechanical Systems By Weak Hamiltonian Formulation". *Computers & Structures*, 20(1-3):495–508, 1985.

[22] C. Boyer. Adapative" optics:interaction matrix measurements and real time control algorithm for the come-on project". In *Proceedings of the SPIE*, volume 1237, page 406, 1990.

[23] A. Chellabi, Y. Stepanenko, and S. Dost. "A new Control Algorithm for Bimorph Mirrors". In *Proccedings of IEEE Sytstems Man and Cybernitics*, volume 1, pages 569–573, Vancouver, BC, 1995.

[24] C. T. Chen. " *Linear Systems Theory and Design*". Holt, Rinehart and Winston, Inc., New York, 1984.

[25] E. S. Claflin and N Bareket. "Configuring an Electrostatic Membrane Mirror by Least-Square Fitting Analytically derived INfluence Functions". *Journal of the Optical Society of America*, 3(11):1833–1839, 1986.

[26] R. L. Clark. "adaptive optics: Aims for earthy applications". *Photonics*, pages 100–106, April 1997.

[27] G. P. Collins. "Making stars to see stars: DOD Adaptive Optics work declassified.". *Physics today*, February 1992.

[28] R. Cubalchini. "Modal Wavefront Estimation From Phase Derivative Measurements". *Journal of the Optical Society of America*, 69(7):972–977, 1979.

[29] M. A. Ealey. "Active and Adaptive Optical Components:The Technology and Future Trends". In *Proceedings of SPIE*, volume 1543, pages 2–34, 1991.

[30] M. A. Ealey and J. F. Washeba. "Continuous Facesheet Low Voltage Deformable Mirrors". *Optical Engineering*, 29(10):1191–1198, 1990.

[31] F. Forbes *et al.* "Segmented Bimorph Deformable Mirror". *Journal of Physics E: Scientific Instruments*, 22:402–405, 1989.

[32] F. Roddier *et al.* " One-dimensional spectra of turbulence-iduced Zernike aberrations: time-delay and isoplanicity error in partial compensationala ". *Journal of the Optical Society of America*, 10(5):957–965, May 1993.

[33] R. Q. Fugate *et al.* "Two Generations of Laser Guide Atar Adaptive optics Experiments at the Starfire Optical Range". *Journal of the Optical Society of America A*, 11, 1994.

[34] D. L. Fried. " Least square Fitting a Wavefront Distortion Estimate to an Array of Phase Difference Measurements". *Journal of the Optical Society of America*, 67(3):370–375, March 1977.

[35] B. Friedland. *Control System Design*. Mc Graw Hill, 1986.

[36] J. P. Gaffard and C. Boyer. "adaptive optics: a method for real time optimization of the loop gains in a. o. systems". In *Proceedings of SPIE*, volume 2201, 1994.

[37] J. E. Graves, F. Roddier, M. J. Northcoott, and J. Anuskiewicz. "Adaptive Optics at the University of Hawaii IV: A photon Counting Curvature WavefrontS ensor". In *Proceedings of SPIE*, volume 2201, pages 502–507, 1994.

[38] D. P. Greenwood. " Bandwidth Specification for Adaptive Optics Systems". *Journal of the Optical Society of America*, 67(3), March 1977.

[39] D. P. Greenwood and D. L. Fried. " Power Spectra Requirements for Wavefront Compensation Systems". *Journal of the Optical Society of America*, 66(3), 1976.

[40] R. P. Grosso and M. Yellin. " The Membrane Mirror as an Adaptive Optical Element.". *Journal of the Optical Society of America*, 67(3):399–406, 1977.

[41] P. Halevi. "Bimorph Piezoelectric Flexible Mirror: Graphical Solution and Comparison with Experiment". *Journal of the Society of America*, 73(1):110–113, 1983.

[42] W. R. Hamilton. "On a General Method in Dynamics; by Which the Study of Motion of all Free Systems Attracting or Repelling Points is Reduced to the Search and Differentiation of One Central Relatioon, or Characteristic Function". *Philosophical Transactions of the Royal Society of London*, pages 247-308, 1834.

[43] W. R. Hamilton. "Second Essay on a General Method in Dynamics". *Philosophical Transactions of the Royal Society of London*, pages 995–144, 1835.

[44] J. W. Hardy. "Active Optics: A new Technology for the Control of Light". *Proceedings of IEEE*, 66(6):651–697, 1978.

[45] J. Hermann. " Least squares Wavefront Errors of Minimum Norm". *Journal of the Optical Society of America*, 66(6), June 1980.

[46] D. H. Hodges and R. D. Bless. "A Weak Hamiltonian Finite Element Method for Optimal Control Problems". *Journal of Guidance, Control and Dynamics*, 14(1):148–156, 1991.

[47] D. H. Hodges and L. Hou. "shape functions for mixed p-version finite elements in the time domain". *Journal of Sound and Vibartion*, 145(2):169–178, 1991.

[48] J. Huang. *"Design and Analysis of Adaptive Optics Control Systems"*. PhD thesis, Boston University, 1995.

[49] R. H. Hudgin. " Wavefront Reconstruction for Compensated Imaging". *Journal of the Optical Society of America*, 67(3):375–378, March 1977.

[50] P. Jagourel, P. Y. Madec, and M. Sechaud. "Adaptive Optics: A Bimorph Mirror for Wavefront Correction". In *Proceedings of SPIE*, volume 1271, pages 160–171, 1990.

[51] W. Jiang and H. Li. Hartmann-shack wavefrontsensing and wavefront control algoritms. In *Proceedings of SPIE*, volume 1271, 1990.

[52] S. M. Joshi. *Control of Large Flexible Soace Structures.* Springer, Berlin, 1989.

[53] J. L. Junkins, editor. *Mechanics and Control of Large Flexible Structures.* AIAA, Washington, D. C., 1990.

[54] J. L. Junkins and Y. Kim. *Introduction to Dynamics and Control of Flexible Structures.* American Institute of Aeronautics and Astronautics, Washington, D. C., 1993.

[55] S. A. Kokorowski. "Analysis of Adaptive Optical Elements Made From Piezoelectric Bimorphs". *Journal of the Optical Society of America A*, 69(1):181–187, 1979.

[56] C. K.. Lee, T. C. O'Sullivan, and W. W. Chiang. "Piezoelectric Strain Rate Sensor and Actuator Designs for Active Vibration Control.". In *AIAA # 91-1604, Proceedings of the 32nd AIAA/ASME/ASCE/AHS Structure Structural*

Dynamics and Materials Conference, pages 2197–2207, Baltimore, MD, April 1991.

[57] Frank L. Lewis. *Optimal Control.* A Wieley-Interscience Publication, 1986.

[58] C. F. Lin. *Advanced Control Systems Design.* Prentice Hall, Englewood Cliffs, N.J., 1994.

[59] L. Meirovitch. *Dynamics and Control of Structures.* Wiley Interscience, New York, 1990.

[60] M. L. Nagurka and S. K. Wang. "A Chebychev-based State Representation for Linear Quadratic Optimal Control". *ASME Journal of Dynamic Systems Measurement Control*, 115:1–6, 1993.

[61] R. J. Noll. "Zernike Polynomials and Atmospheric Turbulence". *Journal of the Optical Society of America*, 66(2):207–211, 1976.

[62] H. Oz and A. Raffie. "Inverse Response Problem (Control) of Dynamics Systems via Hamilton's Law". *Computer Methods in Applied Mechanics and Engineering*, 62:17–26, 1987.

[63] R. N. Paschall and D. J. Anderson. "Linear Quadratic Gaussian Control of Deformable Mirror Adaptive Optics System with Time-delayed Measurements". *Applied Optics*, 32(31):6347–6358, November 1993.

[64] B. L. Ellerbroek C. Van Loan N. Pitsianis R. Plemmons. " Optimizing Closed loop Adaptive Optics Performance Using Multiple Bandwidths". *Journal of the Optical Society of America A*, 11, 1994.

[65] B. Porter and R. Crossley. *Modal Control.* Taylor and Francis, London, 1972.

[66] N. V. Raybova and V. F. Zakharenkov. "Active and Adaptive Optics in Large Telescopes". *Soviet Journal of Optical Technology*, 59(6):320–340, June 1992.

[67] F. Roddier. " Curvature Sensing and Compensation: A New Concept in Adaptive Optics". *Applied Optics*, 27(7):1223–1225, 1988.

[68] M. C. Roggemann and J. A. Meinhart. "image reconstruction by means of wavefront sensor measuremnts in closed-loop adaptive optics systems". *Journal of the Optical Society of America*, 10(9):1996–2007, September 1993.

[69] C. Schwartz, E. Ribak, and S. G. Lipson. "Bimorph Adaptive Mirrors and Curvature Sensing". *Journal of Optical Society of America A*, 11(2):895–902, 1994.

[70] T. E. Simkins. Finite elements for initial value problems in dynamics. *AIAA Journal*, 19(10):1357–1362, October 1981.

[71] W. H. Southwell. '"Wavefront Estimation from wavefront slope measurements". *Journal of the Optical Society of America*, 70(8):998–1006, 1980.

[72] R. K. Tyson. *Principles of Adaptive Optics*. Academic Press, 1991.

[73] E. P. Wallner. " Optimal Wavefront Correction Using Slope Measurments". *Journal of the Optical Society of America*, 67(3), August 1977.

[74] J. Y. Wang. " Effect of Finite Bandwith on Far Field Performance Model of Wavefront Compensative System". *Journal of the Optical Society of America*, 69(6):819–828, June 1979.

[75] J. Y. Wang and D. E. Silva. "Wavefront Interpretation witn Zernike Polynomials". *Applied Optics*, 19(9):1510–1518, May 1980.

[76] Y. Xin and W. Xueye. "Novel Wavefront Sensor in Adaptive Optics-Zernike Polynomials Coefficients Sensor". In *Proceedings of SPIE*, volume 2201, pages 539–548, 1994.

[77] V. Yen and M. L. Nagurka. "Fourier-based Optimal Control Approach for Structural Systems". *Journal of Guidance, Control and Dynamics*, 13:265–276, 1990.